



**UNIVERSITÀ DEGLI STUDI DELL'AQUILA**  
**DIPARTIMENTO DI SCIENZE CLINICHE, APPLICATE E**  
**BIOTECNOLOGICHE**

Dottorato di Ricerca in **MEDICINA SPERIMENTALE**  
Curriculum **BIOTECNOLOGIE E SCIENZE BIOCHIMICHE**  
XXXV ciclo

Titolo della tesi

Interaction between endosteal niche and dormant breast cancer cells:  
molecular and functional characterization

SSD BIO/17

Dottorando

Michela Ciocca

Matr. 268394

Coordinatore del corso  
Prof.ssa Maria Grazia Perilli

Tutor  
Prof.ssa Anna Maria Teti

a.a. 2021/2022

# Index

<b>ABSTRACT .....</b>	<b>5</b>
<b>Chapter 1 .....</b>	<b>7</b>
<b>1. INTRODUCTION .....</b>	<b>7</b>
<b>1.1 Breast Cancer .....</b>	<b>7</b>
1.1.2 Overview .....	7
1.1.3 Molecular and histological characteristics of BrCa .....	8
1.1.4 Diagnosis and epidemiology .....	11
1.1.5 Risk factors .....	12
1.1.6 Treatments .....	13
1.2 The metastatic process .....	14
1.3 Mimicry .....	15
1.3.2 Vasculogenic mimicry .....	16
1.3.3 Immunological mimicry .....	17
1.3.4 Osteomimicry .....	17
1.4 BrCa bone metastasis .....	18
1.5 BrCa dormancy .....	19
1.5.2 Role of the endosteal niche in BrCa dormancy .....	22
<b>2 AIM OF THE STUDY .....</b>	<b>26</b>
<b>3 REFERENCES .....</b>	<b>26</b>
<b>Chapter 2 .....</b>	<b>30</b>
<b>Role of Neural (N)-Cadherin in BrCa cell stemness and dormancy in the bone microenvironment .....</b>	<b>30</b>
<b>1. ABSTRACT .....</b>	<b>30</b>
<b>2. INTRODUCTION .....</b>	<b>31</b>
<b>3. MATERIAL AND METHODS .....</b>	<b>32</b>
3.1. Materials .....	32
3.2. BrCa cell culture .....	34
3.4. Magnetic-Activated Cell Sorting (MACS) .....	35
3.5. RNA extraction, RNA deep Sequencing (RNAdSeq) analysis and gene expression .....	35

3.6. Flow cytometry .....	36
3.7. Animals .....	36
3.8. Intratibial injection of N-Cadherin <sup>High</sup> and N-Cadherin <sup>Low</sup> MDA cells.....	36
3.9. Limiting Dilution Assay (LDA) .....	37
3.10. Micro-Computed Tomography ( $\mu$ CT) analysis .....	37
3.11. Histology.....	37
3.12. Immunohistochemistry and immunofluorescence .....	37
3.13. Histomorphometry .....	38
3.14. Osteoblast/BrCa cells coculture assay .....	38
3.15. Primary and secondary mammosphere formation assay .....	39
3.16. Statistical analyses.....	39
<b>4. RESULTS</b> .....	<b>39</b>
4.1. N-Cadherin and Notch2 are co-expressed in MDA cells .....	39
4.2. Role of N-Cadherin in in vivo tumor growth and dormancy.....	41
4.3. N-Cadherin mediates BrCa Cell adhesion onto SNOs in vitro .....	43
4.4. The role of N-Cadherin in HSC mimicry and Cancer Stem Cell-like phenotype .....	45
4.5. N-Cadherin status in human primary BrCa and correlation with survival .....	47
<b>5. DISCUSSION</b> .....	<b>51</b>
<b>6. REFERENCES</b> .....	<b>53</b>
<b>Chapter 3</b> .....	<b>57</b>
<b>The endosteal niche regulates BrCa cell dormancy in bone</b> .....	<b>57</b>
1. <b>ABSTRACT</b> .....	57
2. <b>INTRODUCTION</b> .....	58
3. <b>MATERIAL AND METHODS</b> .....	59
3.1 <b>Materials</b> .....	59
3.2 <b>Animals</b> .....	62
3.3 <b>Human samples</b> .....	62
3.4 <b>Cell lines</b> .....	62

3.5	<i>Primary osteoblast cell isolation</i> .....	62
3.6	<i>Magnetic-Associated Cell Sorting (MACS)</i> .....	63
3.7	<i>Flow cytometry</i> .....	63
3.8	<i>Osteoblast/BrCa cell coculture assay</i> .....	63
3.9	<i>Transcriptome analysis</i> .....	63
3.10	<i>Gene ontology and pathway analyses</i> .....	64
3.11	<i>Gene Set Enrichment Analysis (GSEA)</i> .....	66
3.12	<i>Real time and semi-quantitative RT-PCR</i> .....	66
3.13	<i>Western blot</i> .....	67
3.14	<i>In vivo studies</i> .....	67
3.15	<i>Micro-computed tomography</i> .....	67
3.16	<i>Histology</i> .....	68
3.17	<i>Immunohistochemistry and immunofluorescence</i> .....	68
3.18	<i>Statistical analysis</i> .....	68
<b>4.</b>	<b>RESULTS</b> .....	<b>69</b>
4.1.	<i>Notch1 and Notch2 expression in BrCa cells</i> .....	69
4.2.	<i>Role of Notch1 and Notch2 in the interaction of BrCa cells and SNOs</i> .....	72
4.4.	<i>Comparison between Notch1<sup>High</sup> and Notch2<sup>High</sup> MDA cell transcriptomes</i> .....	75
4.4.	<i>Stem cell signature and HSC mimicry</i> .....	77
4.6.	<i>BrCa cells-SNO interactome</i> .....	81
<b>5.</b>	<b>DISCUSSIONS</b> .....	<b>85</b>
<b>6.</b>	<b>REFERENCES</b> .....	<b>88</b>
<b>Chapter 5</b>	.....	<b>92</b>
<b>CURRICULUM VITAE</b>	.....	<b>92</b>

## ABSTRACT

Breast Cancer (BrCa) is the most commonly diagnosed malignancy in women worldwide. Early diagnosis, screening programs and therapies increased the overall chances of survival for patients, with a ten-year survival rate above 95%. The main problem for patients remains the long-term recurrence, which can occur due to a small percentage of the BrCa cells colonizing distant organs that can acquire a quiescent status and remain resistant to conventional therapies for years. After this period, specific stimuli, not yet fully known, prompt the cells to reactivate, generating a new tumor.

In this thesis, it has been provided an overview of BrCa features, diagnosis and treatment, describing in detail the general metastatic process, and in particular the mechanism involved in the development of BrCa bone metastases. Given that the project was focused on the process of cellular dormancy, this latter has been described in detail, with a special emphasis on the “niche” concept that, in the bone microenvironment, is physiologically involved in the maintenance of the Hematopoietic Stem Cell (HSC) pool indispensable for the generation of blood cells. Previous results published by our laboratory had demonstrated the relevance of the endosteal niche enriched in spindle-shaped N-Cadherin+ Osteoblasts (SNOs), known to be involved in the quiescence of Long-Term HSCs, for the maintenance of the quiescent status of dormant BrCa cells. In this article, it was demonstrated that SNOs can reduce the proliferation of human BrCa MDA-MB231 (MDA) cells expressing high level of Notch2, and that Notch2<sup>High</sup> BrCa cells also express genes typical of HSCs, known to physiologically interact with SNOs remaining quiescent.

In the project presented in this thesis, we investigated N-Cadherin as another potential player of BrCa cell-SNO interaction that could induce BrCa cellular dormancy. We also extended the knowledge on the involvement of the Notch family in BrCa dormancy, comparing various cell lines expressing high levels of Notch1, Notch2 or both, and profiling the molecular signatures obtained by RNAdSeq in Notch1<sup>High</sup> and Notch2<sup>High</sup> MDA cells. The results demonstrated that:

- N-Cadherin<sup>High</sup> and Notch2<sup>High</sup> MDA cells show similar HSC-mimicry and SNO-induced dormancy features.
- N-Cadherin mediates MDA-SNO adhesion in the endosteal niche.
- High expression of Notch2, but not of Notch1, confers MDA cells molecular signatures of pluripotency, HSC-mimicry and dormancy
- HSC genes appear not to be implicated in SNO-induced MDA cellular dormancy.

- Notch2<sup>High</sup> MDA cells express high level of CD177 glycosylphosphatidylinositol (GPI)-linked surface glycoprotein that recognizes the plasminogen activator urokinase receptor (uPAR), the CD11b chain of the Mac-1 (alphaMbeta2; Cd11b/CD18; complement receptor-3) integrin and the CarcinoEmbrionic Antigen-related Cell Adhesion Molecule 1 (CEACAM1) expressed by SNOs.

Based on these results, we hypothesize that the CD177 associated pathways could potentially contribute to the SNO-mediated dormancy of Notch2<sup>High</sup> MDA cells. To demonstrate this hypothesis, further work will be necessary beyond the study presented in this thesis. This goal will be achieved through functional studies that will make use of CD177 antagonists in the *in vitro* and *in vivo* models of dormancy described in this thesis.

# Chapter 1

## 1. INTRODUCTION

### 1.1 Breast Cancer

#### 1.1.2 Overview

After skin cancer, Breast Cancer (BrCa) is the second most common cancer found in female bodies.<sup>1</sup> Due to the screening programs, diagnoses of BrCa are increasingly carried out during the earlier stages of tumor development. Thanks to these early diagnoses and the associated conventional therapies, the overall survival rate for patients is very high, resulting in a ten-year survival rate above 95%,<sup>1</sup> the leading cause of death being the metastatic relapse.<sup>2</sup>

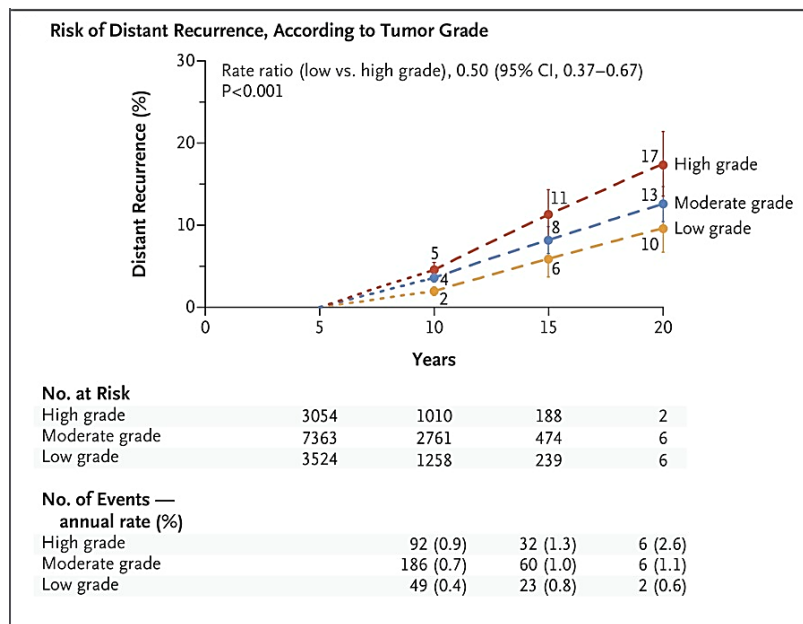


**Figure 1.** Association of Tumor Grade with the Risk of Distant Recurrence during years 5 to 20. Adapted from “20-Year Risks of Breast-Cancer Recurrence after Stopping Endocrine Therapy at 5 Years”.<sup>2</sup>

BrCa is a heterogeneous group of tumors with different pathological features, molecular signatures, and clinical outcomes. This heterogeneity implies the usage of an array of different therapies in order to target specific molecular pathways and reduce the adverse effects of treatment.

### 1.1.3 Molecular and histological characteristics of BrCa

From a molecular point of view, BrCa are classified based on their differentiation status and the expression of specific markers, such as estrogen receptors (ER), progesterone receptors (PR), human epidermal growth factor receptor 2 (HER2), and the cell proliferation regulator, Ki-67. BrCa are also classified in luminal A, luminal B, HER2-positive and triple negative (TNBC) or basal-like subtypes.<sup>3</sup> This classification is useful to predict the prognosis and to guide the therapeutic choice (Figure 2, Table 1).

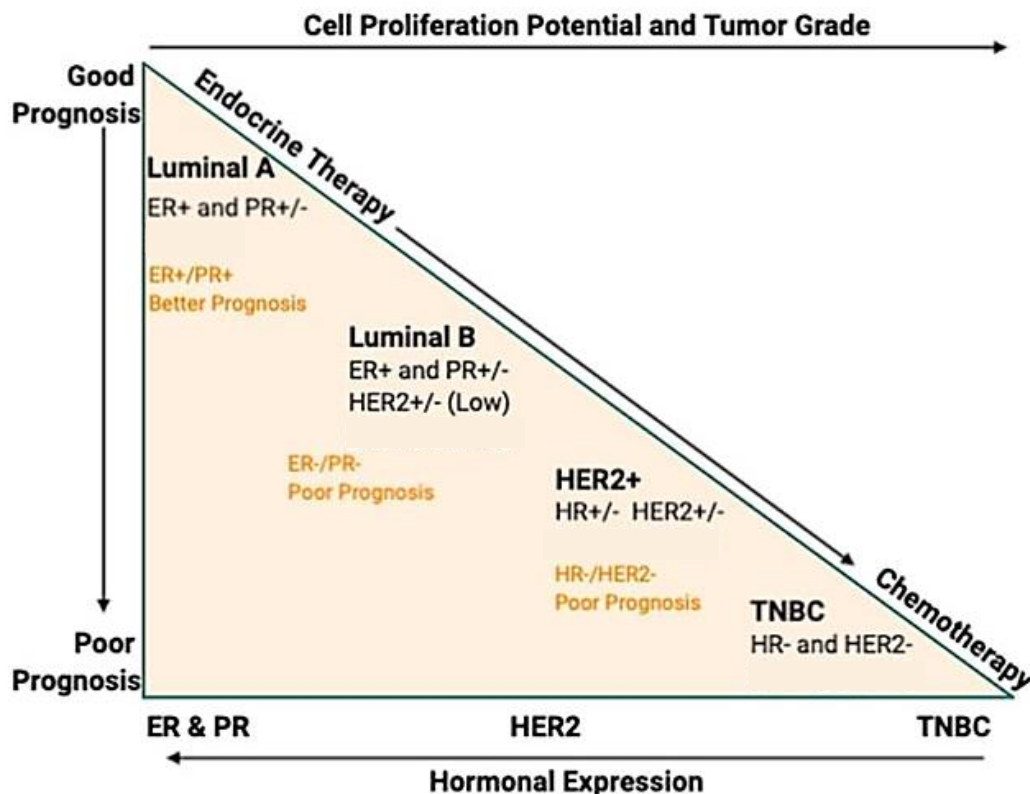


**Figure 2.** Classification of BrCa based on molecular stratification, relative grading, therapy requirement, and prognosis. Adapted from “Advanced Approaches to Breast Cancer Classification and Diagnosis”<sup>4</sup>

#### Luminal A BrCa ( $ER^+$ $PR^+$ $HER2^-$ $Ki67^{low}$ ):

This tumor has characteristics of the luminal epithelial cells of the breast, it is well differentiated and expresses both estrogen and progesterone receptors. It is the most differentiated subtype, with slow growth and a better prognosis. Luminal A tumors represent 40-50% of all BrCa cases. From the histological point of view, this type of tumor represents the low grade invasive ductal carcinoma.



Luminal B BrCa (ER+ PR- HER2-/+ Ki67<sup>high/low</sup>)

This subtype is responsible for approximately 20-30% of invasive ductal BrCa. It is more aggressive than type A and is not well differentiated. Luminal B tumor is also known as basoluminal or molecular apocrine BrCa which might be derived from a stem cell midway along the differentiation.

HER2+ BrCa (ER- PR- HER2+ Ki67<sup>high</sup>)

This tumor subtype is characterized by a poorer differentiation. It does not express estrogen or progesterone receptors, but it is enriched in the expression of the epidermal growth factor receptor, HER2. It represents 15% of invasive BrCa cases and has a high proliferation ability. Therefore, it is classified as high grade invasive ductal carcinoma.

Triple negative (TNBC) or basal-like BrCa (ER- PR- HER2- Ki67<sup>high</sup>)

This subtype is characterized by the lack of the expression of HER2, estrogen and progesterone receptors. Furthermore, it is the highest proliferative tumor subtype, according to the Ki67 most elevated expression. It represents 10-20% of the high grade invasive ductal carcinomas, with a high risk of loco-regional recurrence, contralateral disease and distant relapse.

**Table 1.** Molecular subtypes of BrCa

<b>Molecular BrCa subtypes</b>				
	<b>Luminal A</b>	<b>Luminal B</b>	<b>HER+</b>	<b>TNBC</b>
<b>Molecular markers</b>	ER+ PR+ HER2- Ki67 <sup>low</sup>	ER+ PR- HER2-/+ Ki67 <sup>high/low</sup>	ER- PR- HER2+ Ki67 <sup>high</sup>	ER- PR- HER2- Ki67 <sup>high</sup>
<b>Clinical and biological properties</b>	40-50% of invasive BrCa, ER/PR positive, HER2 negative	20-30% of invasive BrCa, ER/PR positive, HER2 expression variable, higher proliferation than Luminal A, higher histologic grade than Luminal A	15% of invasive BrCa, ER/PR negative, HER2 positive, high proliferation, high histologic grade and nodal positivity	10-15% of invasive BrCa, most ER/PR/HER2 negative (triple negative), high proliferation
<b>Histological correlation</b>	Low grade invasive ductal carcinoma	Invasive ductal carcinoma	High grade invasive ductal carcinoma	High grade invasive ductal carcinoma, high risk of relapse and metastasis

The World Health Organization (WHO) classifies BrCa in 19 subtypes according to the histological categories.<sup>5</sup> Firstly, they are divided into non-invasive and pre-invasive types, when they manifest locally in the breast; whereas when they show features which indicate their ability to spread in other sites, they are classified as invasive.

A further classification divides them in ductal or lobular cancers, depending on the breast structure involved.

According to the Elston- and Ellis-modified Scarff–Bloom–Richardson system<sup>6</sup>, BrCa can be classified by histological grade, based on three tumor features:

- the proportion of cancer cells that are in the phase of tubule formation,
- the variation of nuclear size and shape between the cells (anisokaryosis),
- the number of mitoses.

Based on the scores from all three categories above, the tumors are classified by grades. (Figure 3 and Table 2)

**Table 2. Histological grade of BrCa.** BrCa can be divided by histological grades. This is a prognostic factor and is representative of the "aggressive potential" of the tumor. In a broad generalization, "low grade" cancers tend to be less aggressive than "high grade" cancers.

<b>Grade</b>	<b>Glandular/Tubular Differentiation</b>	<b>Nuclear Pleomorphism</b>	<b>Mitotic Count</b>
<b>Grade 1</b>	>75% of tumor forms glands	Uniform cells with small nuclei similar in size to normal breast epithelial cells	< 7 mitoses per 10 high power fields
<b>Grade 2</b>	10% to 75% of tumor forms glands	Cells larger than normal with visible nucleoli and moderate variability in size and shape	8-15 mitoses per 10 high power fields
<b>Grade 3</b>	<10% of tumor forms glands	Cells with prominent nucleoli, marked variation in size and shape	> 16 mitoses per 10 high power fields

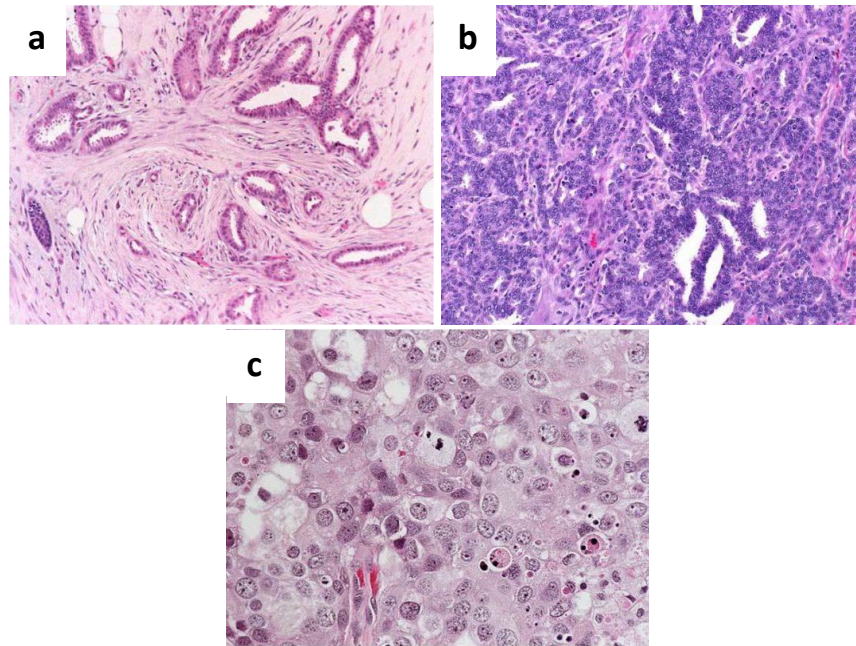


**Figure 3. Histologic sections of Grades I-III BrCa.** (a) Histologic Grade I Invasive Ductal Carcinoma. This tumor consists of small glands with uniform nuclei. Grade I carcinomas tend to be less aggressive and have a better prognosis than higher grade carcinomas. They are also often ER positive, which is another feature associated with a more favorable prognosis. (b) Histologic Grade II Invasive Ductal Carcinoma. Portions of this invasive carcinoma form tubular gland structures, but the remaining areas present poorly formed glands with nests of cells containing moderately atypical nuclei. Grade II carcinomas have an intermediate prognosis between Grade I and Grade III cancers. (c) Histologic Grade III Invasive Ductal Carcinoma. This carcinoma consists of sheets of individual and nest cells with marked nuclear atypia and mitotic activity. They tend to be aggressive and have a worse prognosis than the lower grade carcinomas. They are also more often triple negative, which is another feature associated with aggressive behavior and worse prognosis. Adapted from “Staging & Grade - Breast Pathology “. <sup>7</sup>

#### *1.1.4 Diagnosis and epidemiology*

As mentioned in the first paragraph, in recent years, screening programs for BrCa have been implemented allowing early diagnosis. This greatly reduces the time of intervention, increasing the survival rate of patients. Imaging represents a gold standard to detect cancer and to monitor progression and response to therapies.<sup>8</sup> The first level of diagnosis featured in the screening programs is the mammography, which consists of a low- dose X- ray imaging of the breasts.<sup>8</sup> It was recently confirmed that women who attended a mammography screening have a lower risk of death due to BrCa within 10 years (about 40% less than unscreened women).<sup>9</sup>

Other imaging techniques are ultrasounds and Magnetic Resonance Imaging (MRI). (Figure 4)

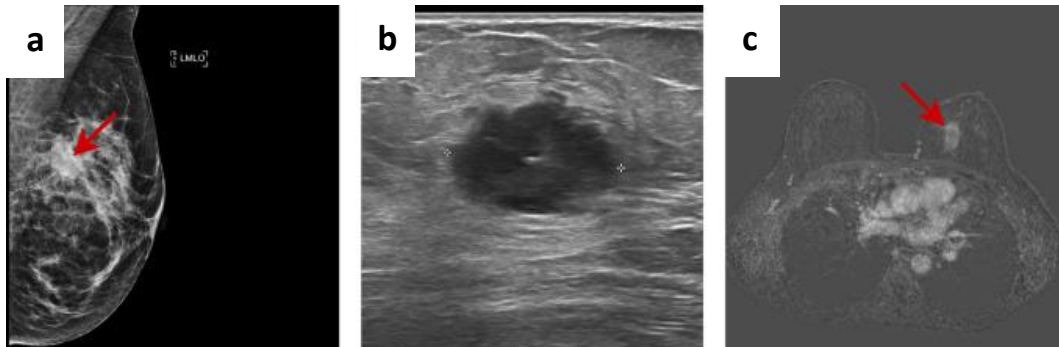


**Figure 4.** (a) Digital mammography, (b) ultrasound and (c) magnetic resonance scans of a 45-year-old woman with an infiltrating ductal carcinoma in the left breast, indicated with the red arrows. Adapted from “Application of Deep Learning in Breast Cancer Imaging”.<sup>10</sup>

The second level of diagnosis is the needle biopsy of malignant mass and lymph nodes to investigate the tumor histology, grade and marker expression, select neoadjuvant therapy, and predict sentinel lymph node status.<sup>11</sup> Finally, if a metastatic cancer is suspected, further computed tomography (CT) on chest, abdomen and pelvis, as well as chest CT with abdomen and pelvis MRI, and bone scan or sodium fluoride positron emission tomography (PET)/CT are performed.

Due to differences in the screening programs and in the availability of medical care, the BrCa incidence varies worldwide. The highest BrCa incidence is found in North America, Australia, New Zealand, and Northern and Western Europe.<sup>12</sup> It is also worth mentioning that BrCa is diagnosed at an earlier stage and the prognosis is usually better in developed countries. This is not the case in less-developed countries, where BrCa is often diagnosed at a later stage and for this reason it is associated with lower chances of survival.<sup>12</sup>

There are also some variations in BrCa incidence, subtype, and prognosis between ethnic groups. Indeed, black women have a high risk of TNBC compared to the other groups, which is correlated with a higher death rate. On the other hand, Asian/Pacific Islander women are more likely to be diagnosed with localized BrCa, with a lower death rate.<sup>13</sup>

#### *1.1.5 Risk factors*

Half of the cases of BrCa develop in women without risk factors. However, age, obesity, use of alcohol and tobacco, history of radiation exposure, reproductive history, previous familiar BrCa cases and postmenopausal hormone therapy can increase the risk.

Moreover, mutations in the suppressor genes BrCa Susceptibility protein type 1 and 2 [*BRCA1* (17q21) and *BRCA2* (13q13)] show an autosomal-dominant inheritance pattern accounting for 1-7% of BrCa. Other genes possibly related to the high risk of BrCa development are *ATM*, *CHEK2*, *PALB2*, *PTEN*, *STK11* and *TP53*.<sup>14</sup>

#### 1.1.6 Treatments

Ninety percent of women with an early diagnosis have a favorable prognosis.<sup>15</sup> Treatments generally consist in:

- surgery
- chemo- and radiotherapy
- endocrine therapy
- immunotherapy or targeted therapy

In the past, the surgery involved total mastectomy, including the resection of the uterus and ovaries when needed. Currently, if the cancer is not too extensive, it can be removed with a partial mastectomy, with which only the affected area is removed from the breast. This procedure requires radiotherapy to prevent recurrence.<sup>16</sup> Together with breast surgery, a sentinel lymph node biopsy is needed to check for lymph node involvement, an indication of cancer spreading.<sup>17</sup>

The medical treatment after surgery depends on the BrCa subtype. Cancers that express ER and PR, can be treated using endocrine therapies such as tamoxifen or aromatase inhibitors. This treatment prevents the risk of recurrence by half, although it is not free of side effects, which consists in menopause symptoms however reversible.<sup>18</sup>

If the cancer is negative for hormone receptors, the only effective treatment is chemotherapy with combination drugs such as cyclophosphamide, epirubicin, anthracycline and taxanes (paclitaxel or docetaxel), depending on subtype aggressivity.<sup>18</sup> However, chemotherapy has cytotoxic, mutagenic, teratogenic, and/or carcinogenic effects and it needs to be managed carefully.

The HER2+ subtype of cancer has a specific treatment that reduces the risk of recurrence by 45-50%, using a blocking monoclonal antibody direct to the HER2 receptor. Some of these drugs are trastuzumab, pertuzumab, neratinib and lapatinib.<sup>18</sup>

## 1.2 The metastatic process

The most frequent cause of death in BrCa patients is the development of distant metastasis, which consists in a multi-step process where tumor cells spread from the primary tumor to other organs (Figure 5).<sup>19</sup> This process includes local invasion, intravasation, migration through lymphatic or blood vessels and colonization of distant organs with the formation of new tumors.

### - Local invasion

BrCa cells in the primary site detach from the tissue through the breaking of the cell-cell or cell-extracellular matrix (ECM) bindings. In addition, molecules released from the degrading ECM stimulate the BrCa cell metastatic process. In this phase, tumor cells lose the expression of epithelial markers, such as E-Cadherin, essential for the formation of anchoring junctions, stimulating cell migration. Conversely, they upregulate the mesenchymal markers Vimentin and N-Cadherin, acquiring the ability to detach from the cell cluster and move through the ECM barriers. This process, called Epithelial to Mesenchymal Transition (EMT), facilitates the invasion of the ECM.<sup>20</sup> When the tumor cells reach the distant metastatic site, this process can be reverted by the Mesenchymal to Epithelial Transition (MET), a phenotypic change opposite to the EMT. MET allows mesenchymal-like cancer cells to regain the epithelial phenotype needed to form cell-cell junctions for the colonization of the secondary site. Moreover, this transition supports tumor cell survival and escape from cytotoxic agents.<sup>21</sup>

### - Intra and extravasation

From the primary site, a small proportion of cancer cells enter the bloodstream through a process called intravasation, in which cancer cells migrate through the vascular endothelium. After the transendothelial migration, they cross the endothelial basement membrane<sup>22</sup> and spread throughout the body as circulating tumor cells. Finally, they leave the circulation through extravasation, invading the potential secondary tumor sites. Extravasation involves interaction of cancer cells with vascular endothelial cells via cell adhesion and chemokine-related processes.<sup>23</sup>

### - Colonization and new tumor formation

In the metastatic site, tumor cells find a “fertile soil” which favors their growth, influenced by resident cells and by the microenvironment.

Furthermore, they acquire genetic instability, stem-like properties and the ability of clonal expansion, required to generate the metastasis.

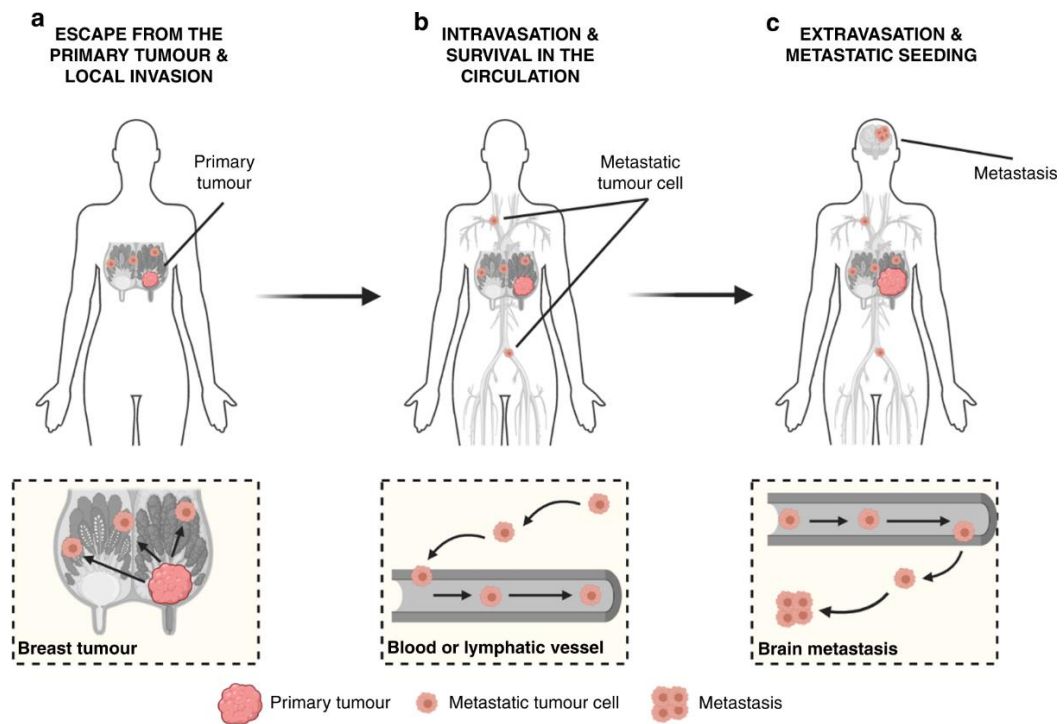


**Figure 5. Schematic representation of the metastatic process.** (a) From the primary tumor, cancer cells start the local invasion, (b) moving in the blood or lymphatic circulation and (c) reaching distant organs where they can generate new tumors. Adapted from “The lingering mysteries of metastatic recurrence in breast cancer”.<sup>19</sup>

Some changes occur also in the host tissues, creating an immunosuppressive microenvironment, which favors the tumor colonization and evolves in a pre-metastatic niche.<sup>24</sup> Other changes of the pre-metastatic niche include inflammation, increased vascular permeability and angiogenesis.

### 1.3 *Mimicry*

Cancer cell metastasis have different organotropism. Preferred metastatic site for BrCa are bones, lungs and liver.<sup>25</sup> (Figure 6).

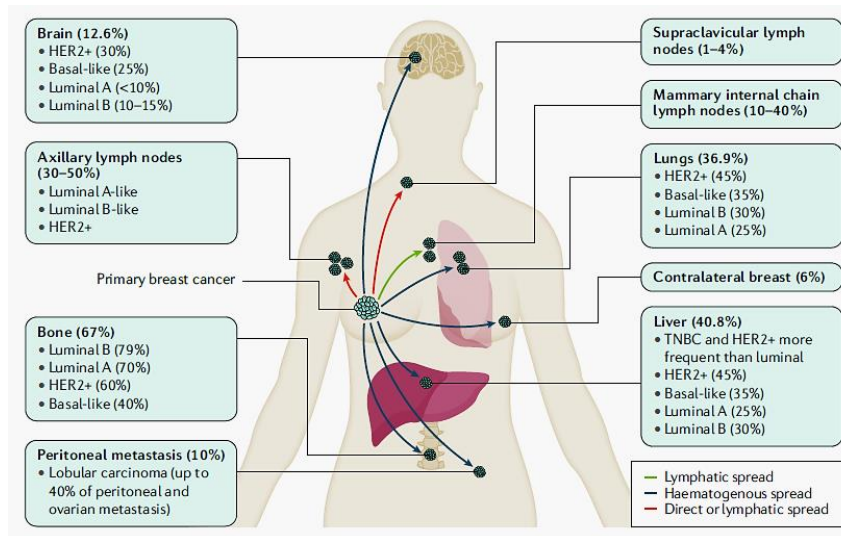


**Figure 6. Most common metastatic sites in BrCa.** The bone is most affected by BrCa distant metastasis (67%), followed by liver (40.8%) and lungs (36.9%). Adapted from “New insights into the metastatic behavior after breast cancer surgery, according to well-established clinicopathological variables and molecular subtypes”.<sup>26</sup>

To survive in the host environment, tumor cells express a genetic profile similar to that of resident cells and “behave” like them. This feature is called mimicry, with vasculogenic, immunological and osteo-mimicry prominent in BrCa.

### 1.3.2 *Vasculogenic mimicry*

The vasculogenic mimicry is the ability of cancer cells to form vascular channels, in the absence of endothelial cells. These cancer cells are periodic acid-Schiff staining positive, and negative for the expression of the endothelial marker, CD31 (Figure 7).

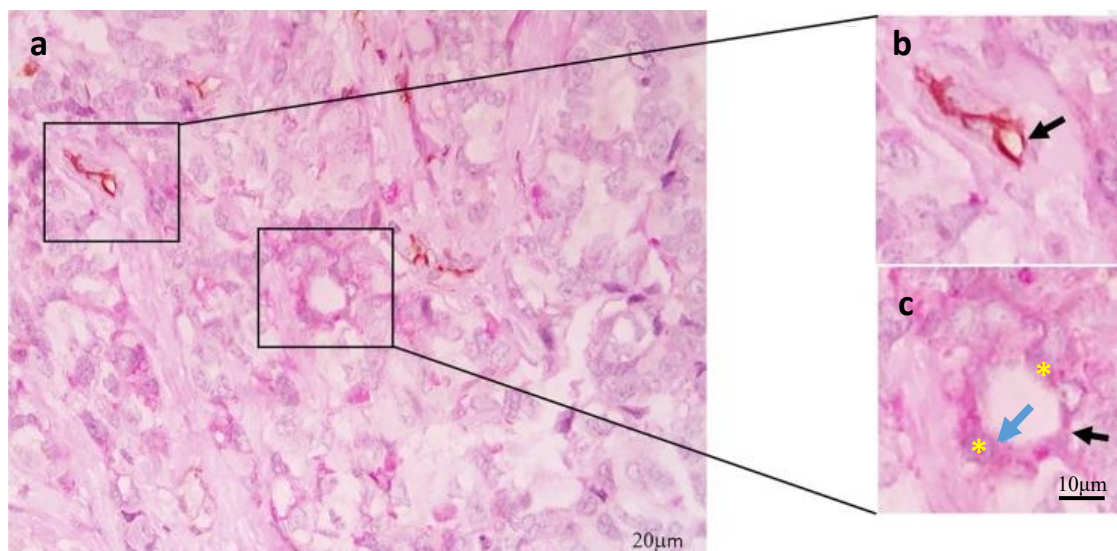




**Figure 7. Vasculogenic mimicry in Triple Negative BrCa.** (a) Low magnification of CD31-PAS Double-staining. (b) High magnification of CD31 positive blood vessel (black arrow), and (c) tubular-type vasculogenic mimicry channel (black arrow), with PAS-positive cuboidal tumor cells (yellow asterisks) and PAS reaction in the luminal surface (blue arrow). From “An Overview of Vasculogenic Mimicry in Breast Cancer”.<sup>12</sup>

These vessel-like structures are functional, as demonstrated by the presence of erythrocytes and their perfusion capacity. In BrCa, the presence of these structures is associated with a poor prognosis and, in line with this observation, there is a higher proportion of triple-negative tumors with vasculogenic mimicry compared to tumors positive for ER, PR, and/or HER2.<sup>12</sup>

### 1.3.3 *Immunological mimicry*

It is still little known about this type of mimicry. It is increasingly confirmed that cells of the immune system can positively or negatively regulate the behavior of cancer cells in a context-dependent manner. Rui Gao et al. (2021) demonstrated that BrCa expresses a high level of immune genes compared to the normal breast epithelium. Using single-cell gene set enrichment analysis (ssGSEA) it was established that the enrichment scores of B cell, T cell and myeloid cell signatures were higher in BrCa compared to normal epithelial cells. In this study, they showed an “immune mimicry program” in cancer cells suggesting that “tumor-infiltrating cells” could be the cancer cells themselves, expressing immune-related genes.

### 1.3.4 *Osteomimicry*

BrCa cells preferentially metastasize in the bone before spreading to visceral organs such as liver, lungs and brain.<sup>28</sup> They exhibit osteomimicry, expressing bone-related genes and upregulating factors that normally regulate bone mineralization and remodeling.<sup>28,29</sup> Bellahcène and colleagues demonstrated that BrCa cells located into the bone are characterized by a significant overexpression of osteoblast related genes<sup>30</sup>, including Runt-related transcription factor 2 (Runx2), bone sialoprotein (BSP) and osteopontin (OPN). BrCa cells also produce the bone pro-osteoclastogenic cytokine Receptor Activator of Nuclear Factor  $\kappa$  B ligand (RANKL), and its decoy molecule, osteoprotegerin (OPG). RANKL stimulates osteoclast bone resorption, increasing the space for BrCa cell growth and establishing a vicious cycle with the resident cells, giving tumor cells more chances to survive and proliferate into the bone microenvironment.

#### 1.4 *BrCa bone metastasis*

The bone marrow is a complex microenvironment, which includes ECM, osteoclasts, osteoblasts, adipocytes, vascular cells, nerve cells as well as mesenchymal and hematopoietic stem cells. The bone is the ideal environment for tumor engraftment and survival. In fact, it is a dynamic tissue continuously undergoing remodeling that causes the release of important factors including Transforming growth factor beta 1 (TGF- $\beta$ ), Fibroblast Growth Factor (FGF), interleukins (IL), Calcium (Ca<sup>+</sup>) and others.

BrCa bone metastasis leads to pathological bone loss due to increased osteoclast-induced bone resorption enhanced by the release of tumor factors, including IL-6, IL-1 $\beta$  and Tumor Necrosis Factor alfa (TNF $\alpha$ ).<sup>31</sup> The increase of bone resorption generates more space in which tumor cells can proliferate. Furthermore, the bone matrix degradation process leads to the release of products, including Bone Morphogenetic Proteins (BMPs), TGF- $\beta$ , FGF, and Platelet-Derived Growth Factor (PDGF). In this pathological condition, these factors contribute to BrCa growth and survival. BrCa cells also induce the expression of RANKL by osteoblasts, through the release of the Parathyroid Hormone-related Protein (PTHrP), further stimulating osteoclast differentiation. This series of reciprocal overstimulation of resident and cancer cells is called vicious cycle (Figure 8).

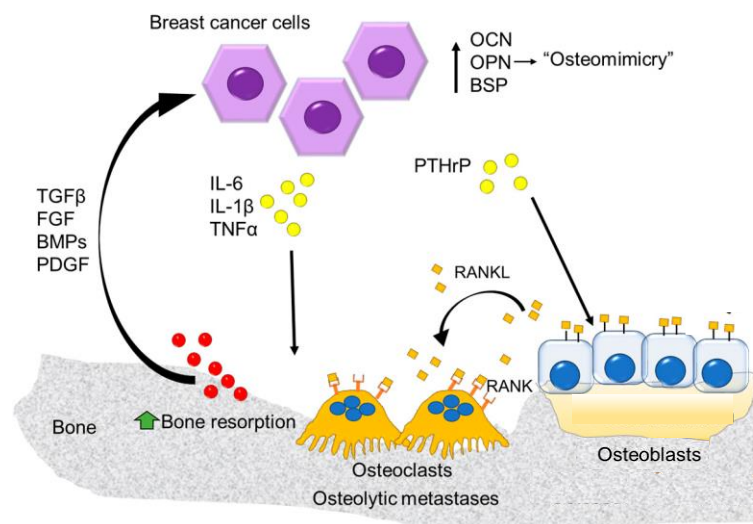


**Figure 8. The BrCa bone metastasis vicious cycle.** BrCa cells can release factors that enhance osteoclast differentiation and bone resorption (osteolytic lesions). Osteoclast activity leads to the release of products from the bone matrix that contributes to the BrCa growth and survival. Adapted from “The Osteoclast in Bone Metastasis: Player and Target”.<sup>31</sup>

### 1.5 *BrCa dormancy*

A small population of BrCa cells that reach the bone microenvironment becomes quiescent for years, escaping the immune system and the conventional therapies. Even after decades, this small population can be reactivated and relapse into a new tumor in bone which then spreads in other organs. This process, called tumor dormancy, is still poorly understood.<sup>32</sup> It represents a state of cell cycle arrest, characterized by the reversible entry into the G<sub>0</sub> phase and the acquisition of latent pluripotency. Cell quiescence is observed physiologically in the stem cell compartment, which includes the HSCs, ensuring a reserve of cells indispensable for the generation of blood cells (Figure 9).

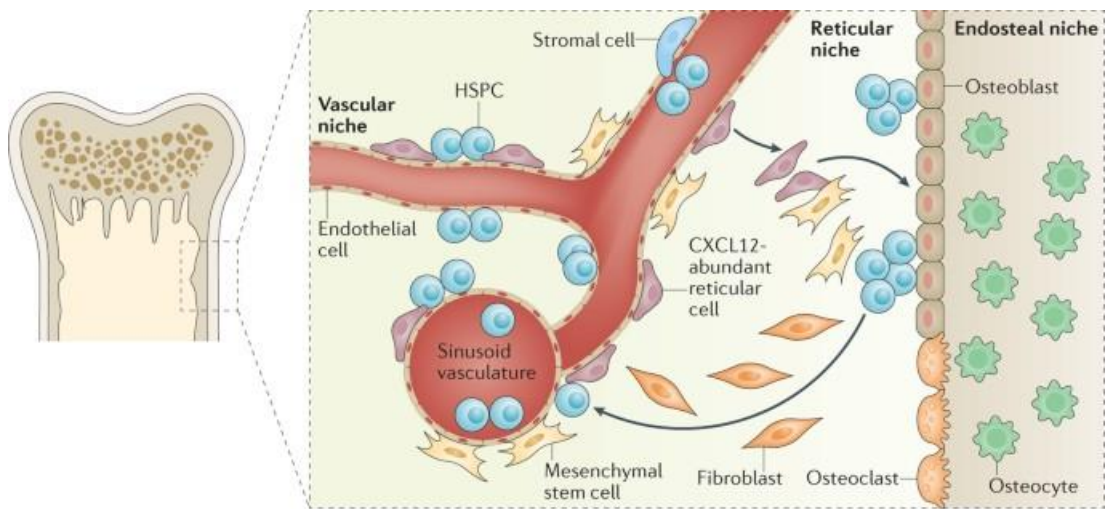


**Figure 9. The bone marrow niches.** The self-renewal and quiescence of HSCs is maintained by the bone-marrow microenvironment, which is composed of different niches. The vascular niche regulates HSC self-renewal and expansion, the reticular niche regulates the production of stem cell factors, and the endosteal niche regulates the HSC reservoir promoting their quiescence and long-term storage. Adapted from “The bone-marrow niche in MDS and MGUS: implications for AML and MM”.<sup>33</sup>

HSCs are multipotent precursors that have self-renewal capacity and ability to generate the Hematopoietic cell lines. Schofield was the first to propose the concept of niche as the HSC localization site, needed for them to exist and fulfill their functions. He also hypothesized that the niche influences the self-renewal of HSCs, considering, that leaving the niche, embark HSCs in their differentiation.<sup>34</sup>

To date, two main niches are described in the bone microenvironment: the vascular niche and the endosteal niche.

The vascular niche is located in the bone marrow, in a region rich in venous sinuses surrounded by reticular cells and endothelial cells, allowing exchanges with the venous

circulation. The vascular niche has been shown to promote HSC mobilization, proliferation and differentiation.<sup>35</sup>

The endosteal niche is located in the interface between the bone marrow and the endosteal surface. It includes a particular type of osteoblasts expressing high levels of Neural(N)-Cadherin, called Spindle Shape N-Cadherin High CD45- osteoblasts (SNOs). In 2003, Zhang and colleagues demonstrated that the SNO cells maintain the Long Term-HSCs (LT-HSCs)<sup>36</sup>. They showed that LT-HSCs are in direct contact with SNOs through anchoring junctions involving N-cadherin homophilic interaction. In addition, SNO-HSC interaction is mediated by Notch, expressed by HSCs, and its ligand Jagged expressed by SNOs. The endosteal niche promotes the quiescent status of the HSCs, maintaining the HSC reservoir. Although they are independent microenvironments, the interaction between endosteal and vascular niches is crucial for many physiological processes, such as maintenance of the HSC pool, maturation and differentiation of their cell progeny, angiogenesis and osteogenesis. Interestingly, in our laboratory, it has been previously demonstrated that BrCa cells that reach the endosteal surface enriched in SNOs, show low proliferation ability similar to LT-HSCs.<sup>37</sup> The above-mentioned study also demonstrated that BrCa cells compete with HSCs for the engraftment of the bone marrow.<sup>37</sup>

Generally speaking, the dormancy process consists of four main stages. In the first three phases tumor cells enter in the dormant status and adapt themselves to the niche through (1) the homing of the cells into the niche, (2) the engraftment to the niche and (3) the cell reprogramming and the long-term dormancy. In the last phase, (4) called reactivation, the tumor cells activity and proliferation can be stimulated by specific mechanisms, not yet fully defined, allowing them to generate a new tumor (Figure 10).

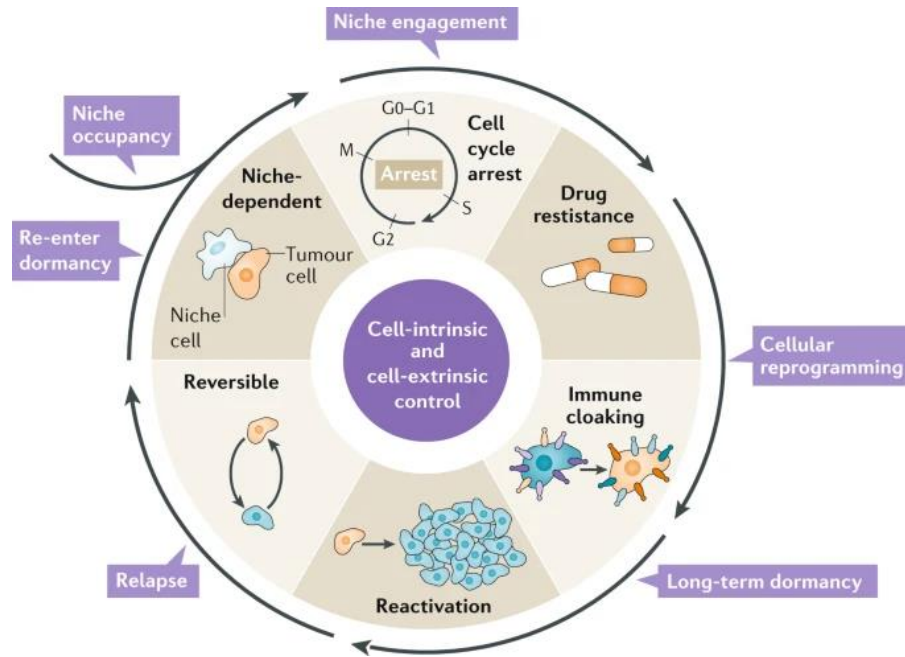


**Figure 10. The dormant cancer cell life cycle.** Tumor cells reach the niche. After the engraftment to the niche, they undergo  $G_0$ – $G_1$  cell cycle arrest and cellular reprogramming to adapt themselves to the microenvironment and survive. To this scope, dormant tumor cells activate immune evasion mechanisms to escape from the immune system and to enable long-term dormancy. Subsequently, after niche modifications, they are reactivated, producing new metastasis in bone and in other organs. Adapted from “The dormant cancer cell life cycle”.<sup>38</sup>

- Niche homing

In the first phase the C-X-C motif chemokine ligand 12 (CXCL12)/C-X-C motif chemokine receptor 4 (CXCR4) signaling axis is known to guide the BrCa cells to the bone marrow microenvironment. Bone cells release CXCL12 and attract CXCR4 overexpressing BrCa cells, promoting their migration and bone colonization.<sup>39</sup> In addition,  $\alpha\beta 3$  integrin expression allows BrCa cells to adhere to the bone matrix proteins containing the Arg-Gly-Asp motif (RGD), including fibronectin and osteopontin.<sup>40</sup>

- Niche engraftment

In the second phase, BrCa cells interact with the niche microenvironment and the resident cells. One of the most important factors that induce the dormant status is oxygen deficiency. Hypoxia arrests tumor cell cycle in the  $G_0$ – $G_1$  phase.<sup>41</sup> Moreover, in the endosteal niche BrCa cells contact the niche resident SNOs through cadherins, favoring the dormant phenotype.<sup>42</sup>

- Cell reprogramming and long-term dormancy

After the niche homing and engraftment, BrCa cells activate different mechanisms to survive in this microenvironment. The most widely accepted one is regulated by the mitogen-activated protein kinase/extracellular signal-regulated kinases, p38/ERK activity. During ERK-induced proliferation, the high level of p38 functions as an inhibitory regulator of ERK and prevents cell proliferation by inducing G<sub>0</sub>-G<sub>1</sub> arrest or triggering senescence and apoptosis.<sup>43</sup> This stop of proliferation is due to the regulation of a variety of transcription factors, such as nuclear receptor subfamily 2 group F member 1 (NR2F1) or the cyclin-dependent kinase inhibitors, p27 and p21. Additionally, p38<sup>high</sup>/ERK<sup>low</sup> downregulates G<sub>1</sub> exit-promoting transcriptional factors, such as FOXM1 and c-Jun.<sup>44</sup> Furthermore, important processes enacted by dormant cancer cells to survive in the niche are the chemotherapy resistance and the immune system escape. All these mechanisms allow dormant BrCa cells to survive for years, generating the so-called long-term relapse, only when changes reactivate their ability to proliferate and initiate a new tumor.

- Reactivation

The reactivation mechanism is still largely unknown but there are some hypotheses. After a period of starvation, due to a nutrient-poor environment, dormant cells accumulate enough nutrients to escape from dormancy and proliferate. Additionally, in the bone the osteoclast-mediated bone resorption may release factors that disrupt the dormant BrCa cellular interactions with the microenvironment that hold the tumor cells quiescent. Furthermore, the immunosuppressive environment facilitated by the loss of immune cells due to therapies could contribute to dormant cell reactivation.<sup>45</sup>

1.5.2 Role of the endosteal niche in BrCa dormancy

Studies by Kolb and colleagues demonstrated that osteoblasts are altered by BrCa and diverted from depositing new matrix to producing cytokines implicated in cancer cell maintenance, including IL6, IL8 and vascular endothelial growth factor (VEGF). They also defined a subpopulation of osteoblast called “Educated Osteoblasts” that have a functional role in suppressing BrCa growth.<sup>46</sup>

Moreover, in our laboratory it has been demonstrated that Notch2 plays a central role in the inhibition of BrCa cells in direct contact with SNOs, which express high levels of the Notch2 ligand Jagged1.<sup>37</sup> They demonstrated that dormant BrCa cells compete with

HSCs for the engraftment of the bone marrow (figure 11a). Furthermore, single non proliferating BrCa cells were found to lodge the endosteal sites (figure 11b) enriched in SNOs (figure 11c).

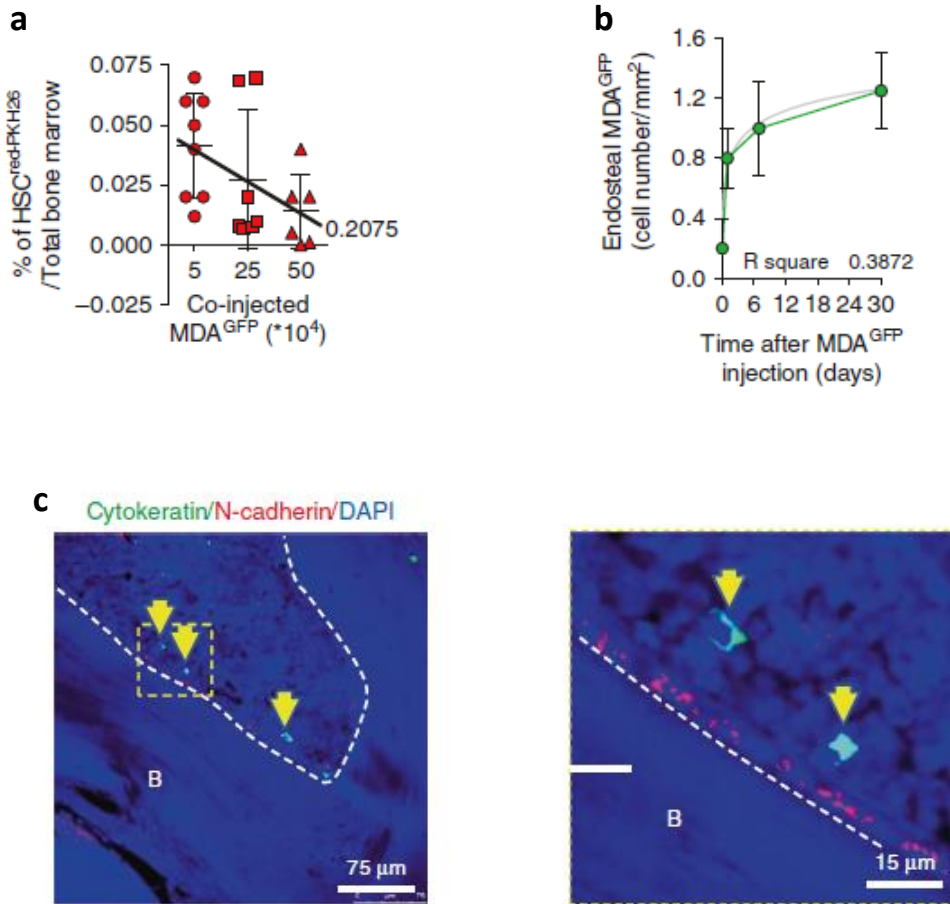


**Figure 11. In vivo engraftment of MDA cells in the endosteal niche.** (a) Sub-lethally myeloablated CD1 nu/nu mice received an intratibial co-injection of HSCs<sup>redPKH26</sup> cells and increasing numbers of MDA<sup>GFP</sup> cells. Marrow cells were then flushed out from the bone and subjected to flow cytometric analysis to retrieve and count engrafted HSC<sup>redPKH26</sup> cells. (b) CD1 nu/nu mice received an intratibial injection of MDA-turboGFP (MDA<sup>GFP</sup>) cells, and the number of endosteal BrCa cells/tissue surface were quantified. B: bone. (c) Imaging by confocal laser scanning microscopy (left panel) and inset (right panel) showing high magnification of the left panel yellow square of MDA<sup>GFP</sup> cells localized closed to the SNO cells (red). Yellow arrowheads: single cancer cells; B: bone.

In line with these observations, when BrCa cells were co-cultured with SNO monolayers a lower proliferation was observed compared to the same cells plated on NON SNOs (Figure 12).

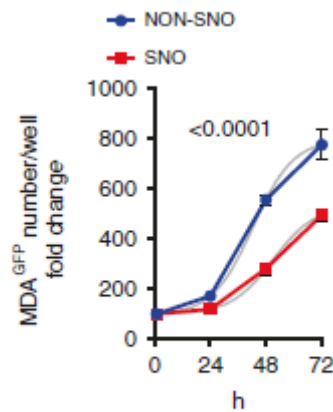


**Figure 12. SNOs inhibit BrCa cell proliferation in vitro.** MDA<sup>GFP</sup> cells were seeded onto MACS sorted SNOs and NON-SNOs and allowed to attach for 1 h at 37 °C, followed by extensive washing and culture for further 72h. Number of MDA<sup>GFP</sup> cells attached on SNOs or NON SNOs at time = 0 (after 1 h of adhesion) and at the indicated times of co-culture.

They also demonstrated that this process is driven by Notch2. In fact, treatment of the co-cultures with a  $\gamma$ -secretase inhibitor that blocks the Notch activity (dibenzazepine – DBZ) restored the BrCa cell ability to proliferate on SNOs (Figure 13a). Furthermore, selective downregulation of Notch1-4 mRNAs, by specific siRNAs, showed that only inhibition of Notch1 and Notch2 expression increased the ability of BrCa cells to proliferate when they were plated on SNOs compared to cells treated with control scramble siRNA, with Notch2 siRNA more potent than Notch1 siRNA (Figure 13b).

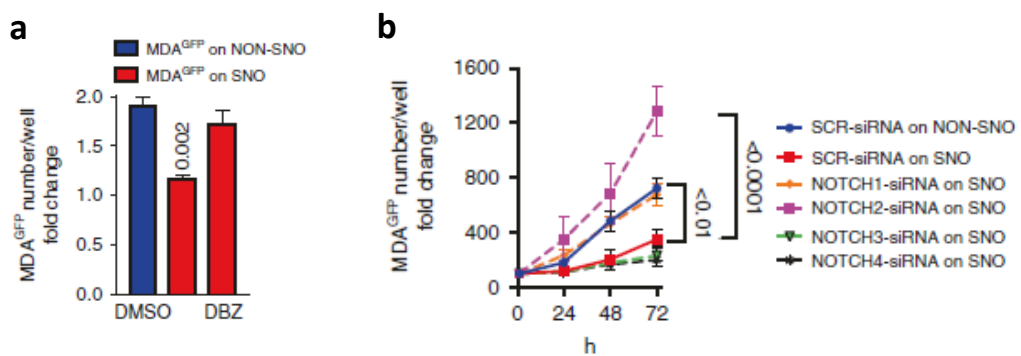


**Figure 13. BrCa inhibition of SNO-dependent proliferation is mediated by Notch2.** (a) MDA<sup>GFP</sup> cells were treated with the  $\gamma$ -secretase inhibitor dibenzazepine (DBZ) and seeded onto SNOs and NON SNOs. Cell number was evaluated after 1 h (time 0) and 24 h. The graph expresses the fold change vs time 0 and results are compared vs cells treated with vehicle (dimethyl sulfoxide - DMSO). (b) Number of MDA<sup>GFP</sup> cells treated with Notch-1–4-specific siRNAs, seeded onto SNOs and NON SNOs and evaluated at time 0 (1 h of adhesion) and after 24–72 h, compared with control-siRNA-treated MDA<sup>GFP</sup> cells.



In addition, we used an *in vivo* model of dormancy in which female immunocompromised CD1 nu/nu mice were intratibially injected with MDA cells. Mice were monitored for the development of osteolytic lesions and those that did not show overt signs of disease after 30 days were assumed to be positive for dormancy. These mice were treated with DBZ and showed a greater distance of single tumor cells from the endosteum compared to the control group. (Figure 14a, b).

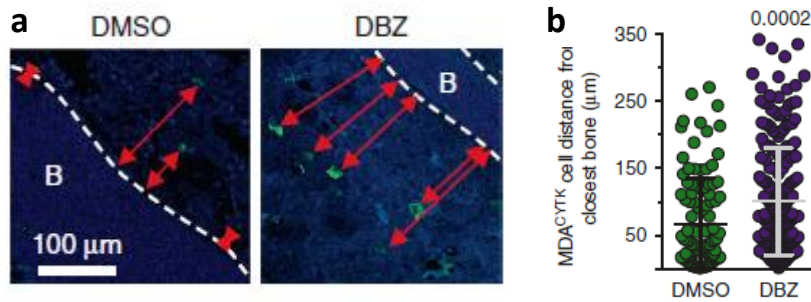


**Figure 14.** MDA intratibially injected mice positive for dormancy were treated with a single injection of vehicle (dimethyl sulfoxide - DMSO) or of 4.28 mg/kg of the  $\gamma$ -secretase inhibitor dibenzazepine (DBZ) and sacrificed 8 weeks later. (a) Immunofluorescence staining for human cytokeratin (green) of tibias allow the (b) quantification of the distance of cytokeratin positive MDA cells from the endosteal surface.

An important characteristic of MDA cells expressing high level of Notch2 (Notch2<sup>High</sup> MDA) is their HSC-like phenotype and stem feature demonstrated by the high expression of the canonical HSC genes, *CD34*, *CXCR4* and *TIE2* (Figure 15a) along with the increased formation of larger mammospheres (Figure 15b) compared to the Notch2<sup>Low</sup> MDA cells.

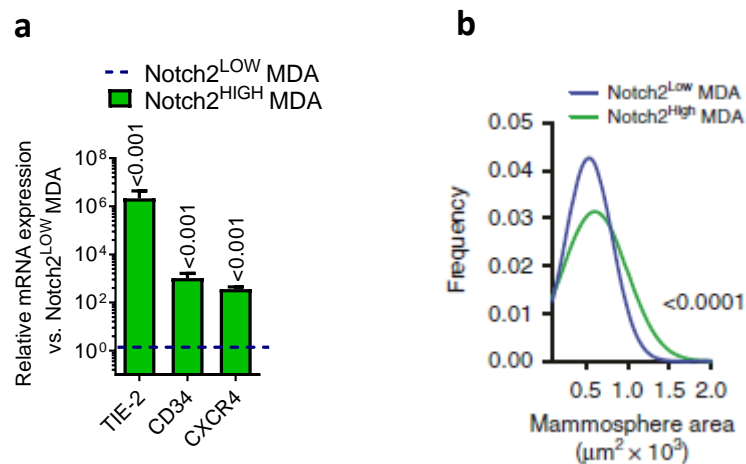


**Figure 15.** HSC-like stem phenotype of Notch2<sup>High</sup> BrCa cells. MDA cells were sorted in Notch2<sup>Low</sup> and Notch2<sup>High</sup> by MACS. (a) Real-time RT-PCR for the transcriptional expression of the indicated HSCs markers. (b) Area of the MACS-sorted Notch2<sup>Low</sup> and Notch2<sup>High</sup> MDA mammospheres correlated with their frequency.

From this previous work they concluded that Notch2 represents an important factor involved in BrCa dormancy in the bone microenvironment and in the acquisition of HSC-like phenotype.

## 2 AIM OF THE STUDY

On the basis of the background information previously obtained in my laboratory, the aims of this project are:

- To understand the role of N-Cadherin in BrCa dormancy.
- To dissect new molecular pathways mediating the interaction between dormant BrCa cells and the endosteal niche.

## 3 REFERENCES

1. Institute, National Cancer for surveillance, epidemiology and E. result program. Female Breast Cancer - Cancer Stat Facts. <https://seer.cancer.gov/statfacts/html/breast.html> (2018).
2. Pan, H. *et al.* 20-Year Risks of Breast-Cancer Recurrence after Stopping Endocrine Therapy at 5 Years. *New England Journal of Medicine* **377**, 1836–1846 (2017).
3. Sims, A. H., Howell, A., Howell, S. J. & Clarke, R. B. Origins of breast cancer subtypes and therapeutic implications. *Nat Clin Pract Oncol* **4**, 516–525 (2007).
4. Zubair, M., Wang, S. & Ali, N. Advanced Approaches to Breast Cancer Classification and Diagnosis. *Front Pharmacol* **11**, 2487 (2021).
5. Sinn, H.-P. & Kreipe, H. Breast Care A Brief Overview of the WHO Classification of Breast Tumors, 4th Edition, Focusing on Issues and Updates from the 3rd Edition. (2013) doi:10.1159/000350774.
6. ELSTON, C. W. & ELLIS, I. O. pathological prognostic factors in breast cancer. I. The value of histological grade in breast cancer: experience from a large study with long-term follow-up. *Histopathology* **19**, 403–410 (1991).
7. Staging & Grade - Breast Pathology | Johns Hopkins Pathology. <https://pathology.jhu.edu/breast/staging-grade>.
8. Nelson, H. D. *et al.* Effectiveness of Breast Cancer Screening: Systematic Review and Meta-analysis to Update the 2009 U.S. Preventive Services Task Force Recommendation. *Ann Intern Med* **164**, 244–255 (2016).
9. Duffy, S. W. *et al.* Mammography screening reduces rates of advanced and fatal breast cancers: Results in 549,091 women. *Cancer* **126**, 2971–2979 (2020).
10. Balkenende, L., Teuwen, J. & Mann, R. M. Application of Deep Learning in Breast Cancer Imaging. *Semin Nucl Med* **52**, 584–596 (2022).
11. James, T. A. *et al.* Troubleshooting Sentinel Lymph Node Biopsy in Breast Cancer Surgery. *Ann Surg Oncol* **23**, 3459–3466 (2016).

12. Torre, L. A., Siegel, R. L., Ward, E. M. & Jemal, A. Global cancer incidence and mortality rates and trends - An update. *Cancer Epidemiology Biomarkers and Prevention* **25**, 16–27 (2016).
13. Breast Cancer Statistics | How Common Is Breast Cancer? <https://www.cancer.org/cancer/breast-cancer/about/how-common-is-breast-cancer.html>.
14. Taylor, A. *et al.* Consensus for genes to be included on cancer panel tests offered by UK genetics services: guidelines of the UK Cancer Genetics Group. *J Med Genet* **55**, 372–377 (2018).
15. Oeffinger, K. C. *et al.* Breast Cancer Screening for Women at Average Risk: 2015 Guideline Update From the American Cancer Society. *JAMA* **314**, 1599–1614 (2015).
16. Gradishar, W. J. *et al.* NCCN Guidelines® Insights: Breast Cancer, Version 4.2021. *J Natl Compr Canc Netw* **19**, 484–494 (2021).
17. Rubio, I. T. *et al.* Sentinel lymph node biopsy for staging breast cancer. *Am J Surg* **176**, 532–537 (1998).
18. Breast Cancer Treatment | Treatment Options for Breast Cancer. <https://www.cancer.org/cancer/breast-cancer/treatment.html>.
19. Riggio, A. I., Varley, K. E. & Welm, A. L. The lingering mysteries of metastatic recurrence in breast cancer. *British Journal of Cancer* *2020 124:1* **124**, 13–26 (2020).
20. Monteran, L. *et al.* Bone metastasis is associated with acquisition of mesenchymal phenotype and immune suppression in a model of spontaneous breast cancer metastasis. *Scientific Reports* *2020 10:1* **10**, 1–14 (2020).
21. Drasin, D. J., Robin, T. P. & Ford, H. L. Breast cancer epithelial-to-mesenchymal transition: Examining the functional consequences of plasticity. *Breast Cancer Research* **13**, 1–13 (2011).
22. Salminen, A. T. *et al.* In vitro Studies of Transendothelial Migration for Biological and Drug Discovery. *Front Med Technol* **2**, 600616 (2020).
23. Reymond, N., D'Água, B. B. & Ridley, A. J. Crossing the endothelial barrier during metastasis. *Nature Reviews Cancer* *2013 13:12* **13**, 858–870 (2013).
24. Akhtar, M., Haider, A., Rashid, S. & Al-Nabet, A. D. M. H. Paget's 'Seed and Soil' Theory of Cancer Metastasis: An Idea Whose Time has Come. *Adv Anat Pathol* **26**, 69–74 (2019).
25. Smid, M. *et al.* Subtypes of breast cancer show preferential site of relapse. *Cancer Res* **68**, 3108–3114 (2008).
26. Buonomo, O. C. *et al.* New insights into the metastatic behavior after breast cancer surgery, according to well-established clinicopathological variables and molecular subtypes. *PLoS One* **12**, (2017).
27. Rucci, N. & Teti, A. Osteomimicry: How the seed grows in the soil. *Calcif. Tissue Int.* **102**, 131–140 (2018).

28. Awolaran, O., Brooks, S. A. & Lavender, V. Breast cancer osteomimicry and its role in bone specific metastasis. *Breast* **30**, 156–171 (2016).
29. Bellahcène, A. *et al.* Transcriptome analysis reveals an osteoblast-like phenotype for human osteotropic breast cancer cells. *Breast Cancer Res Treat* **101**, 135–148 (2007).
30. Maurizi, A. & Rucci, N. The osteoclast in bone metastasis: Player and target. *Cancers (Basel)* **10**, (2018).
31. Holmgren, L., O'reilly, M. S. & Folkman, J. Dormancy of micrometastases: balanced proliferation and apoptosis in the presence of angiogenesis suppression. *Nat Med* **1**, 149–153 (1995).
32. Ghobrial, I. M., Detappe, A., Anderson, K. C. & Steensma, D. P. The bone-marrow niche in MDS and MGUS: implications for AML and MM. *Nature Reviews Clinical Oncology* 2018 15:4 **15**, 219–233 (2018).
33. Schofield, R. The relationship between the spleen colony-forming cell and the haemopoietic stem cell. *Blood Cells* **4**, 1–2 (1978).
34. Doan, P. L. & Chute, J. P. The vascular niche: home for normal and malignant hematopoietic stem cells. *Leukemia* 2012 26:1 **26**, 54–62 (2011).
35. Zhang, J. *et al.* Identification of the haematopoietic stem cell niche and control of the niche size. *Nature* **425**, 836–841 (2003).
36. Capulli, M. *et al.* Notch2 pathway mediates breast cancer cellular dormancy and mobilisation in bone and contributes to haematopoietic stem cell mimicry. *Br J Cancer* **121**, 157–171 (2019).
37. Phan, T. G. & Croucher, P. I. The dormant cancer cell life cycle. *Nature Reviews Cancer* vol. 20 398–411 Preprint at <https://doi.org/10.1038/s41568-020-0263-0> (2020).
38. Price, T. T. *et al.* Dormant breast cancer micrometastases reside in specific bone marrow niches that regulate their transit to and from bone. *Sci Transl Med* **8**, (2016).
39. NP McCabe, S. D. A. V. J. B. T. B. Prostate cancer specific integrin  $\alpha\beta 3$  modulates bone metastatic growth and tissue remodeling. *Oncogene* **26**, 6238–6243 (2007).
40. Butturini, E., de Prati, A. C., Boriero, D. & Mariotto, S. Tumor Dormancy and Interplay with Hypoxic Tumor Microenvironment. *Int J Mol Sci* **20**, (2019).
41. Capulli, M. *et al.* Notch2 pathway mediates breast cancer cellular dormancy and mobilisation in bone and contributes to haematopoietic stem cell mimicry. *Br J Cancer* **121**, 157–171 (2019).
42. Aguirre-Ghiso, J. A., Liu, D., Mignatti, A., Kovalski, K. & Ossowski, L. Urokinase receptor and fibronectin regulate the ERK(MAPK) to p38(MAPK) activity ratios that determine carcinoma cell proliferation or dormancy in vivo. *Mol Biol Cell* **12**, 863–879 (2001).
43. Adam, A. P. *et al.* Computational identification of a p38SAPK-regulated transcription factor network required for tumor cell quiescence. *Cancer Res* **69**, 5664–5672 (2009).

44. Park, S. Y. & Nam, J. S. The force awakens: metastatic dormant cancer cells. *Experimental & Molecular Medicine* 2020 52:4 **52**, 569–581 (2020).
45. Kolb, A. D., Shupp, A. B., Mukhopadhyay, D., Marini, F. C. & Bussard, K. M. Osteoblasts are ‘educated’ by crosstalk with metastatic breast cancer cells in the bone tumor microenvironment. *Breast Cancer Research* **21**, 1–30 (2019).

# Chapter 2

## **Role of Neural (N)-Cadherin in BrCa cell stemness and dormancy in the bone microenvironment**

Adapted from <https://doi.org/10.3390/cancers14051317>

Antonio Maurizi, Michela Ciocca, Cristiano Giuliani, Ilaria Di Carlo and Anna Teti

### **1. ABSTRACT**

BrCa cells that interact with spindle-shaped N-Cadherin<sup>+</sup> Osteoblasts (SNOs) are recognized to become dormant through a Notch2-dependent mechanism. We found that Notch2<sup>High</sup> human BrCa MDA cells also expressed high levels of N-Cadherin. This prompted us to hypothesize that N-Cadherin might have a role in MDA-SNO interaction. We observed that the expression of N-Cadherin in MDA cells reduced tumor incidence and bone osteolysis in mouse model of BrCa bone metastasis. Similar to Notch2<sup>High</sup> MDA cells, the N-Cadherin<sup>High</sup> MDA cells revealed a high expression of canonical HSC markers, suggesting an HSC mimicry and stem-like phenotype associated with a higher ability to form mammospheres. Interestingly, N-Cadherin<sup>High</sup> MDA cells showed greater capacity to adhere to SNOs, while the inhibition of SNO-mediated MDA cell proliferation was independent of the N-Cadherin expression. In conclusion, we demonstrated that:

- N-Cadherin<sup>High</sup> and Notch2<sup>High</sup> MDA cells show similar HSC mimicry and dormancy features.
- N-Cadherin contributes to mediate MDA-SNO adhesion.
- N-Cadherin plays a role in MDA cell adhesion especially onto SNOs, while Notch2 is pivotal in SNO-induced dormancy.

## 2. INTRODUCTION

BrCa represents the second most common malignancy in women, with thousands of new cases diagnosed every year<sup>1</sup> and a five-year survival rate around 90%. It is also estimated that 20–45% of “disease-free” patients experience tumor recurrence 7–25 years after mastectomy.<sup>1,2</sup> This has been correlated with the ability of a subpopulation of BrCa cells to survive in the host environment in a dormant status.<sup>3</sup> Dormant cells are resistant to conventional therapies and are difficult to detect, therefore making their eradication a real challenge in clinical practice.<sup>4,5</sup> The dormancy of BrCa cells is an unharmed event until these cells reactivate and initiate secondary tumors. This shows that dormancy and tumor initiation ability must coexist within the same cancer cell. Indeed, recent studies have demonstrated that dormant BrCa cells have the additional ability to initiate new tumors, displaying cellular and molecular features typical of stem cells.<sup>6,7</sup> The bone marrow microenvironment has been identified as the main site in which BrCa dormant cells are lodged and kept in a quiescence status via specific signals and cell-cell interactions.<sup>8</sup> Bone marrow is known to contribute to the maintenance of long-term (LT)-HSC stemness and quiescence through specific niches. One of these niches is represented by SNOs, a specialized subtype of osteoblasts lining the endosteal surface.<sup>9,10</sup> Recent work has established that the endosteal niche is also implicated in BrCa cell dormancy<sup>11</sup>, and our team has demonstrated that dormant BrCa cells expressing high level of N-Cadherin and Notch2, colonize areas near the endosteal niche enriched in SNOs.<sup>12</sup> This work suggested that SNOs keep the tumor cells dormant by a mechanism similar to LT-HSC quiescence.<sup>12</sup> Moreover, this BrCa subpopulation shows a stem signature comparable to LT-HSCs<sup>12</sup>, thus suggesting an HSC mimicry.

The protein N-Cadherin is a member of the cadherin family, mediating homophilic cell-cell adhesion and migration, encoded by the *Cdh2* gene.<sup>13,14</sup> High N-cadherin expression is often associated with a reduction in cell proliferation,<sup>15,16</sup> which, in osteoblasts, is mediated by the activation of the Wnt3a signaling, resulting in the inhibition of the cyclin D1 expression.<sup>17,18</sup> Moreover, Zhao et al. demonstrated that N-Cadherin<sup>High</sup> bone and marrow stromal progenitors are involved in the maintenance of the reserve HSCs.<sup>19</sup> In cancer, N-Cadherin has a different function according to the cellular context.<sup>16,20,21</sup> For example, in osteosarcoma, N-Cadherin works as a tumor suppressor<sup>22</sup>, while in other cancers it promotes invasion<sup>21</sup>. In normal breast epithelial cells, N-Cadherin interacts with the fibroblast growth factor receptor (FGFR) and the Rho GTPase, activating the ERK signaling pathways and the expression of MMP9, eventually promoting cell motility.<sup>23</sup>

In BrCa cells, N-Cadherin is mis-regulated and increases the Rho GTPase-induced cell motility. In addition, N-Cadherin provides BrCa cells with the capability to interact with the stroma and the endothelial cells, allowing them to migrate and become metastatic.<sup>24,25</sup> Furthermore, a recent work demonstrated that N-Cadherin is expressed by BrCa stem cells in association with connexin 43, mediating the communication between these latter and bone marrow cells.<sup>26</sup>

Finally, although the data about the role of N-Cadherin in HSCs are conflicting<sup>19,27-29</sup>, it is expressed by HSCs and promotes LT-HSC engraftment and quiescence in the bone marrow.<sup>29</sup> Nevertheless, the role of N-Cadherin in mediating SNO-induced BrCa cell dormancy and in HSCs mimicry is not understood and needs investigation.

Based on the background information so far, we hypothesized that N-Cadherin plays a role in BrCa dormancy and HSC-like stemness, cooperating with the Notch2 pathway in the process of dormancy and subsequent new tumor initiation ability. We demonstrated this hypothesis, using human BrCa cells *in vitro* and *in vivo*.

### **3. MATERIAL AND METHODS**

#### ***3.1. Materials***

Dulbecco's Modified Eagle Medium (DMEM) (cat: ECB7501L) penicillin–streptomycin (cat: ECB3001D), Dulbecco's Phosphate Buffered Saline (DPBS) (cat: ECB4004L), Hanks' Balanced Salt Solution (cat: ECB4007L) and disposable plastic were from Euroclone (Milan, Italy). Fetal bovine serum (FBS) (cat: 26140-079), Ethylene-Diamine-Tetra-acetic Acid (EDTA) (cat: 15576-028), TRIzol® (Life Technologies, Carlsbad, CA, USA, cat: 15596018), N2 and B27 supplements (cat: 17502048, 17504044) and primers synthesis were from Invitrogen (Carlsbad, CA, USA). Primers were listed in Table 3 The cDNA Synthesis Kit (cat: K1622) was from ThermoFisher, Waltham, MA, USA. OneTaq® Hot Start 2X Master Mix (cat: M0484S) and Luna® Universal qPCR Master Mix (cat: M3003) were from New England BioLabs (Ipswich, MA, USA). Osteodec (cat: 05-03005E) and all reagents for histology were from Bio-Optica (Milano, Italy). SignalStain® Boost IHC Detection Reagent (cat:8125S (anti-mouse) 8114S (antirabbit)) was from Cell Signaling (Danvers, MA, USA). All reagents for Magnetic-Activated Cell Sorting (MACS) were from Miltenyi Biotec (Bergisch Gladbach, Germany). Supplier, product code and dilution of primary and secondary antibodies used for the study are listed in Table 3. BrCa tissue array was from BioChain® (Newark, CA, USA) (cat: T8235721-5). ON- TARGET



plus Human *CDH2* siRNA (cat: FE5LHUMANXX0005) were purchased from Horizon Discovery, Waterbeach, UK. All other reagents, including Bovine Serum Albumin (BSA) (cat: A9418) and Clostridium histolyticum type IV collagenase (cat: C8051) were from Sigma Aldrich Co. (St. Louis, MO, USA)

**Table 3.** Antibodies information. IF: Immunofluorescence; IHC: Immunohistochemistry; FACS: fluorescence-activated single cell sorting

<b>Antibody</b>	<b>Dilution</b>	<b>Specie</b>	<b>Cat #</b>	<b>Company</b>
<b>N-Cadherin</b>	(IF)(IHC)1:100 (FACS) 1:20	Mouse	NBP1- 48309	Novus
<b>N-Cadherin-PE</b>	(FACS)1:50	Mouse	NBP1- 48309PE	Novus
<b>Pan-Cytokeratin (AE1/AE3)</b>	(IHC)(IF)1:100	Mouse	sc-81714	Santa Cruz Biotechnology
<b>Ki67</b>	(IF)1:500	Rabbit	MA5- 14520	ThermoFisher
<b>Notch2</b>	(FACS)1:50	Rabbit	sc5545	Santa Cruz Biotechnology
<b>AlexaFluor488 anti- Mouse</b>	(IF)1:500	Goat	A11001	Invitrogen
<b>AlexaFluor488 anti- Rabbit</b>	(FACS)(IF)1:500	Goat	A11008	Invitrogen
<b>AlexaFluor594 anti- Mouse</b>	(FACS)1:500	Goat	A11005	Invitrogen
<b>AlexaFluor594 anti- Rabbit</b>	(IF)1:500	Goat	A11037	Invitrogen

**Table 4.** Primers sequences Fw: Forward, Rv: Reverse

<b>Primer Name</b>	<b>Sequence</b>
<b>Human</b>	
<b><i>Gapdh</i></b>	Fw: CAATCTTCCAGGAGCGAGAT Rv: CAGTGATGGCATGGACTGTG
<b><i>Cdh2</i></b>	Fw: CCATTAAGCCGAGTGATGGT

	Rv: GACAATGCCCTCAAGTGTT
<b><i>Notch2</i></b>	Fw: CTGGAGTACAGGAGGCGAAG
	Rv: ATGACTGCCCTAACCACAGG
<b><i>Cxcr4</i></b>	Fw: GACGCCAACATAGACCACCT
	Rv: CTGAGAAGCATGACGGACAA
<b><i>CD34</i></b>	Fw: GCCGAGTCACAATTCGGTAT
	Rv: GCAAGCCACCAGAGCTATTC
<b><i>Tie-2</i></b>	Fw: TGTGAAGCGTCTCACAGGTC
	Rv: CCAAACGTGATTGACACTGG
<b><i>CyclinD1</i></b>	Fw: CCTTCCGGTGTGAAACATCT
	Rv: AGCGCTGTTTTTGTGTGTG
<b><i>Vimentin</i></b>	Fw: GGCTCAGATTCAGGAACAGC
	Rv: GCTTCAACGGCAAAGTTCTC
<b><i>E-Cadherin</i></b>	Fw: TGCCCAGAAAATGAAAAAGG
	Rv: GGATGACACAGCGTGAGAGA

### 3.2. BrCa cell culture

Human MDA-MB-231<sup>GFP</sup> (MDA<sup>GFP</sup>) cell line were generated transfecting MDA cells with an empty turbo-GFP plasmid using the Lipofectamin 2000, then they were stably selected using Geneticin, exploiting the Neo cassette present in the plasmid construct.

Human MDA-MB-231 parental (MDA) or transfected with turbo-GFP (MDA<sup>GFP</sup>), were used for all experiments. Cells were cultured in high glucose Dulbecco's Modified Eagle Medium (DMEM) with the addition of 1% glutamine, 1% penicillin–streptomycin and 10% FBS.

### 3.3. Mouse primary osteoblast cell isolation

Mouse primary osteoblasts were isolated from the calvariae of 8-day-old CD1 mice using three-step enzymatic digestion with a solution containing 25 mg/mL of porcine trypsin and 1 mg/mL of Clostridium histolyticum type IV collagenase in Hanks' Balanced Salt Solution. The supernatant from the first digestion, containing mainly fibroblasts, was discarded, while those from the second and the third digestions, enriched in primary murine osteoblasts, were centrifuged at 300g for 8 min and the cells were then cultured in high

glucose DMEM supplemented with 1% glutamine, 1% penicillin–streptomycin and 10% FBS. At confluence, cells were trypsinised and re-plated according to the experimental protocol.

#### 3.4. Magnetic-Activated Cell Sorting (MACS)

MDA or MDA<sup>GFP</sup>, and primary mouse osteoblasts were sorted using MACS. Cells were detached with sorting buffer containing DPBS, 5% BSA and 0.5M of EDTA. Resuspended cells were incubated for 20 min at 4°C using N-Cadherin or Notch2 biotinylated primary antibodies. Then, cells were incubated again in the same condition using streptavidin-conjugated magnetic microbeads and were eluted through the magnetic column to separate the antigen-depleted and antigen-enriched cell populations. The cells obtained from this procedure were used for RNA isolation, *in vitro* assays, and *in vivo* experiments. Supplier, product code and dilution of the primary and secondary antibodies used for the MACS are listed in Table 3.

#### 3.5. RNA extraction, RNA deep Sequencing (RNAseq) analysis and gene expression

RNA was extracted using TRIzol® according to the manufacturer's instructions. The RNA quality was assessed using electrophoresis agarose gel and was quantified by Nanodrop® using an absorbance of 260 nm wavelength. The RNA purity was assessed measuring the 260/280 nm ratio and 260/230 nm ratio for the protein and phenol presence respectively. For RNA dSeq, 3 independent RNA preparations for Notch2<sup>High</sup> and Notch2<sup>Low</sup> MDA cells were precipitated in ethanol and sent to Omega Bioservice (Norcross, GA, USA) for the RNA dSeq analysis. The RNA dSeq was performed by GATC Biotech. Briefly, RNA dSeq reads were aligned to the reference transcriptome (GRCh38.p13, Ensembl; v85 Ensembl) using Bowtie transcriptome alignments. The generated RNA dSeq dataset, containing the expression profile of 36,000 genes for each sample/condition, was interrogated to examine the expression of the *CDH2* gene.

For conventional gene expression analyses, 1 µg of RNA was retro-transcribed using Revertaid First Strand cDNA Synthesis. Semiquantitative PCR was performed using OneTaq® Hot Start 2X Master Mix, while real-time PCR was performed using Luna® Universal qPCR Master. Primer sequences used to assess gene expression are listed in Table 4.

### 3.6. Flow cytometry

Cells were detached with a sorting buffer containing DPBS, 5% BSA and 0.5 M of EDTA. Resuspended cells were incubated with primary antibodies against Notch2 and N-Cadherin for 1h at 4°C. Then, secondary incubation was performed using fluorochrome-conjugated secondary antibodies, then cells were analyzed by the FACS Melody® (BD) and FlowJO software. Unmarked cells were used to set the laser for the fluorescence threshold. Supplier, product code and dilution of the primary and secondary antibodies used for the analyses are listed in Table 3.

### 3.7. Animals

For the *in vivo* experiment, 4-week-old CD1 or Balb-C nude/nude (nu/nu) female mice were purchased from Charles River (Écully, France). Procedures involving animals and their care were conducted in conformity with national and international laws and policies (European Economic Community Council Directive 86/609, OJ L 358, 1, 12 December 1987; Italian Legislative Decree 116/92, Gazzetta Ufficiale della Repubblica Italiana no. 40, 18 February 1992; National Institutes of Health Guide for the Care and Use of Laboratory Animals, National Institutes of Health, 8th edition, 2011). The procedures were approved by the Institutional Ethical Review Board of the University of L'Aquila and by the Ministry of Health (Authorizations n 270/2018-PR and 1151/2020-PR). The study was conducted according to the Animal Research Reporting *In Vivo* Experiments (ARRIVE) requirements.

### 3.8. Intratibial injection of N-Cadherin<sup>High</sup> and N-Cadherin<sup>Low</sup> MDA cells

Human MDA BrCa cells were injected into the left tibia of 4-week-old female Balb/c nu/nu immunocompromised mice (1x10<sup>4</sup> cells/0.01 mL PBS) anesthetized with intraperitoneal injection of 80 mg/kg of ketamine and 10 mg/kg of xylazine. Animals were monitored daily for body weight, food intake, behavior, and survival. To follow the progression of osteolytic lesions, mice were subjected to weekly X-ray analysis (X-ray parameters: peak kilovoltage [kVp] = 36 kV for 10 s) using a Cabinet X-ray system (Faxitron model no. 43855A; Faxitron X-Ray Corp., Buffalo Grove, IL, USA). At the end of the experiment, mice were subjected to final X-ray analysis and then sacrificed to perform anatomical dissection for the evaluation of bone and visceral metastases

### 3.9. Limiting Dilution Assay (LDA)

Different dilutions (50,000 to 100 cells/mice) of human MDA cells MACS-sorted into N-Cadherin<sup>High</sup> and N-Cadherin<sup>Low</sup> subpopulations were subcutaneously injected in Balb/c nu/nu immunocompromised female mice anesthetized with intraperitoneal injection of 80 mg/kg of ketamine and 10 mg/kg of xylazine. Animals were monitored daily for body weight, food intake, behavior, and survival. The tumor incidence was evaluated after 4 weeks from the injection of the tumor cells. The stem cell frequency was estimated using the Extreme Limiting Dilution Assay (ELDA)<sup>30</sup> available at <https://bioinf.wehi.edu.au/software/elda/> (accessed on 25 February 2022).

### 3.10. Micro-Computed Tomography ( $\mu$ CT) analysis

Left tibias harvested from the tumor cell-injected mice were fixed in 4% formaldehyde for 48 h and then scanned by  $\mu$ CT SkyScan 1174. The scan was performed with a 9.80  $\mu$ m resolution using the X-ray voltage of 50 kV. The Skyscan NRecon software was used to reconstruct the images using a modified Feldkamp algorithm. Three-dimensional (3D) analysis was carried out employing a marching cubes-type model with a rendered surface. The cortical bone parameters were calculated on 300 consecutive slices starting from 100  $\mu$ m below the growth plate, where the osteolytic lesions were located. Pratt's algorithm was adopted to take 2D measurements. Threshold values were applied for segmenting trabecular bone. Bone cortical variables were evaluated according to Bouxsein et al.<sup>31</sup>

### 3.11. Histology

Left tibias were decalcified for 48h in Osteodec and then embedded in paraffin. Livers were fixed in 4% paraformaldehyde and embedded in paraffin. Microtome sectioning was used to obtain tissue slices of 5- $\mu$ m thickness. Liver sections were stained with hematoxylin and eosin while tibia sections were also processed for immunohistochemistry or immunofluorescence staining.

### 3.12. Immunohistochemistry and immunofluorescence

For immunohistochemistry, mouse tibia sections and human primary BrCa tissue arrays were deparaffinized and incubated with 0.07 M citrate buffer (pH 6) for 30 min at 96°C and for 10 min at room temperature. The blocking was made with 3% H<sub>2</sub>O<sub>2</sub> and 5% BSA. Then samples were incubated overnight at 4°C with primary antibodies against N-Cadherin or human pan-Cytokeratin AE1/AE3. The staining signals were revealed using the

SignalStain® Boost IHC Detection Reagent (HPR rabbit or mouse). Sections were counterstained using Gill's No.3 hematoxylin for 10 s. Positive and negative controls were performed in parallel.

For immunofluorescence, tissue sections or fixed cells (4% paraformaldehyde) were incubated with primary antibodies against human pan-Cytokeratin AE1/AE3, N-Cadherin or Ki67, either singularly or in combinations. Primary antibody incubations were carried out at room temperature for 1 h, then overnight at 4°C. Then, incubations with secondary antibodies conjugated with AlexaFluor 488 or 594 were performed for 1 h at room temperature.

Nuc-Spot® or DAPI were used to stain the nuclei. The supplier, product code and dilution of the primary and secondary antibodies used for the analyses are listed in Table 3.

### 3.13. Histomorphometry

Endosteal niche colonization analysis was performed counting the number of cytokeratin positive cells in proximity of the endosteum (4 mm<sup>2</sup> in area, 50 µm away from the growth plate and 20 µm away from the endocortical surface)<sup>12</sup>, and their distance from the endosteal surface was measured. For liver metastases, sections were evaluated for metastasis number/mm<sup>2</sup> and percentage of metastasis area over total tissue area. Primary BrCa tissue arrays were analyzed counting the number of N-Cadherin+ cells on the total surface. All histomorphometric analyses were performed using the software Fiji® by ImageJ (version 1.53).

### 3.14. Osteoblast/BrCa cells coculture assay

Mouse primary calvarial osteoblasts were MACS-sorted into SNOs or NON-SNOs using anti-N-Cadherin-biotin antibody and streptavidin-conjugated magnetic microbeads, as described above. For the knock-down experiment, MACS-sorted MDA cells were incubated with *CDH2*- or Scramble (SCR)-siRNA for 48 h before proceeding with the coculture. 7x10<sup>4</sup>–1x10<sup>5</sup> sorted cells were seeded in 96-well plates and incubated overnight in a humidified CO<sub>2</sub> incubator (5% CO<sub>2</sub>, 37°C). The day after, the MDA<sup>GFP</sup>, MACS-sorted into N-Cadherin<sup>High</sup> and N-Cadherin<sup>Low</sup> or Notch2<sup>High</sup> and Notch2<sup>Low</sup> were seeded on SNO or NON-SNO monolayers as above. After 1 h, cultures were extensively washed and the number of GFP+ cells were counted using an Olympus Fluoview IX81 confocal microscope. The counting was repeated after 24, 48, 72 h. BrCa cell density in the

cocultures were  $1 \times 10^3$ .

### 3.15. Primary and secondary mammosphere formation assay

Primary mammosphere assays were performed using a clonal dilution of  $8 \times 10^3$  suspended cells seeded in non-adhesive Petri dishes with serum-free DMEM, supplemented with 1% N2, 1% B27, 1% penicillin/streptomycin and 1% L-glutamine. They were incubated for 6 days in a humidified CO<sub>2</sub> incubator. For secondary mammospheres, the primary mammospheres were disaggregated using trypsin to obtain single-cell suspensions and cultured again under the same conditions used for the primary mammosphere assay. Imaging for the analysis was performed using the SXView Software (version 2.2.0.172). Mammosphere volume was calculated using the formula:  $V = 3/4\pi r^3$

### 3.16. Statistical analyses

Results are expressed as mean  $\pm$  Standard Deviation (SD). Sample size is indicated in the figure legends. Groups' comparisons were performed carrying out independent samples Student's t-tests and non-linear regression, fitting with F-test when dealing with continuous parameters. Data from RNA dSeq were analyzed using a false discovery rate (FDR)-adjusted p-value. To assess the distributional pattern of the BrCa cells in the bone marrow in relation to the endosteal surface we used a cumulative frequency distribution with Gaussian regression and the F-test. For the Extreme Limiting Dilution Assay, the p-value was calculated using a Student's t-tests with 95% of confidence<sup>30</sup>. The statistical methods are indicated in the figure legends and the p values are indicated in the figures.

## **4. RESULTS**

### 4.1. N-Cadherin and Notch2 are co-expressed in MDA cells

Previous data from our laboratory has indicated that the Notch2<sup>High</sup> MDA BrCa cell line, which behaved as *in vitro* and *in vivo* BrCa dormancy models, also expressed N-Cadherin.<sup>12</sup> RNAdSeq confirmed that Notch2<sup>High</sup> MDA cells were enriched in N-Cadherin mRNA (Figure 1a). Then, analysis carried out by real-time RT-PCR and immunofluorescence on independent samples of MACS-sorted Notch2<sup>High</sup> and Notch2<sup>Low</sup> MDA cells showed higher N-Cadherin expression in Notch2<sup>High</sup> compared to the Notch2<sup>Low</sup> MDA cells (Figure 1b, c). Next, FACS analysis showed the presence of an N-Cadherin<sup>High</sup> subgroup in the MDA cell population (Figure 1d). Moreover, an expanded analysis confirmed the presence of an MDA subpopulation co-expressing both Notch2 and N-Cadherin (Figure 1e). Finally,

immunofluorescence for cytokeratin, performed on tibia sections of CD1 nu/nu female mice sacrificed after 4 weeks from intratibial injection of MDA cells, revealed the presence of single N-Cadherin/cytokeratin double-positive tumor cells close to the endosteal surface (Figure 1f).

These results suggested the presence of an MDA cell subpopulation co-expressing higher levels of both Notch2 and N-Cadherin that lodged in proximity of the endosteal area, prompting us to further investigate the role of N-Cadherin in the BrCa phenotype and dormancy.

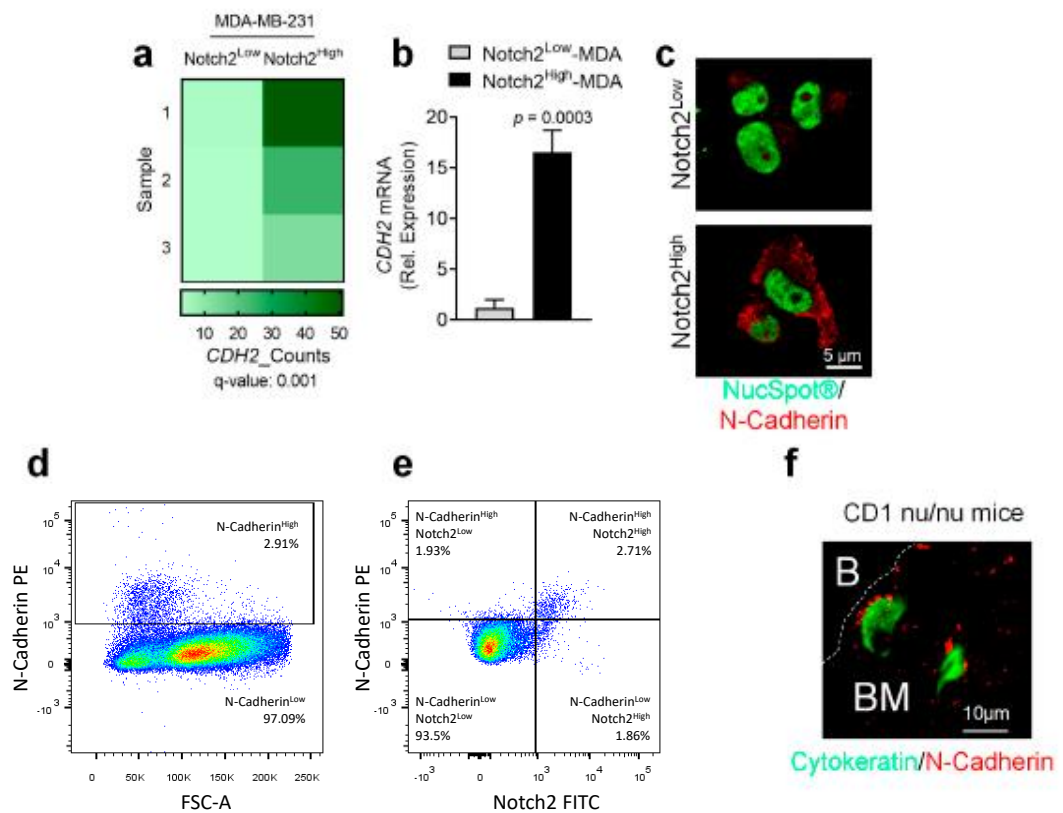


**Figure 1. Analysis of N-Cadherin expression in Notch2<sup>High</sup> MDA human BrCa cells.** Total MDA BrCa cells were MACS-sorted into Notch2<sup>High</sup> and Notch2<sup>Low</sup> subpopulations and the isolated RNA was subjected to RNA deep sequencing (RNA dSeq) analysis. (a) Heat map showing *CDH2* expression in Notch2<sup>High</sup> and Notch2<sup>Low</sup> MDA cells. (b) Real-time RT-PCR performed using a specific primer pair for human *CDH2*. Human *GAPDH* was used to normalize gene expression. (c) Immunofluorescence staining performed on MACS-sorted Notch2<sup>High</sup> and Notch2<sup>Low</sup> MDA subpopulation to evaluate the expression of the N-Cadherin protein (red). NucSpot@ reagent was used to stain the nuclei (green). (d) Flow cytometry analysis of MDA cells whole population stained with antibody for N-Cadherin only. (e) Flow cytometry analysis of MDA cells whole population double stained with N-Cadherin and Notch2 antibodies. (f) Paraffin-embedded tibia sections harvested from CD1 nu/nu female mice after 4 weeks from intratibial injection with MDA cells, double-stained



with antibodies for Cytokeratin (green) and N-Cadherin (red). B: bone; BM: bone marrow. (c, f) Scale bars are shown in the pictures. Data are the mean  $\pm$  SD and pictures are representative of (a) three independent RNA dSeq datasets, (b–d) three independent cell cultures. Statistical analysis: (a) FDR-adjusted p-value, (b) Student's t-test

#### 4.2. Role of N-Cadherin in *in vivo* tumor growth and dormancy

To address the relevance of N-Cadherin in *in vivo* tumor growth and dormancy, MACS-sorted N-Cadherin<sup>High</sup> and N-Cadherin<sup>Low</sup> MDA cells were injected into the tibial medullary cavity of female Balb-c nu/nu mice. After 4 weeks, X-rays and  $\mu$ CT analyses showed a trend of reduction of osteolytic lesion incidence (chi-square test;  $p = 0.06$ ) (Figure 2a) along with a reduced osteolytic area (Figure 2b, c) in the tibiae of N-Cadherin<sup>High</sup> compared to N-Cadherin<sup>Low</sup> cell-injected mice. Accordingly,  $\mu$ CT analysis revealed a higher cortical bone volume in N-Cadherin<sup>High</sup> cell-injected mice (Figure 2d, e). Notably, histopathological analyses revealed that the liver metastases were smaller in N-Cadherin<sup>High</sup> compared to N-Cadherin<sup>Low</sup> cell-injected mice (Figure 2f, h), with a trend of reduction in their number and incidence and a significant reduction of their percentage (Figure 2g). Lung metastases were however undetectable.

Next, the endosteal niche colonization capability of Cadherin<sup>High</sup> and N-Cadherin<sup>Low</sup> MDA cells at 3- and 7-days post-injection has been analyzed, evaluating the tumor cell distribution in relation to their vicinity to the endosteal surface. Histomorphometric analysis demonstrated that the distance of cytokeratin+ MDA cells from the endosteal surface was lower in the N-Cadherin<sup>High</sup> compared to the N-Cadherin<sup>Low</sup> cell-injected mice at all the time points analyzed (Figure 2i, j). In line with this observation, the number of MDA cells near the endosteal surface was higher in the N-Cadherin<sup>High</sup> cell-injected mice after 7 days (Figure 2k, l).

Altogether, these results demonstrated that the expression of N-Cadherin is associated with reduced MDA cell aggressiveness in the bone microenvironment and increased ability to engraft to the endosteal niche.

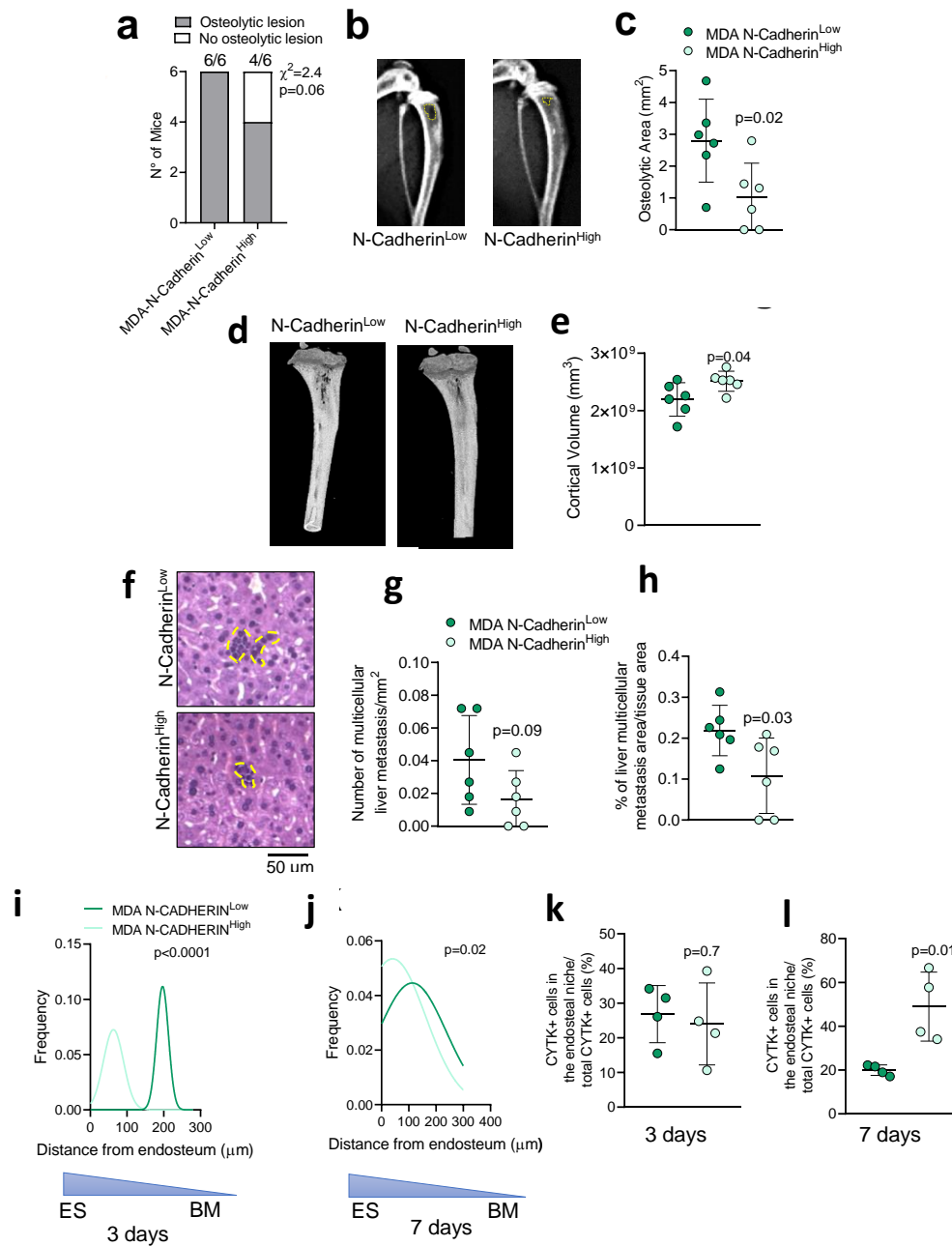


**Figure 2. In vivo analysis of N-Cadherin<sup>High</sup> BrCa MDA cells.** Four-week-old Balb-c nu/nu female mice were intratibially injected with  $1 \times 10^4$  MDA cells and MACS-sorted into N-Cadherin<sup>High</sup> and N-Cadherin<sup>Low</sup> subpopulations. (a) After 4 weeks, mice were sacrificed and tibia osteolytic lesion incidence and (b, c) area were analyzed by X-rays while, (d)  $\mu$ CT 3D analysis and (e) cortical volume measurement of the injected tibia were performed. (f) Paraffin embedded livers isolated from MDA N-Cadherin<sup>High</sup> and N-Cadherin<sup>Low</sup>-injected mice stained with hematoxylin and eosin to quantify (g) the number of multicellular liver metastases over square millimeters and (h) the % of multicellular liver metastases area over tissue area by the ImageJ® software. (i) Four-week-old Balb-c nu/nu female mice were intratibially injected with  $1 \times 10^4$  MDA cells MACS sorted into N-Cadherin<sup>High</sup> and N-Cadherin<sup>Low</sup> subpopulations and sacrificed 3- and 7-days post-injection. Paraffin-embedded tibiae were harvested from the injected mice immuno-stained for cytokeratin to visualize the tumor cells in the bone tissue and measure the cell distribution after 3 and (j) 7 days post injection in relation to the

endosteum, and (k) the number of cells in the endosteal niche after 3 and (l) 7 days post injection. Data are the mean  $\pm$ SD and pictures are representative of 4–6 mice per group. Statistical analysis: (a) square analysis, (c, e, g, h, k, l) Student's t-test, (i, j) Gaussian curve regression fitting and F-test. Scale bar is in the pictures.

#### 4.3. *N-Cadherin mediates BrCa Cell adhesion onto SNOs in vitro*

To establish the role of N-Cadherin in the SNO-mediated tumor cell dormancy, MACS-sorted N-Cadherin<sup>High</sup> and N-Cadherin<sup>Low</sup> MDA<sup>GFP</sup> cells were seeded onto sorted SNOs or NON-SNOs as previously described.<sup>12</sup> N-Cadherin<sup>High</sup> MDA<sup>GFP</sup> cell adhesion, measured after 1 h from plating, was significantly higher when they were plated on SNOs compared to all other conditions tested (Figure 3a). In a time-course of 24–72 h, the number of MDA<sup>GFP</sup> cells was lower in MDA-SNO compared to MDA-NON-SNO cocultures, regardless of the N-Cadherin status (Figure 3b), suggesting that the expression of N-Cadherin does not affect the inhibition of MDA cell proliferation induced by SNOs.<sup>12</sup> In line with this observation, the N-Cadherin knock-down by a specific siRNA reduced the N-Cadherin<sup>High</sup> MDA<sup>GFP</sup> cell adhesion to SNOs (Figure 3c) without affecting the SNO-dependent inhibition of MDA proliferation (Figure 3d).

Interestingly, N-Cadherin<sup>High</sup> MDA cells showed higher Notch2 transcriptional expression when compared with the N-Cadherin<sup>Low</sup> counterpart (Figure 3e), and FACS analysis revealed that 58.4% of the N-Cadherin<sup>High</sup> MDA cells were also Notch2<sup>High</sup> (see Figure 1e). We also co-cultured MACS-sorted Notch2<sup>High</sup> and Notch2<sup>Low</sup> MDA<sup>GFP</sup> cells with SNOs or NON-SNOs. Although cell adhesion measured after 1 h from plating was not significantly different in Notch2<sup>High</sup> and Notch2<sup>Low</sup> MDA<sup>GFP</sup> co-cultured with SNOs and NON-SNOs (Figure 3f), during the subsequent time-course the number of Notch2<sup>High</sup> MDA<sup>GFP</sup> cells increased less when plated on SNOs compared to the co-plating with NON-SNOs (Figure 3g). It is to be noted that co-cultures between Notch2<sup>High</sup> MDA<sup>GFP</sup> cells and NON-SNOs or Notch2<sup>Low</sup> MDA<sup>GFP</sup> cells and SNOs impaired the tumor cell proliferation only partially, suggesting that both players should be present to induce the maximum inhibitory effect.

In light of this data, we can conclude that N-Cadherin plays a role in MDA cell adhesion especially onto SNOs, while Notch2 is pivotal in SNO-induced dormancy.

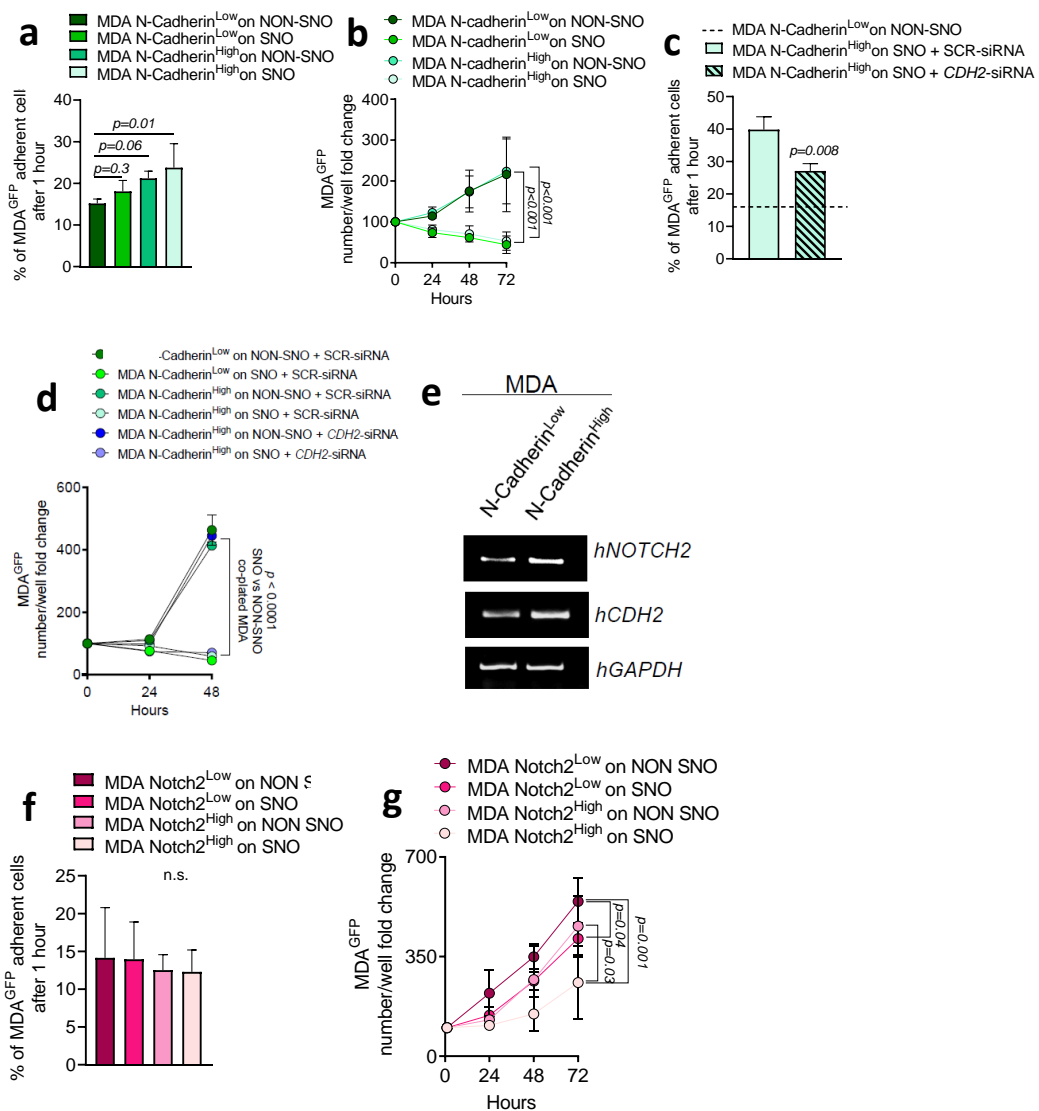


**Figure 3. Role of N-Cadherin and Notch2 in MDA-SNO interaction in vitro.** (a) N-Cadherin<sup>High</sup> and N-Cadherin<sup>Low</sup> MDA<sup>GFP</sup> cells were seeded onto MACS-sorted SNOs and NON-SNOs and allowed to attach for 1 h at 37 °C, followed by extensive washing. Number of MDA<sup>GFP</sup> cells was assessed after 1h of adhesion and (b) after 24–72 h of co-culture. (c) N-Cadherin<sup>High</sup> and N-Cadherin<sup>Low</sup> MDA<sup>GFP</sup> cells, treated with siRNA against the N-Cadherin (*CDH2*-siRNA) or scrambled (SCR siRNA), were seeded onto MACS-sorted SNOs and NON-SNOs. The number of MDA<sup>GFP</sup> cells was assessed after 1h of adhesion. (d) N-Cadherin<sup>High</sup> and N-Cadherin<sup>Low</sup> MDA<sup>GFP</sup> cells treated with *CDH2*-siRNA or SCR-siRNA for 48 hours were seeded onto MACS-sorted SNOs and NON-SNOs and allowed to attach for 1 h at 37 °C, followed by extensive washing and assessment of the number of MDA<sup>GFP</sup> cells after 24–48 h of co-culture. (e) Semiquantitative RT-PCR was used to assess the expression of the indicated genes. Human *GAPDH* was used to normalize the gene expression. (f) Notch2<sup>High</sup> and Notch2<sup>Low</sup> MDA<sup>GFP</sup> cells were seeded onto MACS sorted SNOs and NON-SNOs and allowed to attach for 1 h at 37 °C, followed by extensive washing. The number of MDA<sup>GFP</sup> cells was assessed after 1h of adhesion and (g) after 24–72 h of co-culture. In (b, d, g) cell number per well was normalized for time 0 (number of cells after 1 h of adhesion). Data are the mean ± SD of 4 independent cell preparations. Statistical analysis: (a, c, f) Student's t-test, (b, d, g) Non-linear regression fitting and F-test.

#### 4.4. The role of N-Cadherin in HSC mimicry and Cancer Stem Cell-like phenotype

It has been previously demonstrated that the dormant Notch2<sup>High</sup> MDA cells showed HSC mimicry, along with a cancer stem cell-like phenotype and reduced 2D cell proliferation, when compared with the Notch2<sup>Low</sup> counterpart.<sup>12</sup> To evaluate whether these features were shared by the N-Cadherin<sup>High</sup> BrCa cells, we investigated whether MACS-sorted N-Cadherin<sup>High</sup> MDA cells showed an HSC-like gene signature. Our analysis demonstrated that they expressed higher mRNA levels of the HSC markers, *CD34*, *TIE2*, and *CXCR4* compared to N-Cadherin<sup>Low</sup> MDA cells (Figure 4a), along with a higher expression of the stem cell related genes *SOX2* and *NAGOG* (Figure 4b). In addition, the presence of a canonical cancer stem cell signature independent from N-Cadherin expression has been confirmed. Indeed, both N-Cadherin<sup>High</sup> and N-Cadherin<sup>Low</sup> MDA cells expressed high *CD44*, medium *ALDH* and low *CD24* mRNA (Figure 4c, d). On the contrary, a lower expression of the cell proliferation marker EdU was found in N-Cadherin<sup>High</sup> compared to N-Cadherin<sup>Low</sup> MDA cells (Figure 4e). Primary mammospheres from the N-Cadherin<sup>High</sup> MDA cells were larger (Figure 4f) and more numerous (Figure 4g) than mammospheres generated by N-Cadherin<sup>Low</sup> MDA cells. Secondary mammospheres were larger in the N-Cadherin<sup>High</sup> compared to the N-Cadherin<sup>Low</sup> MDA cells (Figure 4h), while their number was very variable and showed only a trend to increase (Figure 4i). The cancer stem cell-like phenotype was further confirmed employing an *in vivo* Limiting Dilution Assays (LDA) that revealed a higher stem cell frequency in the N-Cadherin<sup>High</sup> compared to the N-Cadherin<sup>Low</sup> MDA cells subpopulation (Table 5). Finally, the analysis of the epithelial-to-mesenchymal transition (EMT) markers revealed a higher expression of E-Cadherin in the N-Cadherin<sup>High</sup> vs. N-Cadherin<sup>Low</sup> MDA cells (Figure 4j).

Overall, these results showed that N-Cadherin<sup>High</sup> MDA cells display an HSC-like gene signature and a canonical cancer stem cell-like CD44<sup>High</sup>/CD24<sup>Low</sup>/ALDH<sup>+</sup> phenotype similar to the Notch2<sup>High</sup> MDA cells.

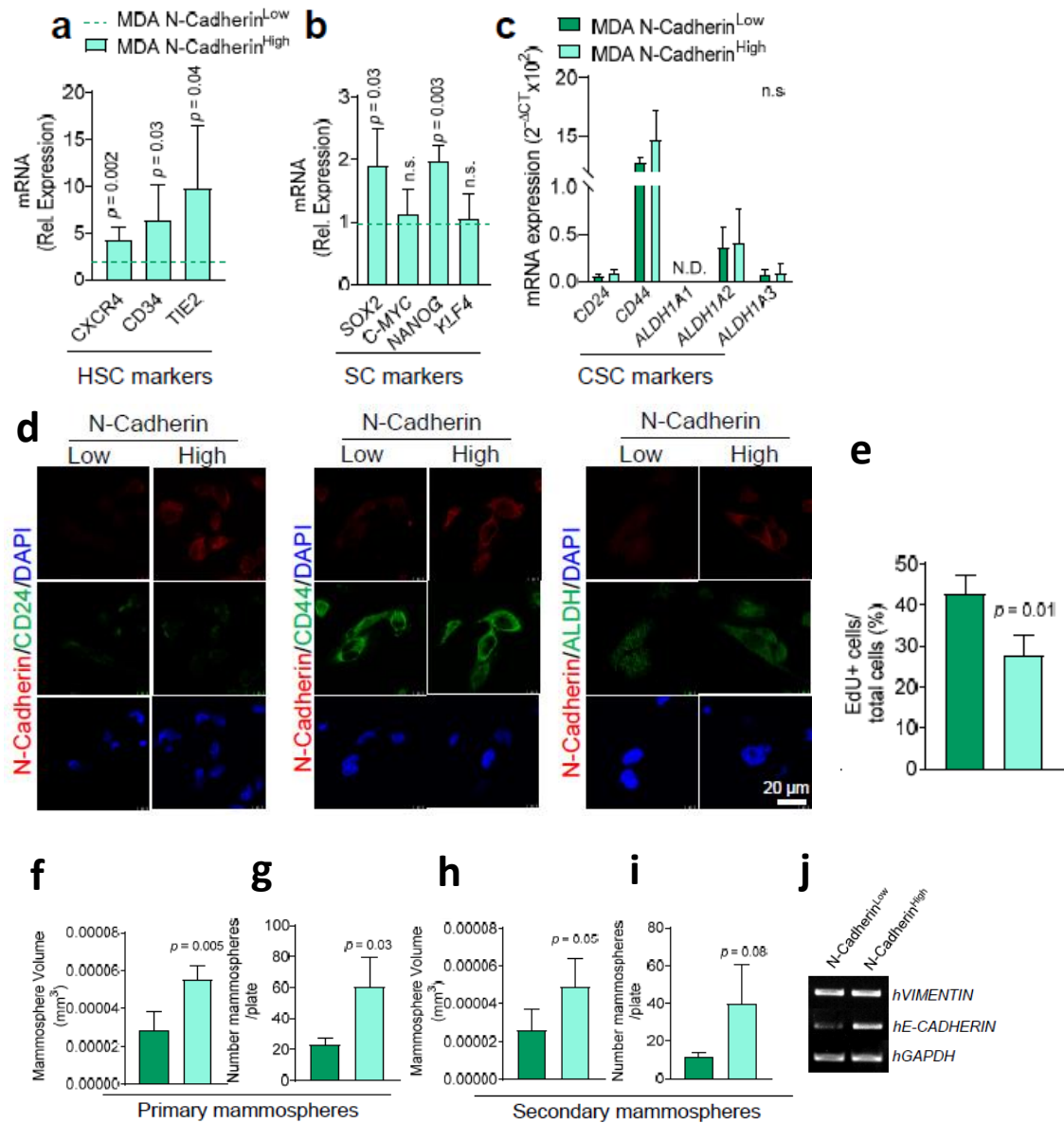


**Figure 4. Effect of N-Cadherin expression on HSC mimicry, stemness and EMT.** MDA cells were sorted into N-Cadherin<sup>High</sup> and N-Cadherin<sup>Low</sup> subpopulations by MACS. Real-time RT-PCR was used to assess the expression of the indicated (a) HSC, (b) Stem Cell (SC) and (c) Cancer Stem Cell (CSC) markers. Human *GAPDH* was used to normalize gene expression. (d) Immunofluorescence was performed using the antibodies for the indicated proteins to evaluate their expression level in N-Cadherin<sup>High</sup> and N-Cadherin<sup>Low</sup> MDA. (e) 5-ethynyl-2'-deoxyuridine (EdU) assay to assess cell proliferation. (f) Size and (g) number of primary mammospheres obtained from MACS-sorted N-Cadherin<sup>High</sup> and N-Cadherin<sup>Low</sup> MDA cells. (h) Size and (i) number of secondary mammospheres obtained after trypsinization and re-plating the single cells harvested from the primary MDA mammospheres. (j) Semiquantitative RT-PCR to assess the expression of the indicated EMT genes. Human *GAPDH* was used to normalize gene expression. Data are the mean ± SD of 3–5 independent cell preparations. Statistical analysis: Student's t-test.

**Table 5.** Stem cell frequency in N-Cadherin<sup>High</sup> and N-Cadherin<sup>Low</sup> MDA tumors.

Cell Models	Cell Number			Stem Cell Frequency (ELDA)	p-Value (vs. N-Cadherin <sup>Low</sup> )
	50,000	10,000	100		
N-Cadherin <sup>Low</sup> -MDA	5/5 (100%)	4/5 (80%)	0/5 (0%)	1/6338	-
N-Cadherin <sup>High</sup> -MDA	5/5 (100%)	5/5 (100%)	2/5 (40%)	1/196	0.002

#### 4.5. *N-Cadherin status in human primary BrCa and correlation with survival*

The KMplot®, containing protein expression data and survival information from four independent cohorts of 1193 BrCa patients, was used to test the correlation between N-Cadherin protein expression and survival. The analysis revealed the presence of a positive correlation between the N-Cadherin and the overall survival when we analyzed the whole dataset (Figure 5a). Furthermore, when data were stratified for estrogen (ER) or progesterone (PR) receptor, Human Epidermal growth factor Receptor 2 (HER2) or triple negative subtypes, a significant and positive correlation between high N-cadherin level and overall survival in patients with either ER- or PR-positive BrCas could be confirmed (Figure 5b, d). On the other hand, no significant correlations were found in the survival of patients with either ER- or PR-negative, HER2 positive and negative, or triple negative BrCas (Figure 5c, e, f-h).

Finally, we investigated the expression of N-Cadherin in a BrCa tissue array containing 64 different samples of primary tumors. We observed that N-Cadherin positive cells represented a small subpopulation ( $0.76 \pm 0.3$  cell/mm<sup>2</sup>) (Figure 5i and Table 6). Furthermore, histopathological analysis revealed that the number of N-Cadherin positive cells was higher in poorly differentiated primary BrCa (Figure 5j). In contrast, the number of N-cadherin positive cells remained unchanged when the tumors were stratified according to the presence of distant metastases (Figure 5k) and PR and HER2 status (Figure 5l, m), while, when samples were stratified for the ER status, a positive trend in the N-cadherin positive cells ( $p = 0.08$ ) was found in the ER-positive compared to the ER-negative primary BrCa (Figure 5n). Moreover, no changes in the number of N-Cadherin positive cells were found when we compared the ER, PR and HER2 single negative with triple negative specimens (Figure 5o).

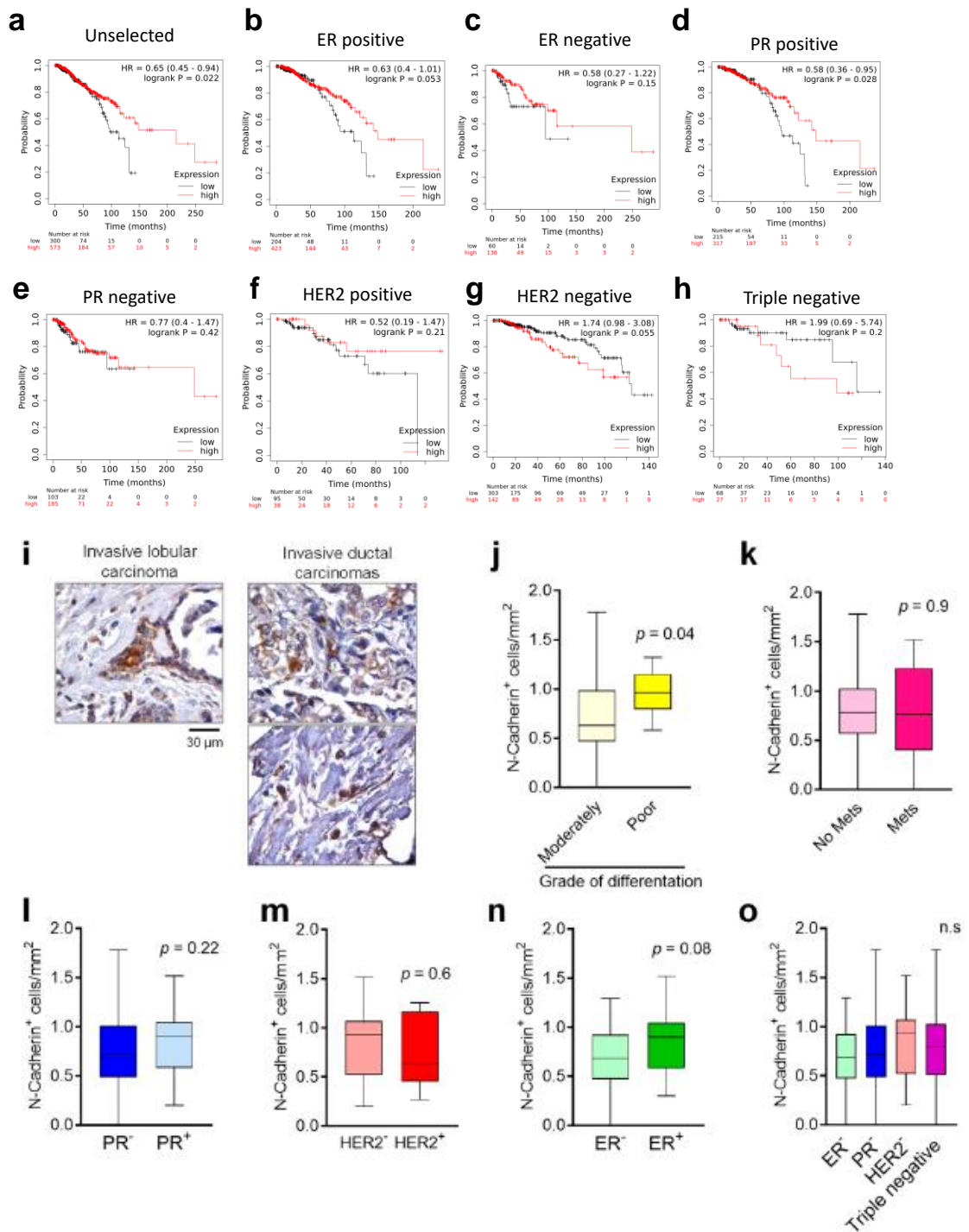


**Figure 5. N-Cadherin expression in primary human BrCa and correlation with survival.** (a) Kaplan–Meier plots on 1229 public proteomics from primary BrCa to correlate N-Cadherin protein expression with patient survival in unselected populations of 300 N-Cadherin<sup>Low</sup> and 573 N-Cadherin<sup>High</sup> samples, (b) in estrogen receptor (ER)-positive of 204 N- Cadherin<sup>Low</sup> and 423 N-Cadherin<sup>High</sup> samples, (c) in ER-negative populations of 60 N-Cadherin<sup>Low</sup> and 136 N-Cadherin<sup>High</sup> samples, (d) in progesterone receptor (PR)-positive of 215 N-Cadherin<sup>Low</sup> and 317 N-Cadherin<sup>High</sup> and (e) progesterone receptor (PR)-negative populations of 103 N-Cadherin<sup>Low</sup> and 185 N-Cadherin<sup>High</sup> samples, (f) in HER2-positive populations of 95 N-Cadherin<sup>Low</sup> and 38 N-Cadherin<sup>High</sup> samples, (g) in HER2-negative populations of 303 N-Cadherin<sup>Low</sup> and 142 N- Cadherin<sup>High</sup>



samples and (h) in triple negative populations of 68 N-Cadherin<sup>Low</sup> and 27 N-Cadherin<sup>High</sup> samples plotted against time (KMPlot®). (i) BrCa tissue array containing 64 primary BrCa samples was stained for N-Cadherin by immunohistochemistry. The number of the N-Cadherin positive cells was quantified, and the results were stratified according to (j) grade of differentiation, (k) presence of distal metastases, expression of (l) PR, (m) HER2 or (n) ER receptors and in (o) triple negative primary tumors. Pictures are representative and data in (j–o) are the mean ± SD of at least 9 primary tumors per condition. Statistical analysis: (a, h) log-rank test; (j–o) Student's t-test.

**Table 6.** BrCa tissue array donor information.

<b>Patient #</b>	<b>N-Cadherin<sup>+</sup> cells (n/mm<sup>2</sup>)</b>	<b>Grade of differentiation</b>	<b>TNM<sup>1</sup></b>	<b>ER</b>	<b>PR</b>	<b>Her2</b>
<b>A3</b>	0.268754733	moderately	T2N2M1	-	-	++
<b>A4</b>	0.489416875	moderately	T2N2M1	-	-	-
<b>A5</b>	0.578140816	moderately	T2N1M0	+	-	-
<b>A6</b>	1.519303172	moderately	T2N2M1	+	+	-
<b>A7</b>	1.172902049	moderately	T2N1M1	-	-	-
<b>A8</b>	0.717111097	moderately	T2N0M0	-	-	-
<b>A9</b>	1.045280582	moderately	T2N0M0	+	++	-
<b>A10</b>	1.238009699	moderately	T2N0M0	++	+	-
<b>A11</b>	0.613798482	moderately	T2N2M1	+	-	-
<b>B1</b>	1.002740094	moderately	T2N0M0	+++	+++	-
<b>B2</b>	1.780623318	moderately	T2N0M0	-	-	-
<b>B3</b>	0.996662881	well	T2N2M0	-	-	-
<b>B4</b>	0.990585668	well	T2N2M0	+	+	-
<b>B5</b>	0.237011295	moderately	T2N1M0	+++	++	-
<b>B6</b>	0.753574373	moderately	T2N2M0	-	+++	-
<b>B7</b>	0.929813541	moderately	T2N1M1	-	-	-
<b>B8</b>	1.294446303	moderately	T2N1M1	-	-	-
<b>B9</b>	0.583412418	poorly	T3N3M0	++	+	-
<b>B10</b>	0.559103567	moderately	T2N1M0	-	-	-
<b>B11</b>	1.02450169	moderately	T2N2M0	-	-	-
<b>C1</b>	0.301716335	moderately	T2N1M0	++	+	-
<b>C2</b>	0.303860634	moderately	T2N0M0	-	-	-
<b>C3</b>	0.47161648	moderately	T2N1M1	+++	-	-
<b>C4</b>	0	moderately	T2N3M1	-	-	++
<b>C5</b>	0.820423713	moderately	T2N2M0	-	-	-
<b>C6</b>	0.924575038	poorly	T2N0M0	++	+	-
<b>C7</b>	1.140809202	poorly	T2N0M0	+	+	-
<b>C8</b>	0.765728799	N/A	T2N1M1	-	-	-
<b>C9</b>	0.653817617	N/A	T1N0M0	-	-	-
<b>C10</b>	1.482839896	N/A	T2N3M1	+	-	-
<b>C11</b>	1.237246384	N/A	T1N0M0	+	+	++
<b>D1</b>	0.88119584	N/A	T2N0M0	+	+	-
<b>D2</b>	0.929813541	moderately	T2N2M0	+	+	-
<b>D3</b>	1.317934063	poorly	T2N0M0	+	++	-

<b>D4</b>	0.963586355	poorly	T2N1M0	++	+++	-
<b>D5</b>	1.173030367	moderately/poorly	T2N1M0	-	-	-
<b>D6</b>	0.814435591	moderately	T2N3M1	-	-	-
<b>D7</b>	0.626021387	moderately	T3N3M0	+	+	-
<b>D8</b>	1.023707197	moderately	T2N0M0	-	-	-
<b>D9</b>	1.13253033	poorly	T2N0M0	-	-	-
<b>D10</b>	0.807312152	poorly	T2N0M0	-	-	-
<b>D11</b>	0.784046204	poorly	T2N0M0	-	-	-
<b>E1</b>	1.291734397	moderately	T2N0M0	-	-	-
<b>E2</b>	0.899525877	moderately	T2N0M0	-	-	-
<b>E3</b>	0.632099265	moderately	T2N0M0	-	+	-
<b>E4</b>	0.583476244	moderately	T2N0M0	-	+++	-
<b>E5</b>	0.634051873	moderately	T2N0M0	-	-	-
<b>E6</b>	0.32212751	moderately	T2N2M1	+	+	-
<b>E7</b>	0.522697469	moderately	T2N0M0	-	-	+++
<b>E8</b>	1.258120652	moderately	T2N0M0	-	-	+++
<b>E9</b>	0	moderately	T2N0M0	-	-	+++
<b>E10</b>	0.819838504	moderately	T2N0M0	-	-	+++
<b>E11</b>	0.613865632	moderately	T2N0M0	-	+	+++
<b>F1</b>	0.480152326	moderately	T2N3M0	-	-	-
<b>F2</b>	1.166952489	poorly	T2N1M0	-	-	+
<b>F3</b>	0.455840816	moderately	T2N0M0	-	-	+++
<b>F4</b>	0.632099265	moderately	T2N0M0	-	-	+++
<b>F5</b>	0.492308081	moderately	T2N0M0	-	-	-
<b>F6</b>	0.200569959	moderately	T2N1M0	+	+	-
<b>F7</b>	0	moderately	T2N0M0	-	-	-
<b>F8</b>	0.747578938	moderately	T2N0M0	-	-	-
<b>F9</b>	0.121557551	moderately	T2N0M0	-	-	-
<b>F10</b>	0.467996571	moderately	TxNxMx	-	-	-
<b>F11</b>	0.583476244	moderately/poorly	TxNxMx	+	+	-

**<sup>1</sup>TNM staging:**

T1: tumor is 2 centimeters (cm) across or less.

T2: tumor is more than 2 centimeters but no more than 5 centimeters across.

T3: tumor is bigger than 5 centimeters across.

TX: the tumor size can't be assessed.

N0: No cancer was found in the lymph nodes or only areas of cancer smaller than 0.2 mm are in the lymph nodes.

N1: cancer has spread to 1 to 3 axillary lymph nodes and/or the internal mammary lymph nodes.

N2: cancer has spread to 4 to 9 axillary lymph nodes. Or, it has spread to the internal mammary lymph nodes, but not the axillary lymph nodes.

N3: cancer has spread to 10 or more axillary lymph nodes, or it has spread to the lymph nodes located under the clavicle, or collarbone.

M0: there is no sign that the cancer has spread (No distal metastases).

M1: cancer has spread to another part of the body (Distal metastases).

## 5. DISCUSSION

Tumor cell dormancy is an intricate mechanism involving different molecular pathways and cell-cell interactions in accordance with the type of cancer and the microenvironmental signaling.<sup>32</sup> In the previous work performed in our laboratory it was demonstrated that dormant BrCa cells interact with a specific osteoblast subpopulation, known as spindle-shaped N-Cadherin<sup>High</sup> osteoblasts (SNOs), remaining cell cycle arrested due to the Notch2 pathway. Moreover, we demonstrated that dormant BrCa cells compete with HSCs for bone marrow engraftment and endosteal niche colonization thanks to their HSC mimicry features.<sup>12</sup> In this work, a new piece was added in this complex puzzle showing a potential role of N-Cadherin in the SNO-mediated BrCa cell dormancy and cellular stemness.

The role of N-Cadherin in tumor biology is very complex and varies according to the cellular context and the type of tumor. N-Cadherin has been reported to induce or suppress tumor development and spreading according to the type of cancer.<sup>22,24,26</sup> In the BrCa context, the role of N-Cadherin is still barely understood, probably because its function is tightly related to cellular and microenvironmental conditions. Data in the literature indicates that the expression of N-Cadherin increases the BrCa cell adhesion to the stroma and stimulates motility, enhancing metastatic spread.<sup>15,25,26,33</sup> In contrast, a recent paper demonstrated that N-Cadherin drives human BrCa dormancy in the bone marrow in association with connexin 43.<sup>26</sup> Also, in line with our findings, the author showed that N-Cadherin was expressed by the stem compartment of BrCa cells, contributing to the maintenance of the cellular dormancy.<sup>26</sup>

An expression of N-Cadherin in the dormant Notch2<sup>High</sup> MDA BrCa cells has been found, confirming the possible association between N-Cadherin expression and BrCa cellular dormancy. In line with this observation, MDA cells expressing high level of N-Cadherin showed a lower aggressiveness in the bone microenvironment associated with a lower incidence of osteolytic lesions alongside an increased endosteal niche engraftment, indicating that the N-Cadherin signaling prompted the tumor cells to acquire a dormant-like phenotype.

The ability to lodge in proximity of the endosteal niche led us to assume that MDA N-Cadherin<sup>High</sup> were able to interact with the SNOs. The assumption was confirmed *in vitro* by experiments showing that MDA cells expressing N-Cadherin were able to interact with SNOs and that the presence of high level of N-Cadherin increased the ability of tumor cells to adhere to SNOs. This observation was further confirmed by the fact that the knock-down of N-Cadherin expression in MDA cells reduced their ability to adhere to SNOs. Of note,

unlike Notch2<sup>High</sup> cells, the proliferation of N-Cadherin<sup>High</sup> MDA cells in the presence of SNOs was unremarkable, suggesting that N-Cadherin mediates the adhesion of BrCa cells to SNOs, while Notch2 mediates the inhibition of SNO-induced cell proliferation. Accordingly, further analyses confirmed that only about 58% of N-Cadherin<sup>High</sup> MDA expressed high levels of Notch2. Altogether these data prompted us to hypothesize that the homophilic N-Cadherin interaction between MDA cells and SNOs is used by tumor cells for engraftment to the endosteal niche, while only a small subpopulation co-expressing Notch2 also acquires the dormant phenotype.

As mentioned above, the ability to colonize the endosteal niche and interact with SNOs is a typical feature of HSCs<sup>10</sup> shared also by the dormant Notch2<sup>High</sup> MDA cells.<sup>12</sup> Although conflicting data about the role of N-cadherin in HSCs are shown in literature<sup>19,27-29</sup>, Arai et al. demonstrated that N-Cadherin is expressed by HSCs and that its overexpression promotes HSC quiescence<sup>29</sup>. In agreement with this observation, the present data has demonstrated that the N-Cadherin expression was associated with the acquisition of a bone marrow-specific cancer stem cell phenotype and HSC like-signature in MDA cells. In fact, a higher expression of the canonical HSC markers CXCR4, TIE-2 and CD34 and of the stem cell related markers SOX2 and NANOG in the N-Cadherin<sup>High</sup> MDA cells along with a lower cell proliferation rate and a higher ability to form primary and secondary mammospheres has been found. In addition, in vivo limiting dilution assay showed a higher stem cell frequency in the N-Cadherin<sup>High</sup> MDA cells, further confirming their ability to initiate a new cancer. Interestingly, the analysis of canonical cancer stem cell markers revealed that both N-Cadherin<sup>High</sup> and N-Cadherin<sup>Low</sup> MDA cells display the typical cancer stem cell phenotype CD44<sup>High</sup>/CD24<sup>Low</sup>/ALDH<sup>+</sup>.<sup>34</sup> These findings suggest that N-Cadherin expression identifies a specific subpopulation, expressing HSC- and stem cell-related markers, within the canonical CD44<sup>High</sup>/CD24<sup>Low</sup>/ALDH<sup>+</sup> cancer stem cell population. These data were in line with the ability of the N-Cadherin<sup>High</sup> cells to colonize the endosteal niche resulting in lower aggressiveness in the bone/bone marrow microenvironment and with the concept that dormant cells should have stem features to initiate a new tumor after their reactivation.<sup>6,7</sup>

Finally, according to the fact that there are no reliable markers to predict tumor dormancy in clinical practice<sup>35</sup>, we investigated whether N-Cadherin could be useful to this scope. The analyses carried out using public datasets demonstrated that N-Cadherin protein expression in primary tumors was correlated with a better prognosis in an unselected BrCa patients' cohort. In line with this, the analyses of a primary BrCa tissues array demonstrated a trend of increase in the number of N-Cadherin positive cells in ER positive tumors, known

to be less malignant, suggesting that N-Cadherin expression could be associated with less aggressive human primary tumors. However, we also found a higher number of N-Cadherin-positive cells in primary tumors classified as less differentiated, which are known to be more aggressive.<sup>36</sup> This is in agreement with a recent publication showing that N-Cadherin expression in patients with ductal carcinoma *in situ* is predictive of synchronous invasion.<sup>36</sup> Another explanation of this conflicting result could be represented by the fact that less differentiated tumor cells usually show a stem-like phenotype. In confirmation, according to our and others'<sup>12,26,37</sup> results, N-Cadherin is likely to be expressed mainly in the stem cellular compartment. A limitation of this study is that most of the tumors analyzed were ductal carcinomas, and that the absence of more differentiated tumors in our BrCa tissue array did not allow a complete correlation analysis between type and differentiation grade of primary tumors and N-Cadherin expression. Besides, even if our data were generated using triple negative BrCa cell lines, we did not find an association between N-Cadherin expression and the overall survival in patients harboring triple negative BrCa. Similar results were found when we analyzed the number of N-Cadherin positive cells in triple negative specimens present in our BrCa tissues array. This could be partially explained by the fact that the number of patients derived from the public dataset carrying a triple negative tumor was relatively low (68 N-Cadherin<sup>Low</sup> and 27 N-Cadherin<sup>High</sup> samples) and the absence of triple positive specimens in our BrCa tissue array forced us to compare the triple negative samples only with the ER, PR and HER2 single negative tumors. For this reason, further and larger studies are needed to clarify the possible role of N-Cadherin as an early dormancy marker in BrCa patients.

## 6. REFERENCES

1. Howlader N, Noone AM, Krapcho M, Miller D, Brest A, Yu M, Ruhl J, T. Z. & Mariotto A, Lewis DR, Chen HS, Feuer EJ, C. K. (eds). Cancer Statistics Review, 1975-2018 - SEER Statistics. [https://seer.cancer.gov/csr/1975\\_2018/](https://seer.cancer.gov/csr/1975_2018/).
2. Osisami, M. & Keller, E. Mechanisms of Metastatic Tumor Dormancy. *J Clin Med* **2**, 136–150 (2013).
3. Páez, D. *et al.* Cancer dormancy: A model of early dissemination and late cancer recurrence. *Clinical Cancer Research* **18**, 645–653 (2012).

4. M, B.-P., F, R. & T, F. Disseminated Tumor Cells and Dormancy in Breast Cancer Progression. *Adv Exp Med Biol* **1220**, 35–43 (2020).
5. Naumov, G. N. *et al.* Ineffectiveness of doxorubicin treatment on solitary dormant mammary carcinoma cells or late-developing metastases. *Breast Cancer Res Treat* **82**, 199–206 (2003).
6. Talukdar, S. *et al.* Dormancy and cancer stem cells: An enigma for cancer therapeutic targeting. *Adv Cancer Res* **141**, 43–84 (2019).
7. De Angelis, M. L., Francescangeli, F. & Zeuner, A. Breast Cancer Stem Cells as Drivers of Tumor Chemoresistance, Dormancy and Relapse: New Challenges and Therapeutic Opportunities. *Cancers (Basel)* **11**, (2019).
8. Roodman, G. D. Mechanisms of Bone Metastasis. *New England Journal of Medicine* **350**, 1655–1664 (2004).
9. Calvi, L. M. *et al.* Osteoblastic cells regulate the haematopoietic stem cell niche. *Nature* **425**, 841–846 (2003).
10. Zhang, J. *et al.* Identification of the haematopoietic stem cell niche and control of the niche size. *Nature* **425**, 836–841 (2003).
11. Haider, M. T., Smit, D. J. & Taipaleenmäki, H. The Endosteal Niche in Breast Cancer Bone Metastasis. *Front Oncol* **10**, 335 (2020).
12. Capulli, M. *et al.* Notch2 pathway mediates breast cancer cellular dormancy and mobilisation in bone and contributes to haematopoietic stem cell mimicry. *Br J Cancer* **121**, 157–171 (2019).
13. Tamura, K., Shan, W.-S., Hendrickson, W. A., Colman, D. R. & Shapiro, L. Structure-Function Analysis of Cell Adhesion by Neural (N-) Cadherin. *Neuron* **20**, 1153–1163 (1998).
14. Walsh, F. S. *et al.* N-Cadherin Gene Maps to Human Chromosome 18 and Is Not Linked to the E-Cadherin Gene. *J Neurochem* **55**, 805–812 (1990).
15. Bremmer, F. *et al.* Role of N-cadherin in proliferation, migration, and invasion of germ cell tumours. *Oncotarget* **6**, 33426–33437 (2015).

16. Derycke, L. D. M. & Bracke, M. E. N-cadherin in the spotlight of cell-cell adhesion, differentiation, invasion and signalling. *International Journal of Developmental Biology* **48**, 463–476 (2004).
17. Hajj, E., Nouraud, A. & Marie, P. J. N-cadherin negatively regulates osteoblast proliferation and survival by antagonizing Wnt, ERK and PI3K/Akt signalling. *PLoS One* **4**, (2009).
18. PJ, M. Role of N-cadherin in bone formation. *J Cell Physiol* **190**, 297–305 (2002).
19. Zhao, M. *et al.* N-Cadherin-Expressing Bone and Marrow Stromal Progenitor Cells Maintain Reserve Hematopoietic Stem Cells. *Cell Rep* **26**, 652-669.e6 (2019).
20. Van Roy, F. Beyond E-cadherin: Roles of other cadherin superfamily members in cancer. *Nat Rev Cancer* **14**, 121–134 (2014).
21. Kaszak, I. *et al.* Role of cadherins in cancer—a review. *Int J Mol Sci* **21**, 1–17 (2020).
22. Gao, Y., Qu, Y., Zhou, Q. & Ma, Y. SIRT6 inhibits proliferation and invasion in osteosarcoma cells by targeting N-cadherin. *Oncol Lett* **17**, 1237–1244 (2019).
23. JL, A., AC, K. & JR, H. The role and function of cadherins in the mammary gland. *Breast Cancer Res* **14**, (2012).
24. Cao, Z. Q., Wang, Z. & Leng, P. Aberrant N-cadherin expression in cancer. *Biomedicine and Pharmacotherapy* **118**, (2019).
25. Nieman, M. T., Prudoff, R. S., Johnson, K. R. & Wheelock, M. J. N-cadherin promotes motility in human breast cancer cells regardless of their E-cadherin expression. *Journal of Cell Biology* **147**, 631–643 (1999).
26. Sinha, G. *et al.* Specific N-cadherin dependent pathways drive human breast cancer dormancy in bone marrow. *Life Sci Alliance* **4**, (2021).
27. Greenbaum, A. M., Revollo, L. D., Woloszynek, J. R., Civitelli, R. & Link, D. C. N-cadherin in osteolineage cells is not required for maintenance of hematopoietic stem cells. *Blood* **120**, 295–302 (2012).
28. Hosokawa, K., Arai, F. & Suda, T. N-Cadherin Induces Hematopoietic Stem Cells in a Quiescent State in the Bone Marrow Niche. *Blood* **106**, 470–470 (2005).

29. Arai, F., Hosokawa, K., Toyama, H., Matsumoto, Y. & Suda, T. Role of N-cadherin in the regulation of hematopoietic stem cells in the bone marrow niche. *Ann N Y Acad Sci* **1266**, 72–77 (2012).
30. Hu, Y. & Smyth, G. K. ELDA: Extreme limiting dilution analysis for comparing depleted and enriched populations in stem cell and other assays. *J Immunol Methods* **347**, 70–78 (2009).
31. Bouxsein, M. L. *et al.* Guidelines for assessment of bone microstructure in rodents using micro-computed tomography. *Journal of Bone and Mineral Research* **25**, 1468–1486 (2010).
32. Gomatou, G., Syrigos, N., Vathiotis, I. A. & Kotteas, E. A. Tumor dormancy: Implications for invasion and metastasis. *Int J Mol Sci* **22**, (2021).
33. Hazan, R. B., Kang, L., Whooley, B. P. & Borgen, P. I. N-Cadherin Promotes Adhesion between Invasive Breast Cancer Cells and the Stroma. *Cell Commun Adhes* **4**, 399–411 (1997).
34. Ricardo, S. *et al.* Breast cancer stem cell markers CD44, CD24 and ALDH1: Expression distribution within intrinsic molecular subtype. *J Clin Pathol* **64**, 937–944 (2011).
35. Gelao, L. *et al.* Tumour dormancy and clinical implications in breast cancer. *Ecancermedicalscience* **7**, (2013).
36. Jögi, A., Vaapil, M., Johansson, M. & Pählman, S. Cancer cell differentiation heterogeneity and aggressive behavior in solid tumors. *Ups J Med Sci* **117**, 217–224 (2012).
37. Yang, C., Zhao, X., Cui, N. & Liang, Y. Cadherins Associate with Distinct Stem Cell-Related Transcription Factors to Coordinate the Maintenance of Stemness in Triple-Negative Breast Cancer. *Stem Cells Int* **2017**, (2017).



# Chapter 3

## The endosteal niche regulates BrCa cell dormancy in bone

Manuscript in preparation

### 1. ABSTRACT

Breast Cancer (BrCa) cellular dormancy is a deleterious condition that prevents full cancer eradication and causes long-term relapse of metastases even after decades from apparent healing. Bone is a preferential site of BrCa metastases and previous studies in our laboratory have established that Notch2 is a leading molecular mechanism implicated in BrCa cellular dormancy in the bone microenvironment. However, dormant BrCa cells also express high level of Notch1, whose implication in endosteal-mediated cellular dormancy is poorly understood, while the role of Notch3 and Notch4 were found to be negligible. In this study, we focused on Notch1 and Notch2 to structure the molecular features of BrCa cells lodging the bone environment, where Spindle-shaped N-Cadherin+ Osteoblasts (SNOs) contribute to the endosteal niche involved in BrCa dormancy. First, we characterized the Notch1 and Notch2 molecular phenotypes of various BrCa cell lines, selecting the MDA-MB231 (MDA) human cell line as leading cellular tool for the study. Next, we performed a global transcriptomic analysis to examine the Gene Ontology (GO) and Kyoto Encyclopedia of Genes and Genomes (KEGG) pathways to establish the Notch1<sup>High</sup> and Notch2<sup>High</sup> dormant cells molecular signatures. From this analysis, we extrapolated that only MDA Notch2<sup>High</sup> cells express a dormant signature determining cellular quiescence along with pluripotent features and hematopoietic stem cell (HSC)-like phenotype. Furthermore, we identified the molecular interactome binding Notch2<sup>High</sup> BrCa cells to SNOs and recognized the glycosylphosphatidylinositol (GPI)-linked surface glycoprotein, CD177, as a potential master molecular pathway involved in SNO-induced BrCa cellular dormancy.

## 2. INTRODUCTION

Cellular dormancy is the mechanism whereby single metastatic cancer cells lodge in the host tissue remaining cell cycle arrested for long time.<sup>5</sup> These cells have high risk of reactivation, relapsing overt metastases also after decades from apparent cancer healing.<sup>5</sup> The bone marrow is a preferential site of BrCa metastases<sup>6</sup>, and cellular dormancy is a typical event that prevents permanent cancer remission after therapy.<sup>7</sup> Understanding the cellular and molecular mechanisms of dormancy in the bone marrow could provide a solid background to identify ways to permanently eradicate dormant cells or to prevent their long-term reactivation and spreading in bone and other organs, lastingly curing BrCa.

The endosteum is the layer of cells that covers the inner surface of the bone facing the bone marrow.<sup>8</sup> It is mainly made by osteogenic cells, called osteoblasts when they are active in the bone formation process, and lining cells when they become quiescent at the end of bone deposition. They also include a subset of cells supporting long-term hematopoiesis and regulating the size of the myeloid cell pool.<sup>8</sup> These cells are known as Spindle-shaped N-cadherin+CD45- osteoblasts (SNOs)<sup>9</sup> and represent a Hematopoietic Stem Cell (HSC) niche.<sup>9</sup> An increase of SNOs is associated with a parallel increase of HSCs. Furthermore, the most primitive Long-Term (LT)-HSCs bind SNOs, with the anchoring junction molecules, N-Cadherin and  $\beta$ -catenin, observed at the SNO-LT-HSC interface<sup>10</sup>. The SNO-LT-HSC interaction is regulated by bone morphogenetic protein and Parathyroid Hormone (PTH)<sup>11</sup> signals. Notably, PTH-activated osteoblasts express high levels of the Notch ligand, Jagged 1, and support the HSC pool expansion with a mechanism involving Notch1 expressed by HSCs.<sup>12</sup> Like LT-HSCs, dormant BrCa cells interact with SNOs at the endosteal interface.<sup>13</sup> In fact, in our laboratory it was previously demonstrated that single, non-proliferating BrCa cells lodge in proximity of the endosteal surface, remaining quiescent for long time. They also compete with HSCs for bone marrow engraftment, showing molecular similarities with this stem cell pool<sup>14</sup>. SNOs are enriched in the endosteal areas where dormant BrCa cells are recruited, show lower expression of osteoblast-specific genes, and are confirmed to be enriched in the Notch ligand, Jagged 1.<sup>14,15</sup>

Among the Notches expressed by BrCa cells, Notch2 promotes their interactions with SNOs, with a mechanism blunted by the  $\gamma$ -secretase inhibitor, dibenzazepine.<sup>14</sup> Notch2<sup>High</sup> BrCa cells represent a small population within the tumor, exhibiting also stem-like features<sup>14</sup>, and are observed likewise in human BrCa tissues in which they show the ability to lodge as single cells at the endosteal surface of human bone metastases.<sup>14</sup> In previous

study, we observed that Notch1 is also more expressed in a subset of BrCa dormant cells, although at lower level compared to Notch2, but its contribution to the interaction with SNOs was not clarified. In contrast, Notch3 and Notch4 appeared irrelevant.<sup>14</sup>

In this study, we aimed at structuring the molecular features of BrCa cells lodging the bone environment, focusing on the Notch1 and Notch2 pathways as determinant of the dormant phenotype. To this end, we characterized the Notch1- and Notch2-related molecular phenotypes of various BrCa cell lines, selecting the MDA human cell line as leading cellular tool for the study. We performed a global transcriptomic analysis to examine the Gene Ontology (GO) and the Kyoto Encyclopedia of Genes and Genomes (KEGG) pathways and establish the Notch1<sup>High</sup> and Notch2<sup>High</sup> BrCa cell molecular signatures. From this analysis, we extrapolated that Notch2<sup>High</sup> cells express a dominant signature determining the molecular alterations of dormant cells and preserving their pluripotent and HSC-like phenotype. Furthermore, we identified the molecular interactome binding Notch2<sup>High</sup> BrCa cells to SNOs, recognizing the glycosylphosphatidylinositol (GPI)-linked surface glycoprotein, CD177, as a potential master molecular pathway involved in SNO-induced BrCa cellular dormancy.

### **3. MATERIAL AND METHODS**

#### **3.1 *Materials***

Dulbecco's Modified Eagles's Medium (DMEM) (cat: ECB7501L) penicillin–streptomycin (cat: ECB3001D), Dulbecco's Phosphate Buffered Saline (DPBS) (cat: ECB4004L), Hanks' Balanced Salt Solution (cat: ECB4007L) and disposable plastic were from Euroclone (Milan, Italy). Foetal bovine serum (FBS) (cat: 26140-079), Ethylene-Diamine-Tetra-acetic Acid (EDTA) (cat: 15576-028), TRIzol® (Life Technologies, cat: 15596018), and primers synthesis were from Invitrogen (Carlsbad, CA). cDNA Synthesis Kit (cat: K1622), RPMI 1640 (31870074) and ProLong™ Diamond Antifade Mountant with DAPI (cat: P36966) were from ThermoFisher. OneTaq® Hot Start 2X Master Mix (cat: M0484S) and Luna® Universal qPCR Master Mix (cat: M3003) was from New England BioLabs (Massachusetts, USA). Osteodec (cat: 05-03005E) and all reagents for histology were from Bio-Optica (Milano, Italy). BrCa tissue array was from BioChain® (Newark, CA, USA) (cat: T8235721-5). All reagents for Magnetic-Activated Cell Sorting (MACS) were from Miltenyi Biotec (Germany). All other reagents, including Bovine Serum Albumin (BSA) (cat: A9418), the protease inhibitor cocktail (cat: P8340) and Clostridium histolyticum type IV collagenase (cat: C8051) were from Sigma Aldrich Co.

(St. Louis, MO, USA). The trypsin powder (cat:85450 C) were from SAFC Biosciences. The Bradford Solution for protein determination (A6932) was from Panreac Applichem. Primers sequences used are listed in Table 1. Supplier, product code and dilution of primary and secondary antibodies used for the study are listed in Table 2.

**Table 1.** Primers sequences Fw: Forward, Rv: Reverse

<b>Primer Name</b>	<b>Sequence</b>
<b>Human</b>	
<i>Gapdh</i>	Fw: CAATCTTCCAGGAGCGAGAT Rv: CAGTGATGGCATGGACTGTG
<i>Notch1</i>	Fw: CTTCAATGACCCCGGAAGA Rv: GAAGTGGAAAGGAGCTCTTGC
<i>Notch2</i>	Fw: CTGGAGTACAGGAGGCGAAG Rv: ATGACTGCCCTAACCACAGG
<i>Cxcr4</i>	Fw: GACGCCAACATAGACCACCT Rv: CTGAGAAGCATGACGGACAA
<i>CD34</i>	Fw: GCCGAGTCACAATTCGGTAT Rv: GCAAGCCACCAGAGCTATTC
<i>Tie-2</i>	Fw: TGTGAAGCGTCTCACAGGTC Rv: CCAAACGTGATTGACACTGG
<i>CyclinD1</i>	Fw: CCTTCCGGTGTGAAACATCT Rv: AGCGCTGTTTTTGTGTGTG
<i>CD24</i>	Fw: GGCTCAGATTCAGGAACAGC Rv: GCTTCAACGGCAAAGTTCTC
<i>CD44</i>	Fw: TGCCCAGAAAATGAAAAGG Rv: GGATGACACAGCGTGAGAGA
<i>ALDH1A2</i>	Fw: TGATCCTGCAAACACTGCTC Rv: CTGGAGCTGGGTGGTAAGAG
<i>CD177</i>	Fw: CAGAAGAGATCTGCCCAAG Rv: AATTTTGAGCCCAACAGTG
<i>CD163L1</i>	Fw: GGGACACAGGTTTCATTGCT Rv: GCCGTTTGTCTCTAAGCAG
<i>NOTCH4</i>	Fw: GGCTTCTACTCCGCTTCCTT Rv: CAACTTCTGCCTTTGGCTTC
<i>IFITM1</i>	Fw: ATGTCGTCTGGTCCCTGTTC Rv: GTCATGAGGATGCCCAGAAT
<i>CD22</i>	Fw: CCGAGATGAACATACCACGA Rv: GAGCAGGTCCACTTCTGGAG
<i>JAG2</i>	Fw: AGGTGGAGACGGTTGTTACG Rv: TTGCACTGGTAGAGCACGTC
<i>KDR</i>	Fw: GTGACCAACATGGAGTCGTG Rv: TGCTTCACAGAAGACCATGC

<i>CD55</i>	Fw: CAGCACCACCACAAATTGAC Rv: CTGAACTGTTGGTGGGACCT
<i>CD63</i>	Fw: TCCCTTCCATGTCTGAAGAAC Rv: TCCCAAACCTCGACAAAAG
<b>Mouse</b>	
<i>Plaur</i>	Fw: CCACAGCGAAAAGACCAACA Rv: TCCTTTCTGTGCTCTGGAGG
<i>Itgam</i>	Fw: CCATCCCATCTTTCCTGCTA Rv: GGATGATCCCATACGGTCAC
<i>Ceacam 1</i>	Fw: CCTTGGCCTCTGCTACTGTC Rv: CAGAGGGTGTGCCTTAGCTC
<i>Cd180</i>	Fw: CCCAACAGAGAAGCTGAAGG Rv: TCGTCATCCATGTCTCTCAA

**Table 2.** Antibodies information. IF: Immunofluorescence; IHC: Immunohistochemistry; FACS: fluorescence-activated single cell sorting; WB: Western Blot

<b>Antibody</b>	<b>Dilution</b>	<b>Specie</b>	<b>Cat #</b>	<b>Company</b>
<b>Ki67</b>	(IF)1:500	Rabbit	MA5-14520	ThermoFisher
<b>Notch1</b>	(IF) 1:200	Mouse	sc-32745	Santa Cruz Biotechnology
<b>Notch1-BV510</b>	(FACS)1:50	Mouse	743907	BD Biosciences
<b>Notch1-FITC</b>	(FACS)1:50	Mouse	MA5-16862	ThermoFisher
<b>Notch1-PE</b>	(FACS)1:50	Mouse	563421	BD Biosciences
<b>Notch2</b>	(FACS)1:50 (IF) 1:200	Rabbit	sc5545	Santa Cruz Biotechnology
<b>Notch2-BV786</b>	(FACS)1:50	Mouse	742294	BD Biosciences
<b>CD177</b>	(IF)1:200 (WB)1:500	Rabbit	PA5-83575	Invitrogen
<b>CD163L1</b>	(IF)1:500 (WB) 1:1000	Rabbit	PA5-53362	Invitrogen
<b>CD55</b>	(IF) 1:200 (WB) 1:500	Rabbit	PA5-82005	Invitrogen
<b>IFITM1</b>	(IF) 1:200	Rabbit	PA5-82165	Invitrogen
<b>β-ACTIN</b>	(WB) 1:500	Mouse	sc-47778	Santa Cruz Biotechnology
<b>AlexaFluor488 anti-mouse</b>	(IF) 1:500	Goat	A11001	Invitrogen
<b>AlexaFluor488 anti-rabbit</b>	(IF) 1:500	Goat	A11008	Invitrogen
<b>AlexaFluor594 anti-mouse</b>	(IF) 1:500	Goat	A11005	Invitrogen

<b>AlexaFluor594 anti-rabbit</b>	(IF) 1:500	Goat	A11037	Invitrogen
<b>Goat Anti-Rabbit IgG-HRP</b>	(WB) 1:3000	Goat	1706515	BioRad
<b>Goat Anti-Mouse IgG-HRP</b>	(WB) 1:3000	Goat	1706516	BioRad

### 3.2 *Animals*

The in vivo studies were conducted in agreement with the national and international guidelines and policies (European Economic Community Council Directive 86/609, OJ L 358, 1, December 12, 1987; Italian Legislative Decree 4.03.2014, n.26, Gazzetta Ufficiale della Repubblica Italiana no. 61, March 4, 2014) and were approved by the Italian Ministry of Health (N.270/2018-PR; N.1551/2020-PR). Mice were humanely sacrificed by CO<sub>2</sub> inhalation. The study was performed according to the Animal Research: Reporting of In Vivo Experiments (ARRIVE) guidelines.

### 3.3 *Human samples*

BrCa tissue arrays were purchased by BioChain® (Newark, CA, USA) (cat: T8235721-5). They included 64 different samples of primary tumors. BrCa tissue array donor information are in table 6 (Chapter 2).

### 3.4 *Cell lines*

The human BrCa cell lines MDA, parental or transfected with the turbo GFP plasmid (MDA<sup>GFP</sup>), T47D, ZR75D, BT474 and the murine BrCa cell line 4T1 were purchased from ATCC® and cultured in high glucose Dulbecco's Modified Eagle Medium (DMEM) or RPMI 1640, with the addition of 1% glutamine, 1% penicillin–streptomycin and 10% FBS. Cells were trypsinised and used for experiments as described in the specific sections.

### 3.5 *Primary osteoblast cell isolation*

Murine osteoblasts were isolated from the calvarias of 7–10-day old CD1 mice. Calvarias underwent 3 steps of incubation at 37 °C with a digestion solution containing trypsin (25 mg/ml) and clostridial type IV collagenase (1 mg/ml) in Hanks' Balanced Salt Solution. Cells from the second and third digestions were osteoblast enriched and pulled together for the experiments.

### 3.6 *Magnetic-Associated Cell Sorting (MACS)*

Cells were detached and suspended in sterile sorting buffer containing 5% BSA and 0.5M EDTA in DPBS. Cell suspensions were incubated for 20 min at 4 °C with primary antibody (3  $\mu\text{L}/10^6\text{--}10^7$  cells) against the surface protein of interest. Then cells were incubated in the same conditions with anti-PE antibody or streptavidin, respectively, conjugated to magnetic microbeads (20  $\mu\text{L}/10^7$  cells). Afterwards, cells were run through the magnetic column to obtain separate antigen-depleted and antigen-enriched cell populations.

### 3.7 *Flow cytometry*

Cells were detached and suspended in sterile sorting buffer containing 5% bovine serum albumin (BSA) and 0.5M EDTA in DPBS. Cell suspensions were incubated for 1 h at 4 °C with 10  $\mu\text{L}$  per  $10^7$  cells of primary antibodies against Notch2-BV786 or Notch1-BV510, Notch1-FITC or Notch1-PE. After a wash in PBS, cells were analyzed using FACS canto II equipped with the FACS Diva software.

### 3.8 *Osteoblast/BrCa cell coculture assay*

Mouse primary calvarial osteoblasts were MACS-sorted into SNOs or NON-SNOs using anti-N-Cadherin-biotin antibody and Streptavidin-conjugated magnetic microbeads, as described above.  $7 \times 10^4\text{--}1 \times 10^5$  sorted cells were seeded in 96-well plates and incubated overnight in a humidified  $\text{CO}_2$  incubator (5%  $\text{CO}_2$ , 37°C). For the T47D BrCa cell line, the cells were labeled with the stable membrane inter-linker, PKH26 following the manufacturer's instructions.  $1 \times 10^3$  T47D<sup>PKH26</sup> or MDA<sup>GFP</sup>, MACS-sorted into Notch1<sup>High</sup> and Notch1<sup>Low</sup> or Notch2<sup>High</sup> and Notch2<sup>Low</sup> were seeded on SNO or NON-SNO monolayers as above. After 1 h, cultures were extensively washed and the number of PKH26+ or GFP+ cells were counted using an Olympus Fluoview IX81 confocal microscope. The counting was performed after 72 h.

### 3.9 *Transcriptome analysis*

The first step of the bioinformatic analysis was performed by GATC Biotech. Briefly, RNA dSeq reads were aligned to the reference transcriptome (GRCh38.p13, Ensembl; v85 Ensembl) using Bowtie transcriptome alignments. TopHat identified the potential exon-exon splice junctions of the initial alignment. Then Cufflinks identified and quantified the transcripts from the pre-processed RNA dSeq alignment assembly. After this, Cuffmerge merged the identified transcript pieces to full-length transcripts and annotated the transcripts based on the given annotations. Finally, merged transcripts from the two

samples were compared using Cuffdiff to determine the differential transcriptional expression levels at the transcript level between samples. After the analyses, the generated RNA dSeq datasets, containing the expression profile of 36,000 genes for each sample/condition, were used for the Gene Ontology (GO) and Kyoto Encyclopedia of Genes and Genomes (KEGG) pathway enrichment analyses using clusteProfiler tool in R environment.<sup>16,17</sup>

### 3.10 *Gene ontology and pathway analyses*

Normalized differential gene expression data generated by RNA dSeq was analyzed by the R package, clusterProfiler.<sup>16,17</sup> This uses an online database to remove any effect that gene length may have on the expression levels of certain genes. The package then calculates which GO categories are significantly enriched with differentially expressed genes. GO terms were considered significantly enriched in differentially expressed genes if they had a Benjamini-Hochberg adjusted  $p < 0.05$ . GO graphical representation was done using the R package ggplot2.<sup>18</sup> The R package clusterProfiler<sup>16,17</sup> was also used to identify the enrichment of differentially expressed genes in KEGG pathways. KEGG pathways with a Benjamini-Hochberg adjusted  $p < 0.05$  were considered significantly enriched by differentially expressed genes. To prevent high false discovery rate (FDR) in multiple testing, q-values<sup>19</sup> are also estimated for FDR control. The R scripts used are reported in Table 3.

**Table 3.** Script used for bioinformatic analysis in R environment.

<b>Analysis</b>	<b>Script</b>
<b>Gene Ontology (GO)</b>	<pre> #Load library library(readxl) library(enrichplot) library(clusterProfiler) library(ggplot2) # Load data sets seqdata &lt;- read_excel("excel file") str(seqdata)  #trasformo in data frame seqdata_df &lt;- data.frame(seqdata)  # Split the differentially expressed genes using foldchange &gt; or &lt; 0 seqdata_split_df &lt;- split(seqdata, seqdata\$log2FoldChange &gt; 0) seqdata_down_df &lt;- data.frame(seqdata_split_df[["FALSE"]]) seqdata_up_df &lt;- data.frame(seqdata_split_df[["TRUE"]])  # Select the differentially expressed genes using p = 0.05 </pre>



---

```

input_up_df<- seqdata_up_df[seqdata_up_df$pvalue<0.05,]
input_down_df<-
seqdata_down_df[seqdata_down_df$pvalue<0.05,]

## Create vector of gene names for all genes
library('org.Hs.eg.db')
gene_ID_up<-mapIds(org.Hs.eg.db, input_up_df$GeneName,
'ENTREZID', 'SYMBOL')
gene_ID_up_vec<- as.vector(gene_ID_up)

gene_ID_down<-mapIds(org.Hs.eg.db,
input_down_df$GeneName, 'ENTREZID', 'SYMBOL')
gene_ID_down_vec<- as.vector(gene_ID_down)

# GO analysis with clusterProfiler (enrichGO)

#enriched GO terms
ego_tot_up <- enrichGO(gene = gene_ID_up_vec,
OrgDb= "org.Hs.eg.db",
ont = "ALL", pAdjustMethod = "BH",
pvalueCutoff = 0.05)
dotplot(ego_tot_up,          split="ONTOLOGY")          +
facet_grid(ONTOLOGY~., scale="free")

#unenriched GO terms
ego_tot_down <- enrichGO(gene = gene_ID_down_vec,
OrgDb= "org.Hs.eg.db",
ont = "ALL", pAdjustMethod = "BH",
pvalueCutoff = 0.05)
dotplot(ego_tot_down,          split="ONTOLOGY")          +
facet_grid(ONTOLOGY~., scale="free")

```

---

### KEGG pathway

```

#Load library
library(readxl)
library(enrichplot)
library(clusterProfiler)
library(ggplot2)
# Load data sets
seqdata <- read_excel("excel file")
str(seqdata)

#trasformo in data frame
seqdata_df <-data.frame(seqdata)

# Split the differentially expressed genes using foldchange > or
< 0
seqdata_split_df <- split(seqdata, seqdata$log2FoldChange>0)
seqdata_down_df<- data.frame(seqdata_split_df[["FALSE"]])
seqdata_up_df<- data.frame(seqdata_split_df[["TRUE"]])

# Select the differentially expressed genes using p = 0.05

```

---

---

```

input_up_df<- seqdata_up_df[seqdata_up_df$pvalue<0.05,]
input_down_df<-
seqdata_down_df[seqdata_down_df$pvalue<0.05,]

## Create vector of gene names for all genes
library('org.Hs.eg.db')
gene_ID_up<-mapIds(org.Hs.eg.db, input_up_df$GeneName,
'ENTREZID', 'SYMBOL')
gene_ID_up_vec<- as.vector(gene_ID_up)

gene_ID_down<-mapIds(org.Hs.eg.db,
input_down_df$GeneName, 'ENTREZID', 'SYMBOL')
gene_ID_down_vec<- as.vector(gene_ID_down)

# KEGG pathway analysis with clusterprofiler (enrichKEGG)
#enriched KEGG pathways
kegg_up <- enrichKEGG(gene_ID_up_vec,
organism = "hsa",
keyType = "kegg",
pvalueCutoff = 0.05,
pAdjustMethod = "BH")
dotplot(kegg_up)

#unenriched KEGG pathways
kegg_down<- enrichKEGG(gene_ID_down_vec,
organism = "hsa",
keyType = "kegg",
pvalueCutoff = 0.05,
pAdjustMethod = "BH")
dotplot(kegg_down)

```

---

### 3.11 *Gene Set Enrichment Analysis (GSEA)*

Data from our RNA dSeq datasets were crossed with datasets containing pluripotency and HSC gene signatures using the Gene Set Enrichment Analysis (GSEA) software.<sup>20</sup>

The normalized enrichment score (NES) was used to analyze the gene set enrichment results by accounting for differences in gene set size and in correlations between gene sets and the expression dataset.

### 3.12 *Real time and semi-quantitative RT-PCR*

Total RNA was extracted using Trizol® reagent and quantified by Nanodrop. RNA quality was evaluated by 1% agarose gel run. For cDNA synthesis, 1 µg of RNA was reverse transcribed using the RevertAid First Strand cDNA Synthesis Kit. Real time PCR reaction was performed loading 0.1 µg of cDNA using the Luna® Universal qPCR Master Mix. Gene expression data were represented as fold change over the control and normalized by *GAPDH*. Conventional PCR reaction was performed loading 0.2 µg of cDNA using the

OneTaq® Hot Start 2X Master Mix and the relative primers. Samples were analyzed by 2% agarose gel run. The samples were normalized by *GAPDH*. Primer sequences are listed in Table 1.

### 3.13 *Western blot*

Cells were lysed in standard Radio Immuno Precipitation Assay (RIPA) buffer (1 M Tris/HCl, pH 7.4, 1 M NaCl, Nonidet P-40, 10% sodium deoxycholate, 0.5 M EDTA, pH 8, 0.1 M NaF, 20 mM Na<sub>3</sub>VO<sub>4</sub>, dH<sub>2</sub>O, 0.1 M PMSF) containing 1% protease inhibitor cocktail and 10 μM sodium fluoride. Proteins concentration was quantified using the Bradford assay. For Western blot, protein lysates (20 μg) were resolved by SDS-PAGE, immunoblotted with primary antibody for CD177, CD163L1 and CD55 overnight at 4°C, detected by horseradish peroxidase (HRP)-conjugated secondary antibodies and enhanced by chemiluminescence on a ChemiDoc® imaging system.

### 3.14 *In vivo studies*

MDA cells were injected into the left tibia of 4-week-old, female CD1 nu/nu mice (1×10<sup>5</sup>/0.01 ml PBS) anesthetized with intraperitoneal injection of 80 mg/kg of ketamine and 10 mg/kg of xylazine, using standard procedures. Animals were monitored daily for body weight, behavior, and survival. Weekly, mice were also subjected to deep anesthesia and X-ray analysis (peak kilovoltage [kVp] = 36 kV for 10 s) using a Cabinet X-ray system (Faxitron model no.43855A; Faxitron X-Ray Corp., Buffalo Grove, IL, USA) to follow the onset and progression of osteolytic lesions. At the end of the experiment, mice were euthanized and subjected to final X-ray analysis and anatomical dissection for evaluation of bone metastasis.

### 3.15 *Micro-computed tomography*

Images from tibias fixed in 4% paraformaldehyde were acquired in a SkyScan 1174 with a resolution of 6 μm (X-ray voltage 50 kV). Skyscan Nrecon software was used to employ the Feldkamp algorithm to reconstruct the images. Three- and two-dimensional (3D and 2D, respectively) morphometric parameters were calculated for the cortical bone. Segmentation of the bone was conducted using threshold values corresponding to bone mineral density values of 0.6 cm<sup>3</sup> calcium hydroxyapatite. Marching cube-type models with a rendered surface formed the basis of the 3D parameters.

### 3.16 *Histology*

Bone samples were fixed in 4% paraformaldehyde, decalcified for 48 h in Osteodec (Bio-Optica, cat: 05-03005E) and, after a wash with PBS, they were embedded in paraffin using the automatic paraffin embedder (Leica, TP1020). Microtome sectioning was used to obtain tissue slices of 5- $\mu$ m thickness.

### 3.17 *Immunohistochemistry and immunofluorescence*

For immunohistochemistry, human primary BrCa tissue arrays were deparaffined and incubated with 0.07 M citrate buffer (pH 6) for 30 min at 96°C and for 10 min at room temperature. The blocking was made with 3% H<sub>2</sub>O<sub>2</sub> and 5% BSA. Then samples were incubated overnight at 4°C with primary antibodies against Notch1 or Notch2. The staining signals were revealed using the SignalStain® Boost IHC Detection Reagent (HPR rabbit or mouse). Sections were counterstained using Gill's No.3 hematoxylin for 10 s. Positive and negative controls were performed in parallel.

For immunofluorescence, cells and tissue sections were labelled with antibodies against human Notch1, Notch2, CD177, CD163L1, CD55, IFITM1 or Ki-67 1:200–1:500, either singularly or in combinations as double immunofluorescences. For all samples, primary antibody incubations were carried out at room temperature for 1 h, then overnight at 4 °C, followed by secondary incubations for 1 h at room temperature with the corresponding secondary antibody at dilution 1:500. Immunofluorescence quantification was done using the Fiji® by Image-J software.

### 3.18 *Statistical analysis*

Data from RNA dSeq analysis are representative of three mRNA datasets derived from 3 independent cultures. For the differential gene expression in Notch 1 and Notch2 High and Low cells, an uncorrected p-value generated by the Cuffdiff analysis was used. The statistical significance for the enrichment analyses was computed using a Benjamini-Hochberg adjusted  $p < 0.05$ . A  $p\text{-value} \leq 0.05$  was considered statistically significant. The statistical methods used for the analyses are reported in the figure legends. Real time RT-PCR and Western blot statistical analyses were carried out using the unpaired Student's t-test with the software Prism® by GraphPad v7.0. p-Values threshold was  $<0.05$ .

## 4. RESULTS

### 4.1. *Notch1 and Notch2 expression in BrCa cells*

To investigate whether Notch1 and Notch2 were expressed in human primary BrCa cells, we performed double immunofluorescence for Notch1 and Notch2 in human BrCa tissue and associated bone metastasis derived from our internal tissue biobank. Figure 1a shows cancer cells co-expressing Notch1 and Notch2. Similar Notch1 and Notch2 co-staining was observed in single cancer cells located near the endosteum in a sample of human BrCa-associated bone metastasis (Figure 1b). Furthermore, single immunohistochemistry for Notch1 and Notch2 in serial sections of human BrCa tissue array revealed a higher number of Notch1<sup>High</sup> cells compared to Notch2<sup>High</sup> cells in contiguous sections. Most Notch1<sup>High</sup> cells were Notch2<sup>Low</sup> (yellow arrows), while only a small number was positive to both Notches (red arrows) (Figure 1c). Quantitative evaluations confirmed that Notch1<sup>High</sup> cells were more numerous in primary BrCas compared to Notch2<sup>High</sup> cells (Figure 1d), with no differences associated with the grade of tumor differentiation (Figure 1e). In contrast, Notch2<sup>High</sup> cells were less numerous in moderately and poorly differentiated cancers versus well differentiated cancers (Figure 1f). The Notch1 and Notch2 expression showed no association with the receptor status of the human primary cancers (Figure 1g, h). Furthermore, *in vitro* analysis on Notch2<sup>High</sup> MDA cells demonstrated that about half of them were also Notch1<sup>High</sup> (Figure 1i, j), prompting us to investigate the functional interactions between these two molecular determinants. FACS analysis on a variety of BrCa cell lines confirmed that a small population of the total human MDA co-expressed Notch1 and Notch2 (Figure 2a) and unveiled a similar co-expression in small populations of human ZR75D cells (Figure 2b), and mouse 4T1 cells (Figure 2c). In contrast, human T47D cells were Notch2-negative and presented a small Notch1<sup>High</sup> population (Figure 2d), while human BT474 cells were Notch1-negative while expressing a small Notch2<sup>High</sup> population (Figure 2e). These observations confirmed the paucity of the Notch1 and Notch2 populations in several BrCa cell lines and demonstrated heterogeneity in the Notch1<sup>High</sup>/Notch2<sup>High</sup> co-expression.

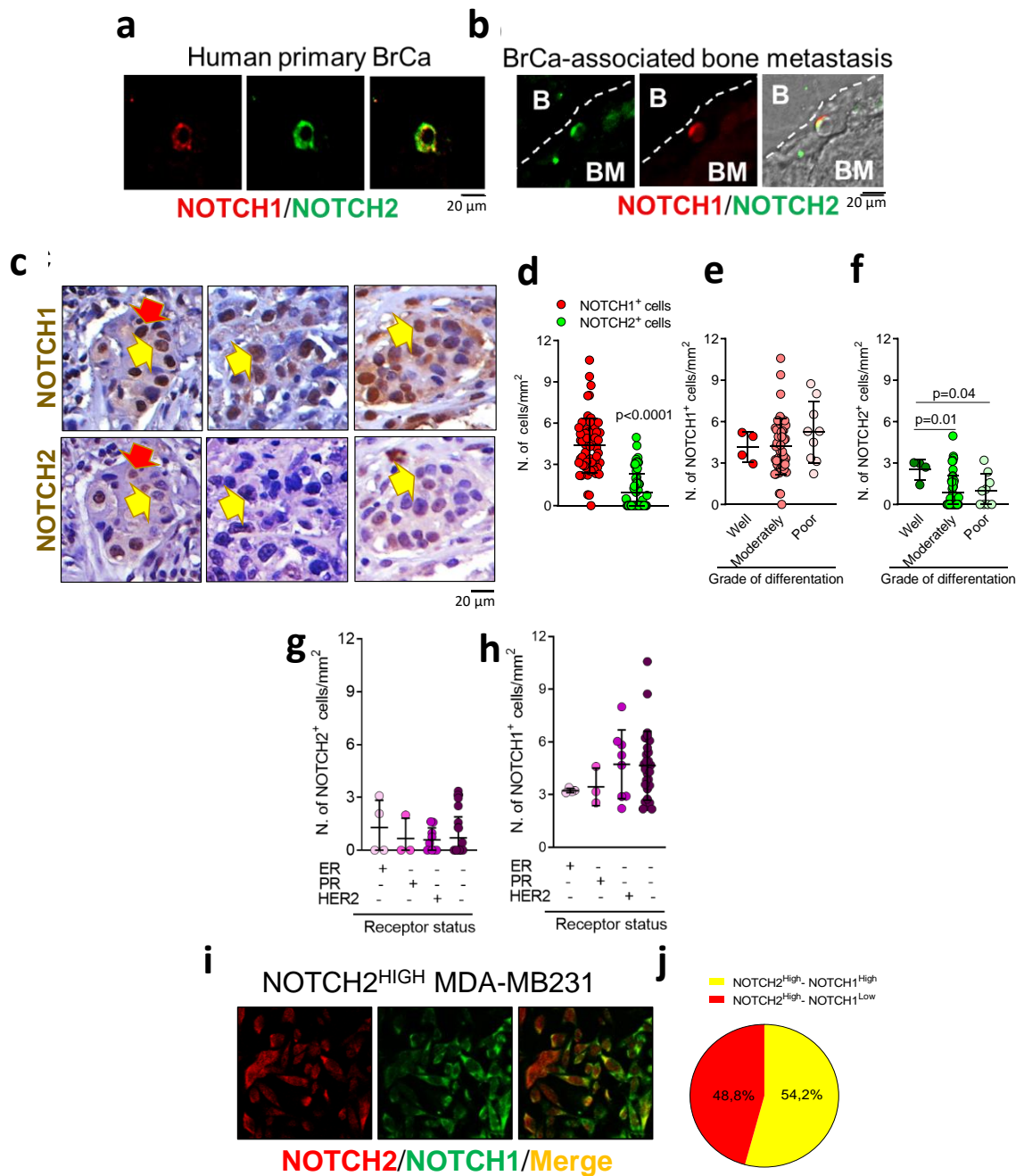


**Figure 1. Notch1 and Notch2 expression in human BrCa samples.** (a) Human primary BrCa tissue and (b) associated bone metastasis, derived from our internal tissue biobank, stained by double immunofluorescence for Notch1 and Notch2. (c) Serial sections of human BrCa tissue arrays analyzed by single immunohistochemistry for Notch1 or Notch2. Yellow arrows: Notch1+ BrCa cells, red arrows: Notch1+Notch2+ BrCa cells. (d) Notch1+ or Notch2+ BrCa cell number quantified counting the number of positive cells/mm<sup>2</sup>. Results were also stratified for (e, f) tumor grade and the (g, h) receptor status. (i) MDA cells were sorted in Notch2<sup>High</sup> and Notch2<sup>Low</sup> by MACS. Notch2<sup>High</sup> MDA cells were stained for Notch1 and Notch2 by immunofluorescence. (j) Quantification of single positive Notch2<sup>High</sup> (red) or double positive Notch1<sup>High</sup>Notch2<sup>High</sup> (yellow) subpopulations. Statistical analysis: (d, e, f, g, h) Student's t-test.

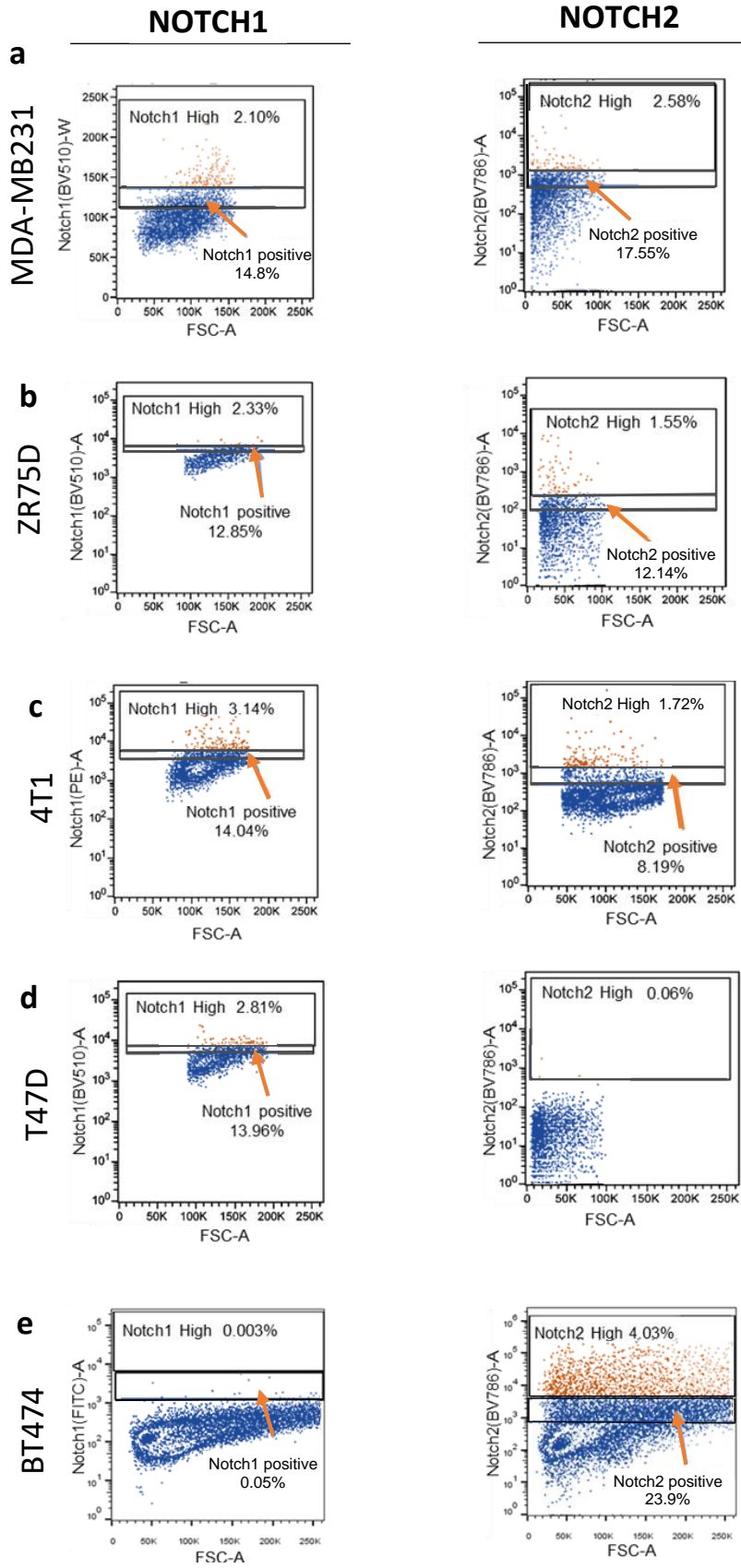


**Figure 2. Notch1 and Notch2 expression in BrCa cell lines.** Flow cytometry analysis of Notch1 and Notch2 expression in (a) MDA-MB231, (b) ZR75, (d) T47D, (e) BT474 and (c) 4T1. Dot plots show the gating strategy to identify the Notch1<sup>+</sup> or Notch2<sup>+</sup> subpopulations (arrows) and the Notch1<sup>High</sup> or Notch2<sup>High</sup> subpopulations (squares). Data are expressed as % over the total population.

#### 4.2. *Role of Notch1 and Notch2 in the interaction of BrCa cells and SNOs*

Notch2<sup>High</sup> MDA cells are known to proliferate less than Notch2<sup>Low</sup> cells when interacting with SNOs.<sup>14</sup> To investigate if Notch1 played a similar role as Notch2, we plated MDA<sup>GFP+</sup> cells MACS-sorted for Notch1<sup>High</sup>, Notch1<sup>Low</sup>, Notch2<sup>High</sup> and Notch2<sup>Low</sup> onto NON-SNO and SNO monolayers, and performed GFP<sup>+</sup> cell counting after 72 hours of co-culture. Results demonstrated that Notch1<sup>High</sup> and Notch2<sup>High</sup> MDA cells were less numerous compared to Notch1<sup>Low</sup> and Notch2<sup>Low</sup> cells (Figure 3a, b) plated on SNOs and on NON-SNOs, and to Notch1<sup>High</sup> and Notch2<sup>High</sup> cells plated on NON-SNOs. However, given that about 50% of the two sorted populations shared high levels of both Notch1 and Notch2 (see Figure 1i, j), this experiment did not clarify the roles of each of the two Notches in the SNO-induced MDA cell dormancy. To remove the confounding effects of the co-expression of Notch1 and Notch2, we performed a similar experiment using T47D cells sorted for Notch1<sup>High</sup>, which were shown to be negative for Notch2 (Figure 2d). In this experiment, cells were loaded with the impermeant cell surface fluorescent dye PKH26, whose fluorescence decreases at each doubling of the cells. Results showed a similar proliferation rate of PKH26-positive cells in each condition tested, demonstrated by the reduced number of PKH26-positive cells in all of them (Figure 3c), ruling out a role of Notch1 in SNO-induced cancer cell dormancy.

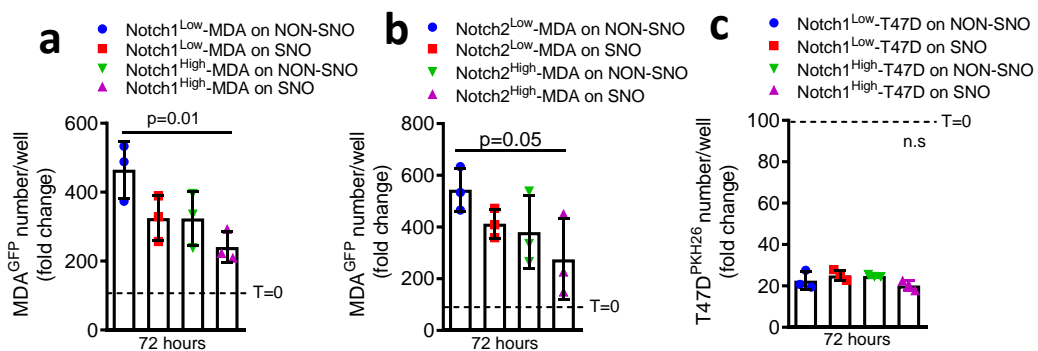


**Figure 3. Role of Notch1 and Notch2 in the BrCa-SNO interaction in vitro.** (a) MDA<sup>GFP</sup> cells MACS-sorted for Notch1 or (b) Notch2, and (c) T47D<sup>PKH26</sup> cells MACS-sorted for Notch1 were seeded onto SNO and NON-SNO monolayers. Number of MDA<sup>GFP</sup> or T47D<sup>PKH26</sup> cells counted at time = 0 (after 1 h of adhesion) and after 72 h of co-culture. Data are the mean±SD of at least 3 independent cell preparations. Statistical analysis: Student's t-test.



#### 4.3. RNAdSeq and Gene Ontology (GO) analysis of the differentially expressed mRNAs in Notch1 and Notch2 High and Low cells

To further characterize the molecular and functional differences between the Notch1<sup>High</sup> and Notch2<sup>High</sup> cell subsets, we settled a broad approach by RNAdSeq analysis, focusing on the MDA cells as primary cellular model. We used a “systemic and systematic” strategy to identify transcriptional differences between MDA cells MACS-sorted for Notch1<sup>High</sup>, Notch1<sup>Low</sup>, Notch2<sup>High</sup> and Notch2<sup>Low</sup> expression. We found 522 genes differentially expressed in the Notch1<sup>High</sup> vs Notch1<sup>Low</sup> cells and 1799 genes differentially expressed in the Notch2<sup>High</sup> vs Notch2<sup>Low</sup> cells (Figure 4 a, b). Then, by bioinformatic analysis the upregulated and downregulated transcripts were normalized and grouped according to the represented biological processes (BPs), molecular functions (MFs) and cellular components (CCs) GO terms and pathways, focusing on the differentially expressed transcripts identified for each condition tested.

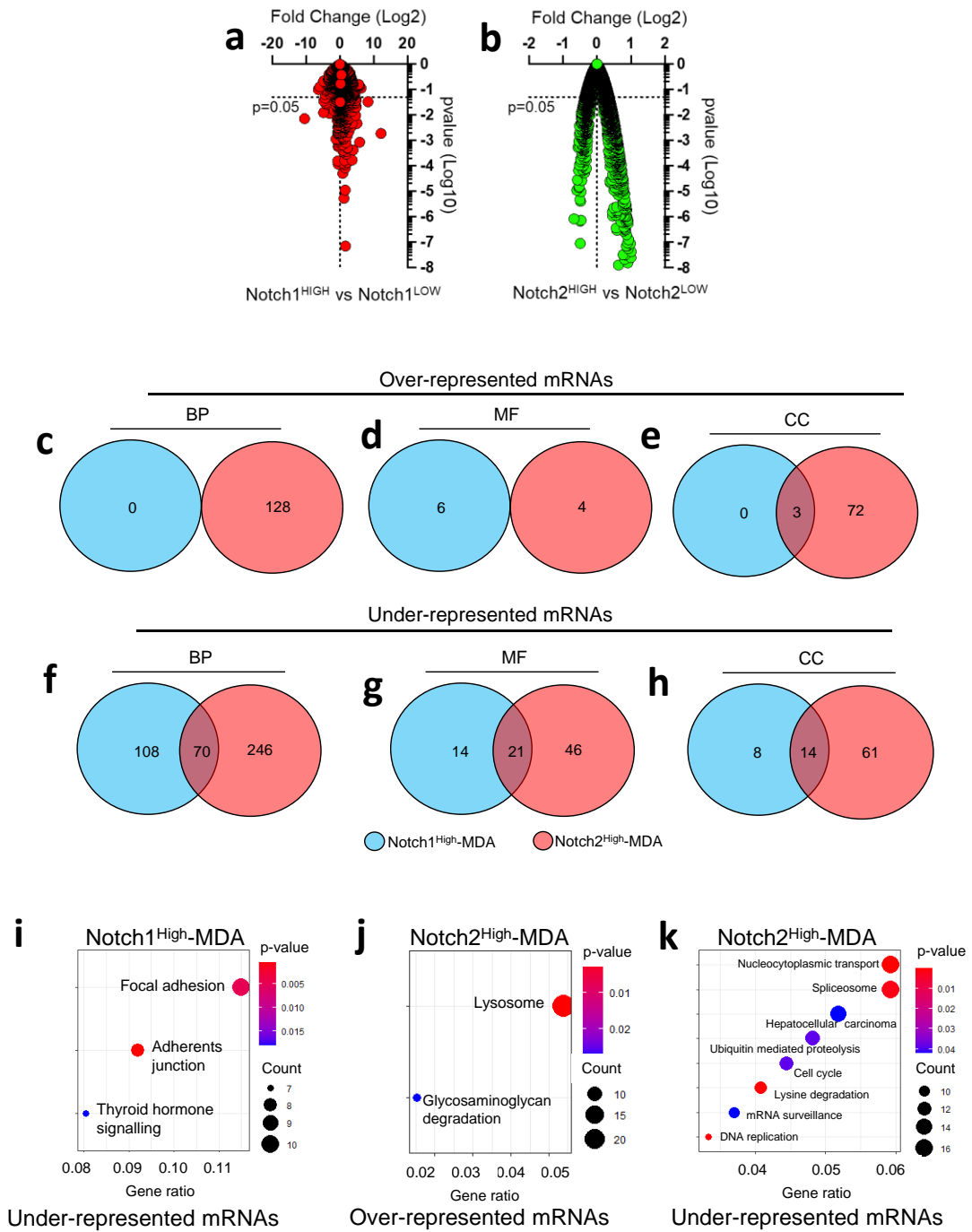


**Figure 4. Transcriptome bioinformatic analysis.** The transcriptomes of MDA cells MACS-sorted for Notch1 or Notch2 were analyzed by R Studio. (a) 522 genes were differentially expressed in Notch1<sup>High</sup> vs Notch1<sup>Low</sup> cells and (b) 1799 genes in Notch2<sup>High</sup> vs Notch2<sup>Low</sup> cells. (c-e) GO terms associated with upregulated and (f-h) downregulated transcripts in Notch1<sup>High</sup> versus Notch2<sup>High</sup> MDA cells to define the shared GO terms represented in Venn-diagrams. (i-k) KEGG pathway analysis of the differentially expressed genes. Node size represents gene ratio; node color represents the P.adjust. Data derived from 3 independent RNA extractions for each condition.

#### 4.4. Comparison between Notch1<sup>High</sup> and Notch2<sup>High</sup> MDA cell transcriptomes

As first step of comparison, we identified statistically significant GO terms associated with upregulated and downregulated transcripts found in Notch1<sup>High</sup> and Notch2<sup>High</sup> cells versus their Low counterparts (Table 4 and 5), then we searched for shared GO terms between Notch1<sup>High</sup> and Notch2<sup>High</sup> cell populations. Interestingly, no shared upregulated biological processes and molecular functions, and only 3 shared cellular components GO terms, including collagen-containing extracellular matrix (GO:0062023), basement membrane (GO:0005604) and endoplasmic reticulum lumen (GO:0005788) were observed between the two groups (Figure 4c-e, Table 6). In contrast, many more unenriched GO terms were shared between Notch1<sup>High</sup> and Notch2<sup>High</sup> cells, with 70 shared BP terms, 21 MF terms and 14 CC terms (Figure 4f-h). Of note, among these shared unenriched terms, the majority was associated with DNA replication, transcription, modification, organization and binding, suggesting a negative impact on cell cycle and proliferation.

Next, the KEGG pathway analysis in Notch1<sup>High</sup> and Notch2<sup>High</sup> cells demonstrated that the underrepresented mRNAs in Notch1<sup>High</sup> cells versus Notch1<sup>Low</sup> cells were associated with pathways involved in focal adhesion and anchoring junctions (Fig. 4i), suggesting a reduced ability to perform cell-substrate and cell-cell interactions, typical of aggressive cancer cells. Interestingly, while Notch2<sup>High</sup> cells showed enriched lysosome and glycosaminoglycan degradation pathways (Fig. 4j) versus Notch2<sup>Low</sup> cells, relevant for the metastatic process, they displayed various downregulated pathways, including nucleocytoplasmic transport, spliceosome, hepatocellular carcinoma, ubiquitin-mediated proteolysis, cell cycle, lysine degradation, mRNA surveillance and DNA replication (Fig. 4k), compatible with the quiescent status associated with a possible cellular dormancy. Therefore, we propose that Notch2 rather than Notch1 affects the molecular machinery necessary for the quiescent status of a small subgroup of human BrCa MDA cells.

**Table 4.** Top 25 statistically significant GO terms associated with upregulated and downregulated transcripts found in Notch1<sup>High</sup> vs Notch1<sup>Low</sup>

ID	Ontology Term	Description	p.adjust
<i>Up-regulated mRNAs</i>			
GO:0030374	MF	nuclear receptor transcription coactivator activity	0.001179
GO:0003713	MF	transcription coactivator activity	0.014041
GO:0042974	MF	retinoic acid receptor binding	0.02894
GO:0035257	MF	nuclear hormone receptor binding	0.02894
GO:0001085	MF	RNA polymerase II transcription factor binding	0.039815

GO:0003712	MF	transcription coregulator activity	0.04891
GO:0062023	CC	collagen-containing extracellular matrix	0.030611
GO:0005604	CC	basement membrane	0.030611
GO:0005788	CC	endoplasmic reticulum lumen	0.030611
<i>Down-regulated mRNAs</i>			
GO:0016570	BP	histone modification	1.7132E-06
GO:0016569	BP	covalent chromatin modification	1.7132E-06
GO:0018205	BP	peptidyl-lysine modification	1.1157E-05
GO:1904837	BP	beta-catenin-TCF complex assembly	0.00024824
GO:0060541	BP	respiratory system development	0.00035603
GO:0060560	BP	developmental growth involved in morphogenesis	0.00137246
GO:0022604	BP	regulation of cell morphogenesis	0.00245783
GO:0003401	BP	axis elongation	0.0031953
GO:0035107	BP	appendage morphogenesis	0.0031953
GO:0035108	BP	limb morphogenesis	0.0031953
GO:0006096	BP	glycolytic process	0.0031953
GO:0006757	BP	ATP generation from ADP	0.0031953
GO:0030518	BP	intracellular steroid hormone receptor signaling pathway	0.0031953
GO:0050769	BP	positive regulation of neurogenesis	0.0031953
GO:0035855	BP	megakaryocyte development	0.0031953
GO:0060562	BP	epithelial tube morphogenesis	0.0031953

GO, gene ontolog; p.adjusted, adjusted P-value; BP, Biological Process; CC, Cellular Component; MF, Molecular Function

**Table 5.** Top 25 statistically significant GO terms associated with upregulated and downregulated transcripts found in Notch2<sup>High</sup> vs Notch2<sup>Low</sup>

<b>ID</b>	<b>GO Term</b>	<b>Description</b>	<b>p.adjust</b>
<i>Up-regulated mRNAs</i>			
GO:0030198	BP	extracellular matrix organization	5.4289E-09
GO:0043062	BP	extracellular structure organization	5.4289E-09
GO:0051924	BP	regulation of calcium ion transport	1.0287E-06
GO:0034612	BP	response to tumor necrosis factor	1.3635E-05
GO:0071356	BP	cellular response to tumor necrosis factor	1.4469E-05
GO:0043122	BP	regulation of I-kappaB kinase/NF-kappaB signaling	1.8844E-05
GO:0060337	BP	type I interferon signaling pathway	1.8844E-05
GO:0071357	BP	cellular response to type I interferon	1.8844E-05
GO:0007249	BP	I-kappaB kinase/NF-kappaB signaling	2.7672E-05
GO:0034340	BP	response to type I interferon	2.7672E-05
GO:1903169	BP	regulation of calcium ion transmembrane transport	2.7672E-05
GO:0043123	BP	positive regulation of I-kappaB kinase/NF-kappaB signaling	2.7916E-05
GO:0009636	BP	response to toxic substance	2.7916E-05

<i>Up-regulated mRNAs</i>			
GO:0016569	BP	covalent chromatin modification	5.2763E-14
GO:0016570	BP	histone modification	5.6491E-13
GO:0018205	BP	peptidyl-lysine modification	1.0602E-12
GO:0033044	BP	regulation of chromosome organization	4.3152E-08
GO:0008380	BP	RNA splicing	4.2616E-07
GO:0045787	BP	positive regulation of cell cycle	7.1436E-07
GO:0006338	BP	chromatin remodeling	1.0991E-06
GO:0016571	BP	histone methylation	1.8405E-06
GO:0090068	BP	positive regulation of cell cycle process	2.0376E-06
GO:0006260	BP	DNA replication	2.1686E-06
GO:0000377	BP	RNA splicing, via transesterification reactions with bulged adenosine as nucleophile	2.5565E-06
GO:0000398	BP	mRNA splicing, via spliceosome	2.5565E-06

GO, gene ontology; p.adjusted, adjusted P-value; BP, Biological Process; CC, Cellular Component; MF, Molecular Function

**Table 6.** Shared Cellular Components (CCs) identified from the enriched GO terms in the Notch1<sup>High</sup> and Notch2<sup>High</sup> MDA cells.

<b>ID</b>	<b>Description</b>	<b>p.adjust</b>
GO:0062023	collagen-containing extracellular matrix	0.03061125
GO:0005604	basement membrane	0.03061125
GO:0005788	endoplasmic reticulum lumen	0.03061125

#### 4.4. *Stem cell signature and HSC mimicry*

An important feature of dormancy is represented by the ability of metastatic cells to retain stem-like features.<sup>21</sup> Furthermore, we had observed in our previous work that dormant cancer cells able to interact with SNOs expressed various stem cell markers.<sup>22,23</sup> Therefore, we next asked whether the transcriptome analysis could unveil if Notch1<sup>High</sup> and Notch2<sup>High</sup> MDA cells shared a pluripotency status. Hence, Gene Set Enrichment Analysis (GSEA) was performed on our RNAdSeq datasets demonstrating that Notch1<sup>High</sup> cells showed no pluripotency signature compared to Notch1<sup>Low</sup> cells (Figure 5a), while Notch2<sup>High</sup> cells displayed a clear-cut enrichment of pluripotency-associated transcripts versus Notch2<sup>Low</sup> cells (Figure 5b). These results support the hypothesis that Notch1 does not drive a stem-like phenotype in MDA cells.

In our previous work, we also observed that Notch2<sup>High</sup> MDA cells displayed similarities with the HSC population.<sup>22</sup> Therefore, we asked whether Notch1<sup>High</sup> and Notch2<sup>High</sup> cells shared HSC signatures. GSEA results ruled out any HSC signature in Notch1<sup>High</sup> cells (Figure 5c), while they showed a prominent HSC signature in Notch2<sup>High</sup> cells (Figure 5d).

Taken together, these data suggest that Notch2 rather than Notch1 displayed HSCs-like molecular signature.

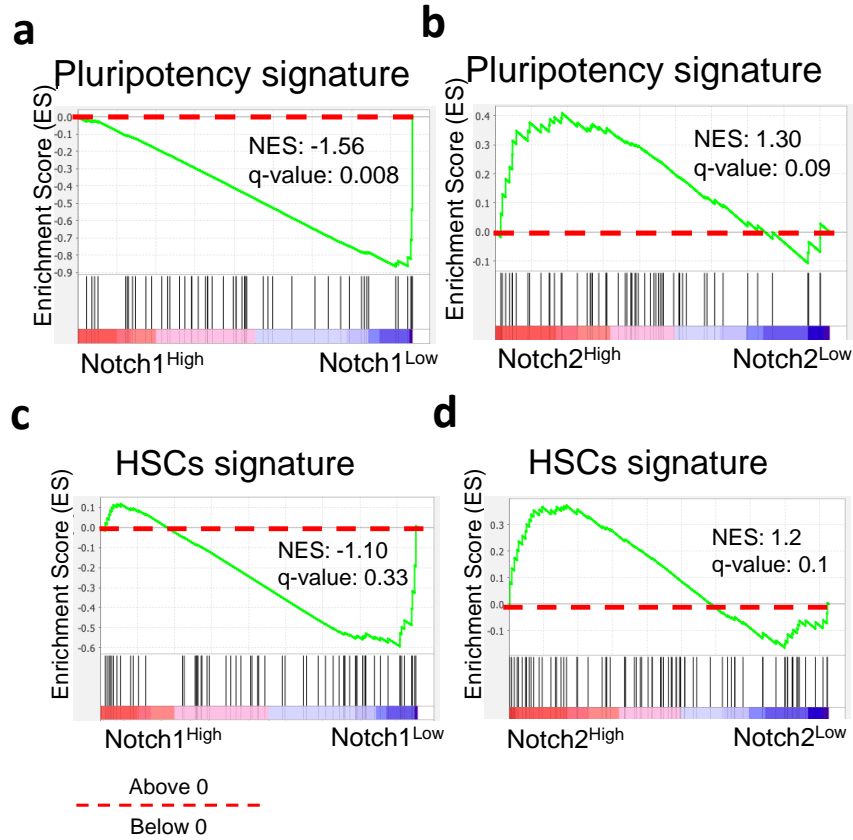


**Figure 5. Gene Set Enrichment Analysis (GSEA).** The transcriptomes of MDA cells MACS-sorted for Notch1 or Notch2 were analyzed by GSEA and crossed in all conditions with datasets containing (a, b) pluripotency and (c, d) HSC gene signature. NES, normalized enrichment score; q-value, measure of the False Discovery Rate. Statistical analysis: False Discovery Rate (FDR)

#### 4.5. Role of HSC genes in BrCa progression

To investigate the role of the HSC mimicry in MDA cell cancer progression in bone, we focused on three HSC genes, *CXCR4*, *CD34* and *TIE2*, that we previously found upregulated in MDA dormant cells<sup>14</sup> and that contributed to the HSC signature shown in Figure 5d. MDA cells were MACS-sorted for CXCR4, CD34 and Tie2 High and Low expression and investigated for the level of each of these mRNAs, and the ability to grow in vitro and generate bone tumors in vivo. CXCR4<sup>High</sup> cells were also CD34<sup>High</sup> (Figure 6a) and expressed more TIE2, albeit at barely detectable level (Figure 6b). Interestingly, they were less positive to the proliferation marker Ki67 (Figure 6c) and incorporated less EdU (6d), suggesting an intrinsic lower proliferation ability. When injected into the tibia of CD1 nu/nu mice, CXCR4<sup>High</sup> cells induced lower incidence and lesser extension of osteolytic lesions, as indicated by the lower number of mice presenting with tibia lytic areas (Figure 6e, f) and their higher tibia cortical volume (Figure 6g) compared to CXCR4<sup>Low</sup> cells.

Like CXCR4<sup>High</sup> MDA cells, CD34<sup>High</sup> cells expressed high level of CXCR4 (Figure 6h) and more, although barely detectable, TIE2 (Figure 6i) compared to CD34<sup>Low</sup> cells. CD34<sup>High</sup> cells also showed less positivity to the proliferation marker Ki67 (Figure 6j) and incorporated less 5-Ethynyl-2'-deoxyuridine (EdU) (Figure 6k). However, CD34<sup>High</sup> and CD34<sup>Low</sup> cells showed similar incidence (Figure 6 l, m) and extension (Figure 6n) of osteolytic lesions.

TIE2<sup>High</sup> MDA cells recapitulated the high expression of CXCR4 and CD34 (Figure 6 o), and the lower proliferation ability showing less positivity to the proliferation marker Ki67 and less ability to incorporate EdU (Figure 6 p, q). TIE2<sup>High</sup> and TIE2<sup>Low</sup> cells induced equal incidence (Figure 6 r, s) but less extension (Figure 6t) of osteolytic lesions in tibias. Finally, the High and Low expression of CXCR4 (Figure 7a), CD34 (Figure 7b) and TIE2 (Figure 7d) did not change the expression of the cancer stem genes *CD24*, *CD44* and *ALDH1A2*, except for a slight increase of *CD24* in CD34<sup>High</sup> compared to CD34<sup>Low</sup> cells (Figure 7b). Altogether these results demonstrated that the expression of HSC genes reduced MDA cell proliferation in vitro and their aggressiveness in vivo, except for the CD34.

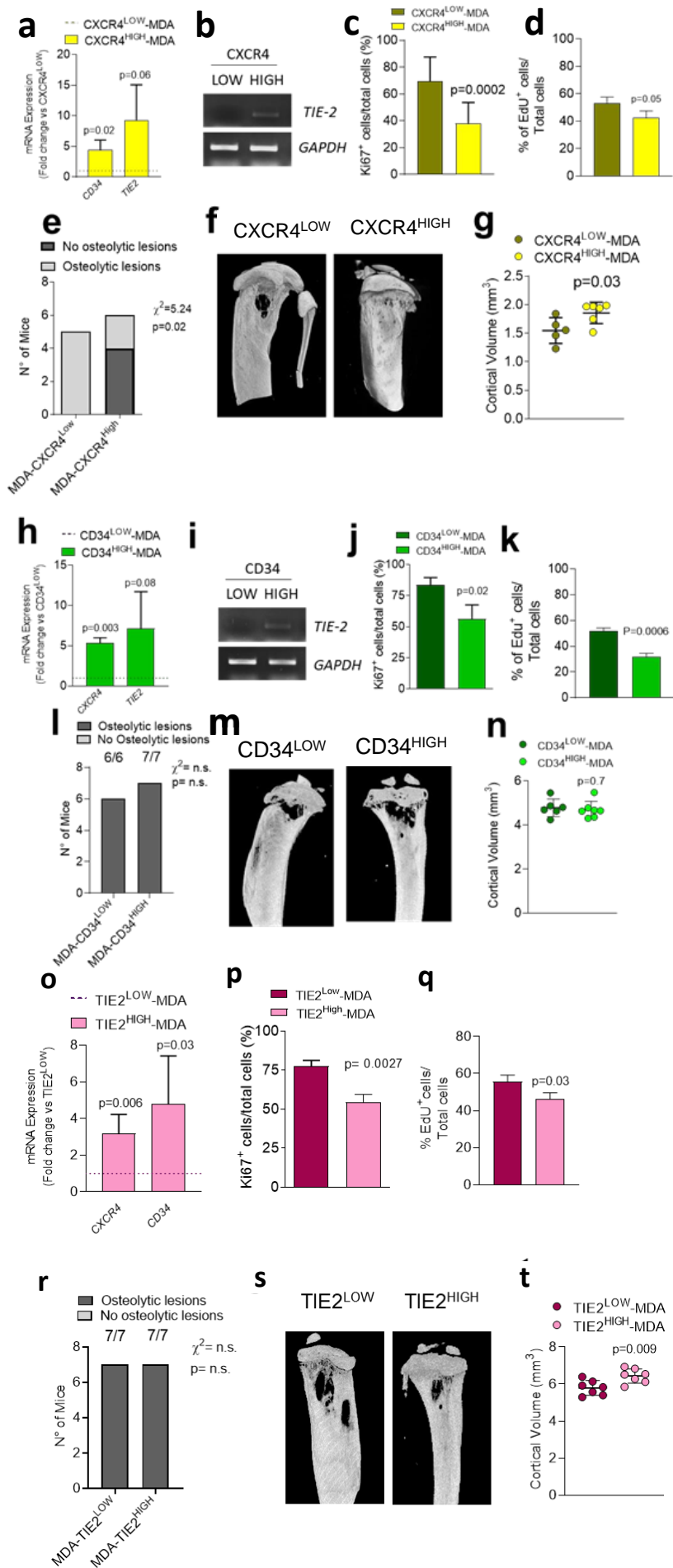




**Figure 6. Role of HSC-mimicry genes in bone metastases.** CXCR4<sup>Low</sup> and CXCR4<sup>High</sup>, CD34<sup>Low</sup> and CD34<sup>High</sup> and TIE2<sup>Low</sup> and TIE2<sup>High</sup> MDA cells were MACS-sorted and analyzed for their role in MDA cell *in vitro* proliferation and *in vivo* growth after intratibial injection in 4-week-old CD1 nu/nu female mice. (a) Real-time RT-PCR and (b) semiquantitative RT-PCR for the indicated genes in CXCR4<sup>Low</sup> and CXCR4<sup>High</sup> MDA cells. Human *GAPDH* was used to normalize gene expression. (c) Ki67 immunostaining and (d) EdU incorporation to measure cell proliferation. (e) Number of mice intratibially injected with CXCR4<sup>Low</sup> and CXCR4<sup>High</sup> MDA cell showing osteolytic lesions. (f)  $\mu$ CT scanning and (g) measurement of cortical bone volume in mice injected with CXCR4<sup>Low</sup> and CXCR4<sup>High</sup> MDA cells. (h) Real-time RT-PCR and (i) semiquantitative RT-PCR for the indicated genes in CD34<sup>Low</sup> and CD34<sup>High</sup> MDA cells. Human *GAPDH* was used to normalize gene expression. (j) Ki67 immunostaining and (k) EdU incorporation to measure cell proliferation. (l) Number of mice intratibially injected with CD34<sup>Low</sup> and CD34<sup>High</sup> MDA cell showing osteolytic lesions. (m)  $\mu$ CT scanning and (n) measurement of cortical bone volume in mice injected with CD34<sup>Low</sup> and CD34<sup>High</sup> MDA cells. (o) Real-time RT-PCR for the indicated genes in TIE2<sup>Low</sup> and TIE2<sup>High</sup> MDA cells. Human *GAPDH* was used to normalize gene expression. (p) Ki67 immunostaining and (q) EdU incorporation to measure cell proliferation. (r) Number of mice intratibially injected with TIE2<sup>Low</sup> and TIE2<sup>High</sup> MDA cells showing osteolytic lesions. (s)  $\mu$ CT scanning and (t) measurement of cortical bone volume in mice injected with TIE2<sup>Low</sup> and TIE2<sup>High</sup> MDA cells. Data are the mean $\pm$ SD of at least 3 independent cell preparations or 6 or 7 mice per group. Statistical analysis: (a, c, e, g, h, j, k, n, o-q, t) Student's t-test, (e, l, r)  $\chi$  square analysis.

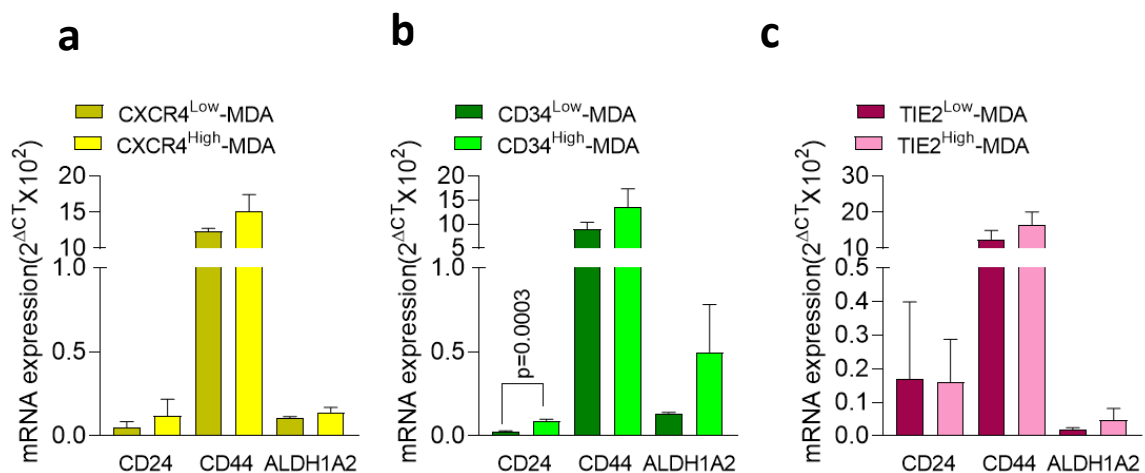


**Figure 7. Effect of HSC marker expression on cancer stem cell phenotype in MDA cells.** MDA cells were MACS-sorted for (a) CXCR4, (b) CD34 and (c) TIE2. Real-time RT-PCR to assess the expression of the indicated cancer stem cell markers. Data are the mean $\pm$ SD of at least 3 independent cell preparations. Statistical analysis: (a-c) Student's t-test.

#### 4.6. *BrCa cells-SNO interactome*

The lack of effect of the HSC genes in the MDA-SNO interaction, prompted us to analyze our Notch2 RNA dataset to identify new determinants mediating this interaction. The RNAdSeq analysis unveiled several transcripts differentially expressed in Notch2<sup>High</sup>

versus Notch2<sup>Low</sup> MDA cells, from which we extracted the data relative to the most regulated mRNAs and focused on the transcripts associated with pluripotency, HSC signatures and Cluster of Differentiation (CD). We then selected mRNAs encoding for cell surface proteins, including *CD177*, *CD163L1*, *NOTCH4*, *IFITM1*, *CD22*, *JAG2*, *KDR*, *CD55* and *CD63*, that could be potentially involved in the interaction with SNOs (Figure 8a).

We then subjected the Notch2<sup>High</sup> and Notch2<sup>Low</sup> cells to conventional real time RT-PCR to validate the differential expression of the selected genes. Results demonstrated that *CD177*, *CD163L1*, *CD55* and *IFITM1* mRNAs were significantly upregulated in Notch2<sup>High</sup> versus Notch2<sup>Low</sup> cells, whereas changes in *CD22* and *KDR* genes were not confirmed (Figure 8b). Finally, although significant, the expression of *CD63* in Notch2<sup>High</sup> was only 1.1-fold higher than in Notch2<sup>Low</sup> cells, whereas the expression of *NOTCH4* and *JAG2* was neglectable in both groups (Figure 8b).

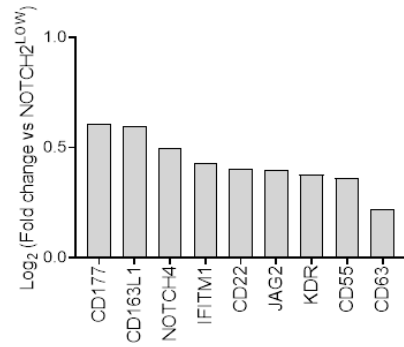
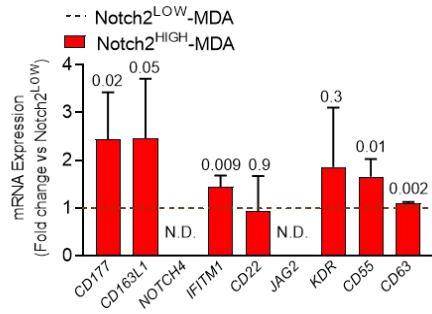
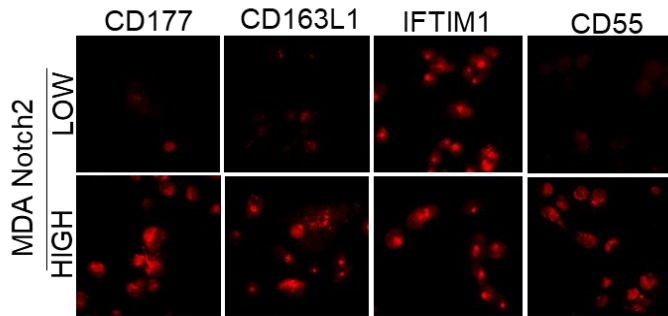
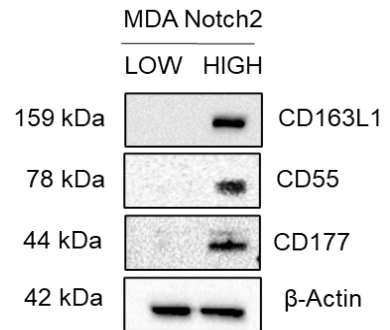
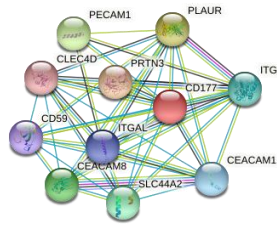
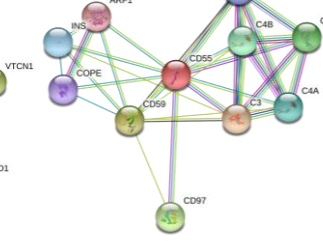
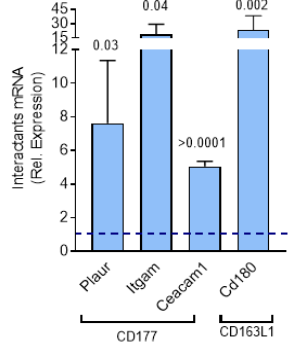
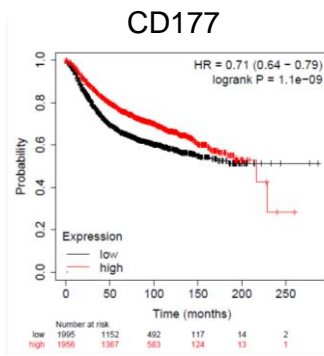
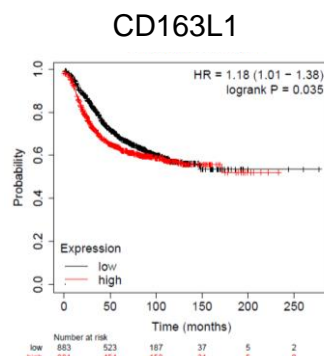
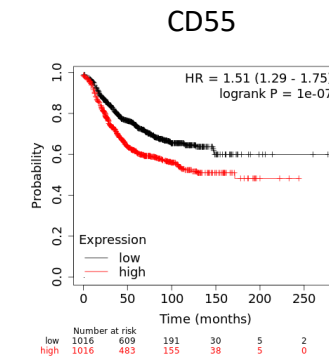
Based on these results we focused on *CD177*, *CD163L1*, *CD55* and *IFITM1* genes and investigated the differential expression of their encoded proteins by immunofluorescence in Notch2<sup>High</sup> and Notch2<sup>Low</sup> MDA cells (Figure 8c). We observed that *CD177*, *CD163L1* and *CD55* proteins were more expressed in Notch2<sup>High</sup> than in Notch2<sup>Low</sup> cells, while *IFTIM1* was equally expressed in the two groups (Figure 8c). Differences in *CD177*, *CD163L1* and *CD55* expression were confirmed also by Western blot analysis (Figure 8d).

We then excluded from the subsequent analysis the *IFTIM1* gene, whose differential expression between Notch2<sup>High</sup> and Notch2<sup>Low</sup> cells was not confirmed and used the String analysis to identify the known cell surface ligands of the *CD177* (Figure 8e), *CD163L1* (Figure 8 f) and *CD55* (Figure 8g) encoded proteins, that could be expressed by SNO and NON- SNO cells. From this list, we extrapolated the cell surface proteins that scored >2 in the String analysis associated with an intracellular signal transduction and evaluated the transcriptomic expression of their genes in SNOs and NON-SNOs. We found that the genes encoding the *CD177* ligands *Plaur*, *Itgam* and *Ceacam 1*, and the gene encoding the *CD163L1* ligand *Cd180* (Figure 8h) were expressed several folds more in SNOs versus NON-SNOs.

To provide a translation meaning to these observations, we investigated if *CD177*, *CD163L1* and *CD55* could correlate with the severity of the human BrCa disease. To this purpose, we interrogated, with the Kaplan–Meier plots method (KMPlot®), a database containing 3951 public transcriptomes from primary BrCas. We observed that there was a

statistically positive correlation in Kaplan-Meyer diagrams between the high expression of CD177 and the overall survival of patients (Figure 8i), whereas this correlation was negative when the CD163L1 and CD55 transcriptomes were interrogated (Figure 8j, k). Given the poor expression in SNOs of the genes encoding for the CD163L1 and CD55 protein ligands and the positive correlation in the Meyer-Kaplan diagrams observed only for the CD177 expression in cancer cells, we can hypothesize CD177 and its ligands Plaur, Itgam and Ceacam1 could represent master genes involved in the MDA-SNO interaction.

Further work is planned to confirm our hypothesis in our models of BrCa cellular dormancy.

**a****b****c****d****e****f****g****h****i****j****k**

**Figure 8. Analysis of the MDA-SNO interactome.** MDA cells were MACS-sorted in Notch2<sup>High</sup> and Notch2<sup>Low</sup>, RNA was extracted and subjected to RNAdSeq. (a) Top 9 genes, encoding for cell surface proteins, associated with pluripotency and HSC signatures, overexpressed by Notch2<sup>High</sup> versus Notch2<sup>Low</sup> MDA cells. (b) Validation of the gene expression showed in figure (a) by real-time RT-PCR. (c) Immunofluorescence imaging of the indicated proteins encoded by the genes selected in figure (b) by statistical significance. (d) Western blot analysis of the proteins upregulated in Notch2<sup>High</sup> versus Notch2<sup>Low</sup> MDA cells. (e) In silico protein-protein interaction network functional enrichment analysis by String for CD177, (f) CD163L1 and (g) CD55. (h) Real-time RT-PCR of the indicated CD177 and CD163L1 cell surface ligands overexpressed by SNOs versus NON SNOs. (i) Kaplan–Meier plots (KMPlot®) of 3951 public transcriptomes from primary human BrCas correlating CD177, (j) CD163L1 and (k) CD55 expression with patient survival. Data are representative of the mean±SD of at least 3 independent cell preparations. Statistical analysis: (b, h) Student's t-test; (i-k) log-rank test.

## 5. DISCUSSIONS

In this study, we used a “from broad to narrow” approach to structure the molecular features of BrCa dormancy in the bone microenvironment. We observed that human primary and bone metastatic BrCas contain rare single cells positive for Notch1 and Notch2, with Notch2 positive cells rarer than Notch1 positive cells. Screening several BrCa cell types, either Notch1<sup>High</sup>, Notch2<sup>High</sup> or Notch1<sup>High</sup>/Notch2<sup>High</sup>, we found that Notch2 and not Notch1 was implicated in SNO-induced inhibition of their proliferation. Using RNAdSeq, a powerful means to investigate the whole cellular transcriptome, we were enabled to delineate the molecular profile of Notch1<sup>High</sup> and Notch2<sup>High</sup> cells, focusing on the MDA cell line that was previously characterized for their ability to lodge the endosteal niche enriched in SNOs, slowing their proliferation ability.<sup>14</sup> Through this approach, it appeared evident that only the high expression of Notch2 conferred to the MDA cells pluripotency signature and HSC-mimicry, while underrepresented pathways were involved in cell proliferation, suggestive of their propensity to remain dormant in a permissive microenvironment. According to our results, this microenvironment could include the SNO-enriched endosteal niche.

Interestingly, the high expression of canonical HSC genes identified in MDA cells, *CXCR4*, *CD34* and *TIE2*, was associated with an intrinsic cellular quiescence. *CXCR4*, also known as *fusin*<sup>25</sup> or *CD184*,<sup>25</sup> encodes for the C-X-C chemokine receptor specific for the lymphocyte chemotactic protein C-X-C motif chemokine ligand 12 (CXCL12), also known as Stromal cell-Derived Factor 1 (SDF1).<sup>26</sup> The CXCR4/CXCL12 axis is known to support quiescence and bone marrow retention of HSCs.<sup>27</sup> *CD34* is a surface marker of HSCs used to distinguish Long-Term (LT)-HSCs from Short-Term (ST)-HSCs.<sup>28</sup> It encodes for the CD34 antigen involved in the adhesion of stem cells to the bone marrow extracellular

matrix and stromal cells.<sup>28</sup> *TIE2* encodes for a receptor of the protein kinase TIE2 family, which binds angiopoietin-1 and regulates angiogenesis.<sup>29</sup> The TIE2/angiopoietin-1 pathway is also involved in HSC quiescence and exhibits antiapoptotic activity.<sup>30</sup> However, in the context of the MDA cellular dormancy, we ruled out that the high expression of these genes was implicated in the SNO-induced inhibition of their proliferation since this was observed also in MDA cells expressing low level of the same genes. Nevertheless, high expression of CXCR4 and TIE2 reduced the extension of the MDA-induced osteolytic lesions in vivo, with CXCR4 also reducing lesion incidence. These results unveiled a high complexity in the HSC-mimicry contribution to the development of MDA tumors in the bone microenvironment, that will require further investigation for a full comprehension of its relevance in BrCa bone metastases.

In this study, we were intrigued by the molecular mechanisms that could promote the physical interaction between dormant BrCa cancer cells and SNOs. We hypothesized that, among them, we could identify a relevant pathway that could be targeted by therapy. Therefore, we interrogated our MDA Notch2<sup>High</sup> RNAseq signatures for high expression of genes encoding for cell surface proteins that could be potentially implicated in MDA-SNO cell-cell interaction and signal transduction. With this successful strategy, we narrowed down a list of nine potential candidates, subsequently excluding those that were not confirmed by conventional RT-PCR and immunofluorescence analysis. The three remaining candidates, *CD177*, *CD163LI* and *CD55* appeared promising. In fact, *CD177* encodes the glycosylphosphatidylinositol (GPI)-linked surface glycoprotein that plays a role in neutrophil activation, binds Platelet Endothelial Cell Adhesion Molecule-1 (PEACAM-1) and facilitates neutrophil transmigration.<sup>31</sup> *CD163LI* encodes a member of the scavenger receptor cysteine-rich superfamily, called CD163 molecule like-1. These are secreted or membrane-anchored proteins associated with the immune system, that mediate protein-protein interaction and ligand binding.<sup>32</sup> Finally, *CD55* encodes the Decay-Accelerating Factor (DAF), another glycosylphosphatidylinositol (GPI)-anchored protein associated with membrane lipid microdomains that is involved in the defense of cells from complement-mediated attack.<sup>33</sup> Given the role we hypothesized for these proteins in the interaction with SNOs, our selection was further refined based on the associated ligands highly expressed by SNOs. Interestingly, compared with NON-SNOs, SNOs expressed high level of three *CD177* ligands encoded by the *Plaur*, *Itgam* and *Ceacam1* genes. *Plaur* encodes the plasminogen activator urokinase receptor (uPAR) involved in tissue remodeling,<sup>34</sup> while *Itgam* encodes the CD11b chain of the Mac-1 (alphaMbeta2; CD11b/CD18; complement receptor-3) integrin, also known as Complement Receptor 3

(CR3), involved in adhesion, inflammation and leukocyte migration.<sup>35</sup> *Ceacam1* encodes the CarcinoEmbryonic Antigen-related Cell Adhesion Molecule 1 (CEACAM1) mediates cell-cell adhesion of leucocytes, epithelia and endothelia via both homophilic and heterophilic binding.<sup>36,37</sup> The CD163L1 ligand highly expressed by SNOs was the CD180 antigen, a protein typical of antigen presenting cells belonging to the family of pathogen receptors.<sup>38</sup> In contrast the CD55 ligand, CD59, shared with the CD177, known as MAC-Inhibitory Protein (MAC-IP), Membrane inhibitor of Reactive lysis (MIRL), or protectin, which prevents the polymerization of complement C9,<sup>39</sup> was downregulated in SNOs and excluded by the list of candidates.

Finally, we completed our selection with a translational observation performed through Kaplan-Meier diagrams obtained by examination of public dataset in which the survival of BrCa patients was evaluated against the expression levels of CD177 and CD163L1. This analysis unveiled that only the high expression of CD177 was associated with a better patient survival, thus prompting us to focus on CD177 for further studies. To the best of our knowledge, the role of CD177 in cancer dormancy has not yet been elucidated. In contrast with our observation, CD177 expression is an indicator of poor survival in patients with non-small cell lung cancer<sup>40</sup> and with cervical cancer.<sup>41</sup> It is also a marker of myeloproliferative diseases<sup>42</sup>, as well as a key molecule of the neutrophil-associated innate immunity<sup>43</sup> that increases in severe bacterial infections.<sup>44</sup> Given the paucity of data on CD177 in the field of BrCa in general, and specifically in BrCa cellular dormancy, we believe that the understanding of its role and relevance requires further studies that will follow the results described in this thesis. To this aim we will perform functional analysis *in vitro* and *in vivo* in the presence of CD177 agonists, with the hypothesis that they should alter MDA-dormancy if this pathway is essential for the SNO-mediated MDA cell cycle arrest in the endosteal niche. If the upcoming latter part of the study will succeed, we might pave the way for further translational investigations that could lighter the intricate mechanisms implicated in the BrCa cellular dormancy in the bone microenvironment.

## 6. REFERENCES

1. Gomatou, G., Syrigos, N., Vathiotis, I. A. & Kotteas, E. A. Tumor dormancy: Implications for invasion and metastasis. *Int J Mol Sci* **22**, (2021).
2. Phan, T. G. & Croucher, P. I. The dormant cancer cell life cycle. *Nature Reviews Cancer* **20**:7 **20**, 398–411 (2020).
3. Páez, D. *et al.* Cancer dormancy: A model of early dissemination and late cancer recurrence. *Clinical Cancer Research* **18**, 645–653 (2012).
4. Park, S. Y. & Nam, J. S. The force awakens: metastatic dormant cancer cells. *Experimental & Molecular Medicine* **52**:4 **52**, 569–581 (2020).
5. Bushnell, G. G. *et al.* Breast cancer dormancy: need for clinically relevant models to address current gaps in knowledge. *npj Breast Cancer* **2021** **7**:1 **7**, 1–12 (2021).
6. Yip, R. K. H. *et al.* Mammary tumour cells remodel the bone marrow vascular microenvironment to support metastasis. *Nature Communications* **2021** **12**:1 **12**, 1–17 (2021).
7. Santos-de-Frutos, K. & Djouder, N. When dormancy fuels tumour relapse. *Commun Biol* **4**, (2021).
8. Lévesque, J. P., Helwani, F. M. & Winkler, I. G. The endosteal ‘osteoblastic’ niche and its role in hematopoietic stem cell homing and mobilization. *Leukemia* **2010** **24**:12 **24**, 1979–1992 (2010).
9. Tamma, R., Ribatti, D., Ranieri, G. & Kumar Vashist, Y. Bone Niches, Hematopoietic Stem Cells, and Vessel Formation. *International Journal of Molecular Sciences* **2017**, Vol. **18**, Page **151** **18**, 151 (2017).
10. Miyamoto, Y., Sakane, F. & Hashimoto, K. N-cadherin-based adherens junction regulates the maintenance, proliferation, and differentiation of neural progenitor cells during development. *Cell Adh Migr* **9**, 183 (2015).
11. Richter, R., Forssmann, W. & Henschler, R. Current Developments in Mobilization of Hematopoietic Stem and Progenitor Cells and Their Interaction with Niches in Bone Marrow. *Transfusion Medicine and Hemotherapy* **44**, 151–164 (2017).
12. Lawal, R. A. *et al.* Notch Ligand Jagged1 Regulates the Osteoblastic Lineage by Maintaining the Osteoprogenitor Pool. *J Bone Miner Res* **32**, 1320 (2017).



13. Haider, M. T., Smit, D. J. & Taipaleenmäki, H. The Endosteal Niche in Breast Cancer Bone Metastasis. *Front Oncol* **10**, (2020).
14. Capulli, M. *et al.* Notch2 pathway mediates breast cancer cellular dormancy and mobilisation in bone and contributes to haematopoietic stem cell mimicry. *Br J Cancer* **121**, 157–171 (2019).
15. Kolb, A. D., Shupp, A. B., Mukhopadhyay, D., Marini, F. C. & Bussard, K. M. Osteoblasts are ‘educated’ by crosstalk with metastatic breast cancer cells in the bone tumor microenvironment. *Breast Cancer Research* **21**, 1–30 (2019).
16. Yu, G., Wang, L. G., Han, Y. & He, Q. Y. ClusterProfiler: An R package for comparing biological themes among gene clusters. *OMICS* **16**, 284–287 (2012).
17. Wu, T. *et al.* clusterProfiler 4.0: A universal enrichment tool for interpreting omics data. *The Innovation* **2**, (2021).
18. Wickham, H. ggplot2. (2016) doi:10.1007/978-3-319-24277-4.
19. Storey, J. D. A direct approach to false discovery rates. *J R Stat Soc Series B Stat Methodol* **64**, 479–498 (2002).
20. Subramanian, A. *et al.* Gene set enrichment analysis: A knowledge-based approach for interpreting genome-wide expression profiles. *Proc Natl Acad Sci U S A* **102**, 15545–15550 (2005).
21. Ayob, A. Z. & Ramasamy, T. S. Cancer stem cells as key drivers of tumour progression. *Journal of Biomedical Science 2018 25:1* **25**, 1–18 (2018).
22. Capulli, M. *et al.* Notch2 pathway mediates breast cancer cellular dormancy and mobilisation in bone and contributes to haematopoietic stem cell mimicry. *Br J Cancer* **121**, 157–171 (2019).
23. Maurizi, A., Ciocca, M., Giuliani, C., di Carlo, I. & Teti, A. Role of Neural (N)-Cadherin in Breast Cancer Cell Stemness and Dormancy in the Bone Microenvironment. *Cancers (Basel)* **14**, (2022).
24. Maurizi, A., Ciocca, M., Giuliani, C., di Carlo, I. & Teti, A. Role of Neural (N)-Cadherin in Breast Cancer Cell Stemness and Dormancy in the Bone Microenvironment. *Cancers (Basel)* **14**, 1–12 (2022).

25. Moriuchi, M., Moriuchi, H., Turner, W., Fauci, A.S., Cloning and analysis of the promoter region of CXCR4, a coreceptor for HIV-1 entry. *Journal of Immunology*. **159**, 4322–9 (1997)
26. Teicher, BA., Fricker, SP., CXCL12 (SDF-1)/CXCR4 pathway in cancer. *Clin Cancer Res*. **16**, 2927-31 (2010)
27. Moll, N.M., Ransohoff, R.M., CXCL12 and CXCR4 in bone marrow physiology. *Expert Rev Hematol*. **3**, 315-22 (2010)
28. Al-Amoodi AS, Li Y, Al-Ghuneim A, Allehaibi H, Isaioglou I, Esau LE, AbuSamra DB, Merzaban JS. Refining the migration and engraftment of short-term and long-term HSCs by enhancing homing-specific adhesion mechanisms. *Blood Adv*. **6**, 4373-4391(2022)
29. Partanen J, Armstrong E, Mäkelä TP, Korhonen J, Sandberg M, Renkonen R, Knuutila S, Huebner K, Alitalo K. A novel endothelial cell surface receptor tyrosine kinase with extracellular epidermal growth factor homology domains. *Mol Cell Biol*. **12**, 1698-707 (1992)
30. Arai F, Hirao A, Ohmura M, Sato H, Matsuoka S, Takubo K, Ito K, Koh GY, Suda T. Tie2/angiopoietin-1 signaling regulates hematopoietic stem cell quiescence in the bone marrow niche. *Cell*. **118**, 149-61(2004)
31. Bayat B, Werth S, Sachs UJ, Newman DK, Newman PJ, Santoso S. Neutrophil transmigration mediated by the neutrophil-specific antigen CD177 is influenced by the endothelial S536N dimorphism of platelet endothelial cell adhesion molecule-1. *J Immunol*. **184**, 3889-96 (2010)
32. Gronlund, J., Holmskov, U., Cloning of a novel scavenger receptor cysteine-rich type I transmembrane molecule (M160) expressed by human macrophages. *J. Immunol*. **165**, 6406-15 (2000)
33. Brodbeck WG, Kuttner-Kondo L, Mold C, Medof ME. Structure/function studies of human decay-accelerating factor. *Immunology*. **101**, 104-11 (2000)
34. Plesner T, Behrendt N, Ploug M. Structure, function and expression on blood and bone marrow cells of the urokinase-type plasminogen activator receptor, uPAR. *Stem Cells*. **15**, 398-408 (1997)
35. Solovjov DA, Pluskota E, Plow EF. Distinct roles for the alpha and beta subunits in the functions of integrin alphaMbeta2. *J Biol Chem*. **280**, 1336-45 (2005)

36. Kim WM, Huang YH, Gandhi A, Blumberg RS. CEACAM1 structure and function in immunity and its therapeutic implications. *Semin Immunol.* **42**, 101296 (2019)
37. Müller MM, Singer BB, Klaile E, Obrink B, Lucka L. Transmembrane CEACAM1 affects integrin-dependent signaling and regulates extracellular matrix protein-specific morphology and migration of endothelial cells. *Blood.* **105**, 3925-34 (2005)
38. Nagai Y, Shimazu R, Ogata H, Akashi S, Sudo K, Yamasaki H, Hayashi S, Iwakura Y, Kimoto M, Miyake K. Requirement for MD-1 in cell surface expression of RP105/CD180 and B-cell responsiveness to lipopolysaccharide. *Blood.* **99**, 1699-705 (2002)
39. Jarvis GA, Li J, Hakulinen J, Brady KA, Nordling S, Dahiya R, Meri S. Expression and function of the complement membrane attack complex inhibitor protectin (CD59) in human prostate cancer. *Int J Cancer.* **71**, 1049-55 (1997)
40. Sakabe T, Azumi J, Haruki T, Umekita Y, Nakamura H, Shiota G. CD117 expression is a predictive marker for poor prognosis in patients with non-small cell lung cancer. *Oncol Lett.* **13**, 3703-3708 (2017)
41. Liao W, Li W, Li Y, Liu T, Wang Y, Feng D, Shen F. Diagnostic, prognostic, and immunological roles of CD177 in cervical cancer. *J Cancer Res Clin Oncol.* (2022)
42. Passamonti F, Pietra D, Malabarba L, Rumi E, Della Porta MG, Malcovati L, Bonfichi M, Pascutto C, Lazzarino M, Cazzola M. Clinical significance of neutrophil CD177 mRNA expression in Ph-negative chronic myeloproliferative disorders. *Br J Haematol.* **126**, 650-6 (2004)
43. Stroncek DF. Neutrophil-specific antigen HNA-2a, NB1 glycoprotein, and CD177. *Curr Opin Hematol.* **14**, 688-93 (2007)
44. Göhring K, Wolff J, Doppl W, Schmidt KL, Fenchel K, Pralle H, Sibelius U, Bux J. Neutrophil CD177 (NB1 gp, HNA-2a) expression is increased in severe bacterial infections and polycythaemia vera. *Br J Haematol.* **126**, 252-4 (2004)

# Chapter 5

## ACHIEVEMENTS

## CURRICULUM VITAE



**Michela Ciocca**

Born in L'Aquila (Italy), December 17, 1994

Italian citizenship



ORCID QR CODE

## AFFILIATION

Department of Biotechnological and Applied Clinical Sciences, via Vetoio – Coppito 2, 67100L'Aquila, Italy

Tel. +39 3290344750

e-mail: [michecio94@gmail.com](mailto:michecio94@gmail.com)

## DEGREES

- 2017** Bachelor's degree in Biology, 95/110
- 2019** Master's degree in Molecular and Cellular Biotechnology, 110/110 cum laude

## PROFESSIONAL EXPERIENCE

- 06/2018-04/2019** Undergraduate Internship at "Bambino Gesù" pediatric hospital (OPBG) at the "Immunology Reserch" Laboratory directed by Dr. Rita Carsetti.
- 04/2019-05/2019** Research contract at the "Translational research laboratory on pediatric idiopathic nephrotic syndrome (INS)" of the OPBG directed by Dr. Francesco Emma.
- 05/2019-10/2019** Research contract at the "Immunological Research laboratory" of the OPBG directed by Dr. Rita Carsetti.
- 11/2019-present** PhD student in Bone Biopathology Lab, Department of Biotechnological and Applied Clinical Sciences, University of L'Aquila

## **PUBLICATIONS**

- Norwood I, Szondi D, Ciocca M, Coudert A, Cohen-Solal M, Rucci N, Teti A, Maurizi A. Transcriptomic and bioinformatic analysis of Clcn7-dependent Autosomal Dominant Osteopetrosis type 2. Preclinical and clinical implications. *Bone*. 2021 Mar;144:115828. doi: 10.1016/j.bone.2020.115828. Epub 2020 Dec 28. PMID: 33359007.
- Ciocca M, Zaffina S, Fernandez Salinas A, Bocci C, Palomba P, Conti MG, Terreri S, Frisullo G, Giorda E, Scarsella M, Brugaletta R, Vinci MR, Magnavita N, Carsetti R, Piano Mortari E. Evolution of Human Memory B Cells From Childhood to Old Age. *Front Immunol*. 2021 Jul 23;12:690534. doi: 10.3389/fimmu.2021.690534. PMID: 34367150; PMCID: PMC8343175.
- Maurizi A, Ciocca M, Giuliani C, Di Carlo I, Teti A. Role of Neural (N)-Cadherin in Breast Cancer Cell Stemness and Dormancy in the Bone Microenvironment. *Cancers (Basel)*. 2022 Mar 4;14(5):1317. doi: 10.3390/cancers14051317. PMID: 35267624; PMCID: PMC8909418.

## **CONFERENCES**

- ECTS 2021 Digital Congress (7-11 May 2021) – Oral Presentation
- ECTS Gemstone PhD Training Course 2021 (24-27 August 2021) – Oral Presentation
- EFF 15th Fellows Forum 2021 (24-25 September 2021) – Oral Presentation
- ECTS congress Helsinki 2022 (6-10 May 2022) – Plenary Oral Presentation

## **AWARDS**

- ECTS congress Helsinki 2022 (6-10 May 2022) – New investigator Award